Continuous Supercritical Emulsion Extraction: process characterization and optimization of operative conditions to produce biopolymer microspheres

Nunzia Falco

Unione Europea

Ministero dell'Istruzione, dell'Università e della Ricerca

UNIVERSITÀ DEGLI STUDI DI SALERNO

Department of Industrial Engineering

Ph.D. Course in Chemical Engineering (X Cycle-New Series)

Continuous Supercritical Emulsion Extraction: process characterization and optimization of operative conditions to produce biopolymer microspheres

Supervisor   **Ph.D. student**
Prof. Ernesto Reverchon   *Ing. Nunzia Falco*

Scientific Referees
Dr. Giovanna Della Porta
Prof. Erdogan Kiran

Ph.D. Course Coordinator
Prof. Paolo Ciambelli

Acknowledgements

I would like to thank here all the kind people around me who made this thesis possible with their help and support.

First of all, I am extremely grateful to my supervisor, Prof. Ernesto Reverchon, for giving me the opportunity to be part of his *"Supercritical Fluid"* team at the University of Salerno and for providing a stimulating and fun environment for me in which to learn and grow as a student and a researcher. His enthusiasm and passion for research, guidance and support, understanding and patience, added considerably to my experience. I appreciated his unsurpassed knowledge and skill in many areas, and his assistance at all levels of the research project. Throughout my PhD work, he provided encouragement, good teaching and wise advice on how to optimize my work.

I would like to thank the other members of my committee, Dr. Giovanna Della Porta and Prof. Erdogan Kiran. Thanks to Giovanna, since this PhD project profited a lot from our several interesting and fruitful discussions. I received from her lots of good ideas and constructive advice during the whole course of my PhD.
My further acknowledgement to Giovanna and Prof. Reverchon, who promoted the collaboration with Prof. Kiran at Virginia Tech University.

I am grateful to Prof. Kiran for his availability to take part in my scientific committee, for kindly giving me the opportunity to join his research group in Blacksburg for several months and for taking his precious time out from his busy schedule to help me every time I needed. His supervision with his expertise and valuable advice were precious for me. It was a great pleasure for me to work with him. I am confident that this experience was helpful for my personal and professional growth. I would also thank his family for their hospitality during my stay at Virginia Tech University, who have been able to let me feel "at home" nevertheless the distance from my family.

Papers produced during this work

International journals:

1) Della Porta G., **Falco N.**, Reverchon E.
   "NSAID Drugs Release from Injectable Microspheres Produced by Supercritical Fluid Emulsion Extraction", Journal of Pharmaceutical Sciences, 99(3), 2010, pp. 1484-1499.

2) Della Porta G., Campardelli R., **Falco N.**, Reverchon E.
   "PLGA Microdevices for Retinoids Sustained Release Produced by Supercritical Emulsion Extraction: Continuous Versus Batch Operation Layouts", Journal of Pharmaceutical Sciences, 100(10), 2011, pp. 4357-4367.

3) Della Porta G., **Falco N.**, Reverchon E.
   "Continuous Supercritical Emulsions Extraction: A New Technology for Biopolymer Microparticles Production", Biotechnology and Bioengineering, 108(3), 2011, pp. 676-686.

4) **Falco N.** and Kiran E.
   "Volumetric Properties of Ethyl Acetate + Carbon Dioxide Binary Fluid Mixtures at High Pressures", The Journal of Supercritical Fluids, 61, 2012, pp. 9-24.

5) **Falco N.**, Reverchon E., Della Porta G.
   "Continuous Supercritical Emulsions Extraction: Packed Tower Characterization and Application to PLGA+Insulin Microspheres Production", submitted to Industrial & Engineering Chemistry Research, 2012.

6) Della Porta G., **Falco N.**, Giordano E., Reverchon E.
"PLGA/Insulin Microdevices Produced by Continuous Supercritical Emulsions Extraction Technology as Active Support for Cardiomioblast Proliferation", submitted to <u>Acta Biomaterialia</u>, 2012.

7) **Falco N.**, Reverchon E., Della Porta G.
"PLGA/Hydrocortisone Microspheres Produced by Continuous Supercritical Emulsions Extraction", submitted to <u>International Journal of Pharmaceutics</u>, 2012.

Proceedings of International Conferences:

1) **Falco N.**, Reverchon E., Della Porta G.
"Continuous Supercritical Emulsions Extraction: An Innovative Process Layout for Microcarriers Production", <u>Proceedings of the 9th Conference on Supercritical Fluids and Their Applications</u>, Sorrento (Italy), 5-8 September 2010.

2) **Falco N.**, Reverchon E., Della Porta G.
"Continuous Supercritical Fluid Emulsion Extraction: a Low Impact Route for Biopolymer Microspheres Production", <u>Proceedings of 2011 AIChE Spring Meeting & 7th Global Congress on Process Safety</u>, Chicago (Illinois) 13-17 March 2011.

3) Della Porta G., **Falco N.**, Reverchon E.
"Continuous Supercritical Emulsions Extraction: Capabilities and Performances of an Innovative Process for Biopolymer Microspheres Production", <u>Proceedings of the 13th European Meeting on Supercritical Fluids</u>, The Hague (Netherlands), 9-12 October 2011.

CONTENTS

II

INDEX OF FIGURES

INDEX OF TABLES

ABSTRACT

Controlled release systems for therapeutic drugs have received extensive attention in recent years, due to their great clinical potential. Biodegradable microspheres are well-recognized systems to control the release rate of a drug out of a pharmaceutical dosage form; they are able to protect these agents against rapid degradation and clearance and release them in the body with a desired controlled rate and amount. Particularly, biopolymer microspheres are attracting increasing attention as drug carriers for injectable controlled release formulations.

Biopolymer microspheres for controlled drug delivery can be conventionally prepared by solvent evaporation/extraction of emulsions, but this technique shows many drawbacks (high temperature, long processing times, large polidispersity, high residual solvents, lower encapsulation efficiency). To overcome the limits of the traditional process, in recent years, Supercritical Emulsion Extraction (SEE) has been proposed for the production of drug/polymer microspheres with controlled size and distribution, starting from *oil-in-water (o-w)* and *water-in-oil-in-water (w-o-w)* emulsions. This process uses supercritical carbon dioxide (SC-CO_2) to extract the "oil" phase of emulsions, leading to near solvent-free microparticles. SEE offers the advantage of being a one-step process and is superior to other conventional techniques for the better particle size control, higher product purity and shorter processing times; but, as traditional processes, it shows problems related to batch-to-batch reproducibility and reduction of the process yield, due to the intrinsically discontinuous operation.

In the present work, a novel SEE configuration is proposed in a continuous operation layout (*Continuous Supercritical Emulsion Extraction, SEE-C*) using a countercurrent packed tower, for the production of controlled-size biopolymer microparticles in a robust and reproducible mode. Particularly, the purpose of this thesis is the optimization and characterization of the SEE-C process to investigate its capabilities and performances in the production of poly-lactic-*co*-glycolic acid (PLGA) microparticles with an engineered size and distribution and charged with different active principles (APs).

Abstract

Before to investigate the possibility to produce AP/PLGA microspheres, an optimization of the process has been performed. Indeed, the thermodynamics of the selected system (ethyl acetate+CO_2) has been studied, together with the analysis of the process operating parameters. Moreover, a fluidodynamic characterization of the packed tower has been carried out to identify the best condition of operation, below the flooding point. The capacity limits for the packing material have been evaluated and, then, directly measured in terms of flooding point at different operating conditions.

Afterwards, firstly blank (drug-free) PLGA microparticles have been successfully produced, starting from single and double emulsions. Secondly, anti-inflammatory drugs (such as Piroxicam and Diclofenac Sodium), corticosteroids (such as Hydrocortisone acetate) and proteins (such as Insulin) have been chosen as model compounds to be entrapped within PLGA microspheres.
All the emulsions produced were stable with non-coalescing droplets. The corresponding microspheres obtained were spherical in shape and well-defined with narrow size distributions, due to the short processing time that prevents aggregation phenomena typically occurring during conventional solvent evaporation process.

The influence of some emulsion formulation parameters (such as polymer concentration and emulsion stirring rate) on particle size has been investigated, showing that the droplet formation step determines size and size distribution of the resulting microspheres; particularly, a significant increase in particle size with the increase of polymer concentration or the decrease of emulsion stirring rate has been observed. Moreover, the effect of kind and formulation of emulsion on the microsphere characteristics has also been investigated, demonstrating that the choice of the encapsulation approach and the emulsion composition have a considerable influence on the attainable drug encapsulation efficiency.

The produced microspheres have been characterized by X-ray, DSC, HPLC and UV-vis analysis. DSC and X-ray analyses confirmed that the microspheres were formed by an AP/PLGA solid solution and the active principle was entrapped in an amorphous state into the polymeric matrix. HPLC analysis revealed that good encapsulation efficiencies have been obtained in the products obtained. Release studies showed uniform drug concentration profiles, confirming a good dispersion of the drug into the polymer particles. The obtained AP/PLGA microspheres can degrade and release the encapsulated active principle slowly with a specific release profile. Active principle loading, particle size and emulsion kind revealed to be the controlling parameters for drug release. A study of PLGA microparticles degradation has also been carried out to monitor any morphological difference in time of the biodegradable devices produced by SEE-C.

Moreover, a comparative study between the characteristics of the PLGA microspheres obtained by SEE-C and the ones produced by the corresponding batch operating mode process (SEE) and conventional evaporation technology (SE) has been performed. PLGA microparticles produced by SEE-C showed a mean particle size always smaller than that associated with particles produced by SEE and SE; physico-chemical properties showed no morphological and structural differences between the processes. Compared with conventional technologies for the preparation of drug delivery systems, e.g. solvent evaporation emulsion techniques, the novel process is environmentally superior and suitable for scaling up to industrial dimensions. Moreover, the higher degree of control, as indicated by the high reproducibility, makes validation of the process very simple.

In conclusion, the SEE-C process has shown to be an attractive way of incorporating active principles into biodegradable microparticles for controlled release formulations. Greater product uniformity, higher throughput with smaller plant volumes and elimination of batch-to-batch repeatability problems are the significant advantages observed.

INTRODUCTION

In recent years, the pharmaceutical industry has focused considerable attention on the development and optimization of formulations that can release an active principle in the body with a desired controlled rate and amount. Biodegradable polymer microspheres are the most promising form for controlled release devices development, especially if produced with a narrow particle size distribution. They can also be used for site specific controlled delivery of small molecular weight drugs and proteins in a large variety of applications such as chemotherapy, cardiovascular disease, hormone therapy, therapeutic protein delivery and vaccine development (Burgess and Hickey, 1994; Cohen et al., 1991; Cao and Schoichet, 1999).

The use of biodegradable polymers as drug carriers has long been of interest in controlled release technology due to the ability of these polymers to be reabsorbed by the body. The field of biodegradable polymers is progressing rapidly, so that researchers now have at their disposal a substantial number of degradable polymers with range of degradation rates (Vert et al., 1993). The most widely used and studied class of biodegradable polymers is the polyesters, including poly-lactic acid (PLA) and poly-lactic-*co*-glycolic acid (PLGA). Microspheres formulated with these polymers have shown wide applicability for oral (Chacón et al., 1996), parenteral (Uchida et al., 1997a; Soriano et al., 1996), respiratory (Emami et al., 2009) and topical (Rolland et al., 1993) administration.

Throughout the past few years, some products based on active principle-loaded biodegradable microspheres have reached the pharmaceutical market place. Well-known examples are Lupron Depot[®] (Abbott Laboratories), Trelstar[®] Depot (Watson Pharmaceuticals), and Risperdal[®] Consta[TM] (Ortho-McNeil-Janssen Pharmaceuticals). These types of injectable depot formulations (intramuscular, IM, or subcutaneous, SC) can provide sustained and controlled delivery of the active substance over a period of weeks. Some of the advantages of these formulations include: decrease in the amount of residual active principle concentrations due to lower dose, targeting of active principles to the affected area in the body, preservation of the efficacy of unstable active principles, reduction of the need for patient follow-up care, and also increase of patient comfort and compliance (Langer, 1998; Bandi et

al., 2004). Therefore, from the perspective of the pharmaceutical companies, microsphere-based depot formulations of existing compounds offer an attractive tool in life cycle management, but most importantly, offer significant value to patients. Although microsphere-based drug delivery is attractive from both market and patient perspective, developers of microsphere formulations have to face many challenges in achieving the desired product performance and process efficiency. Many of these challenges are related to the lack of control over particle size and uniformity of conventional microsphere manufacturing methods. Indeed, conventional methods for producing microspheres, such as solvent evaporation/extraction of emulsions, do not allow for total control of microsphere size and uniformity. Typically, wide particle size distributions with standard deviations of the mean diameter over 50% are achieved. Moreover, conventional processes often show long processing times and toxic solvent residues may remain in the final formulation because the organic solvents used to dissolve polymers are difficult to remove. However, the international regulations for the use of solvents in pharmaceutical industries require controlled use of organic solvents and radical reduction of conventional solvents used in pharmaceutical processes. To obtain narrower size distributions, expensive classification steps with high losses of active compound in the unwanted size ranges are required, as well as further operations are necessary to reduce solvent residue values below safety limits. Given the fact that the current manufacturing processes have difficulties in predictably producing solvent-free microparticles with an engineered size and distribution, a technology that can offer complete control over size distribution and very reduced solvent residues within microspheres is of great industrial value. There are a number of techniques in development designed to overcome issues regarding toxicity, size and uniformity. Among them, a supercritical fluid (SCF) based technique can offer the best and most straightforward opportunity to overcome these challenges. The most common supercritical fluid used is the carbon dioxide (SC-CO$_2$) because it is chemically stable, nonflammable, non toxic, inexpensive, available in high quantity and purity and with critical properties easy to be reached.

SCFs exhibit gas-like (high diffusivity, low viscosity, no surface tension) and liquid-like (high density and high solvent strength) properties. Mild operating conditions and solventless or organic solvent reduced operations are relevant advantages. They also offer several degrees of freedom with respect to process setup and operating conditions, which may be exploited to tune size and shape of product particles (Fusaro et al., 2004; Muhrer et al., 2006). Supercritical fluid technology allows to access domains of miscible as well as of immiscible conditions for the same solvent-SCF system, i.e. by simply changing the operating pressure and temperature. In addition, lower viscosity and higher diffusivity of SCF with respect to the liquid solvent can improve mass transfer, which is often a limiting factor for the extraction

processes. Due to these favorable properties, supercritical fluids are currently proposed in a wide range of extraction applications (Reverchon and De Marco, 2006), microparticle formation (Della Porta and Reverchon, 2008; Della Porta et al., 2006; Reverchon and Adami, 2006; Reverchon and Antonacci, 2007) and membrane drying technologies (Reverchon et al., 2006). For example, in the last 10 years, different supercritical fluid technologies have been proposed in literature to produce microparticles of PLGA and also of drug-PLGA composites, such as the Rapid Expansion of Supercritical Solutions (RESS), the Solution-Enhanced Dispersion by Supercritical Fluids (SEDS) and the Supercritical AntiSolvent (SAS) (Debenedetti, 1993; Della Porta and Reverchon, 2008a).

In RESS technology, SC-CO_2 acts as solvent, solubilizing the compound to be treated and producing microparticles by a rapid decompression of the supercritical solution and the subsequent sovrasaturation of the solubilized biopolymer. SAS technique uses SC-CO_2 as phase-separating anti-solvent to induce the biopolymer precipitation from its liquid solution. In the SEDS technology, the general principle is the same as for the SAS process: the precipitation of the polymer is due to the anti-solvent effect of SC-CO_2. The main problem reported for RESS technology is the very low solubility of almost all PLGA co-polymers in SC-CO_2 that will prevent affordable process yields or will require the use of co-solvent (Kongsombut et al., 2009). On the other hand, the solubility of SC-CO_2 in the PLGA (even if very low) is again the main problem for SAS or SEDS technologies, because it causes strong microparticles agglomeration resulting in products with irregular shapes or recovered with a low yield due to the strong tendency to form a film (Kang et al., 2008; Ginty et al., 2005; Ghaderi et al., 2000). It is worth mentioning that other authors (Young and Johnston, 1999; Pini et al., 2008) also reported a large CO_2 uptake by sorption into PLGA co-polymers, during the supercritical CO_2 antisolvent processing of PLGA, resulting in a significant decrease in PLGA glass transition temperature that will advantage the formation of strong intra-particle adhesion or continuous film structures.

Recently, the use of SC-CO_2 for PLGA microparticles manufacture has also been proposed starting from emulsions. Particularly, SC-CO_2 has been proposed to extract the ''oily'' phase of single *oil-in-water (o-w)* and double *water-in-oil-in-water (w-o-w)* emulsions, leading to near solvent-free microparticles (Chattopadhyay et al., 2006; Della Porta and Reverchon, 2008b; Kluge et al., 2009a). The process, named Supercritical Emulsion Extraction (SEE), produces an aqueous suspension of microparticles after the supercritical extraction of the organic solvent contained in the emulsion. It is described as faster and selective compared to the conventional techniques, and capable of affecting the size distribution of the produced microparticles, since the fast extraction rate results in a narrower particle size distribution because the droplets aggregation is minimized. One of the

major limitations of SEE technology, shared with traditional evaporation/extraction processes, is the intrinsically discontinuous operation. Indeed, emulsions must be treated batch-to-batch, with problems of batch-to-batch variability and reduction of the process yield (Della Porta and Reverchon, 2008b; Kluge et al., 2009).

For this reason, in the present work, Supercritical Emulsion Extraction process is proposed in a Continuous operating mode (SEE-C) (Reverchon and Della Porta, 2007) for the production of biopolymer microspheres with different size and distribution, in a robust and reproducible mode. Particularly, the aim of the PhD research project is to optimize and characterize the SEE-C process to investigate its capabilities and performances in the production of controlled-size active principle/PLGA microspheres for controlled release formulations, starting from single and double emulsion systems. Anti-inflammatory drugs, corticosteroids and proteins have been selected as model active compounds to be entrapped within microspheres.

SEE-C process arrangement is obtained using a high pressure packed column operating in countercurrent flow. Countercurrent extraction is expected to achieve a multistage treatment that should reduce the amount of solvent necessary and increase throughput. This manufacturing technique should provide not only particles having predictable and controllable physical properties such as size distribution, composition and structure, but, it must also conform to the rigorous requirements of product consistency, purity and process scalability.

CHAPTER I
State of the art

In this chapter, the concepts and the parameters involved in the microencapsulation of pharmaceutical agents for controlled release formulations are described. In addition, an in-depth discussion on the emulsions and on the conventional and innovative microencapsulation processes (solvent evaporation/extraction and supercritical extraction emulsions, respectively) for the preparation of microencapsulated drug formulations starting from emulsions is provided.

I.1 Microencapsulation technology in controlled release

formulations

Microencapsulation describes a process of incorporation of micron-sized (very tiny) particles of solids or droplets of liquids or gasses in an inert polymer matrix, which in turn isolates and protects them from the external environment. The inertness is related to the reactivity of the polymer with the entrapped substance. Microencapsulation provides the possibility of combining the properties of different types of material (e.g., inorganic and organic), a process which is difficult to achieve using other techniques.

Microencapsulation technology and its applications have advanced over the last several decades. This technology is used in pharmaceutical, biomedical, agricultural, food, textile, consumer products, cosmetic, veterinary, medicine, industrial chemicals, biotechnology, sensor industries Some applications of microencapsulation are presented in Figure I.1:
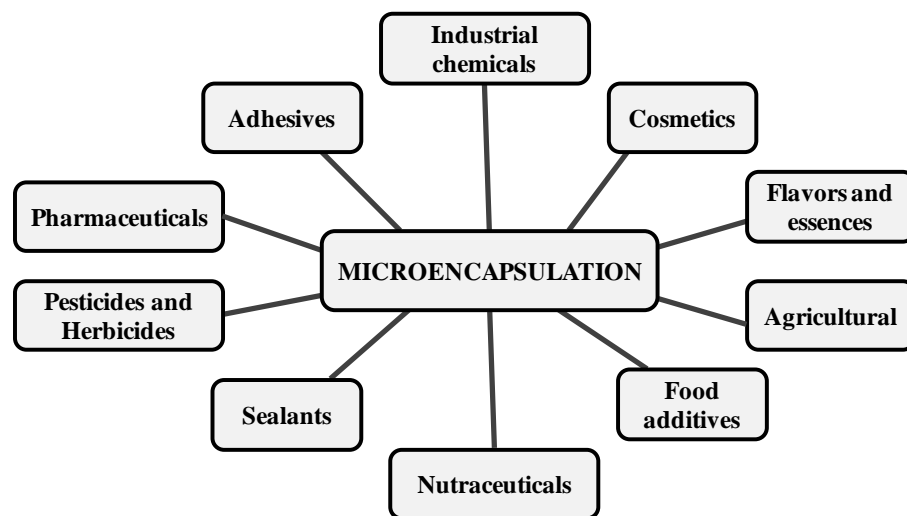
Figure I.1 *Schematic representation of microencapsulation applications.*

The pharmaceutical industry has long used microencapsulation for the preparation of particles containing active principles. The reasons for microencapsulation in the pharmaceutical industries are countless. Microencapsulation is often used to provide a protection for a drug from the reactive surroundings and to prevent drug degradation from light or exposure to oxygen. Furthermore, microencapsulation can be used to improve the formulation characteristics such as taste, stability and wettability. Microencapsulated formulations can also be used to extend the dosage time from a repeated to single administration and to provide controlled release of drugs in a desired part of the body (Tandya et al., 2007).

A large variety of bioactive compounds with different physical and chemical properties have been formulated into polymeric systems, including anti-cancer drugs (Boisdron-Celle et al., 1995), narcotic agents (Mason et al., 1976), local anesthetics (Chung et al., 2001) as well as steroids (Cowsar et al., 1985), therapeutic peptides (Jeyanthi et al., 1997) and proteins (Meinel et al., 2001), DNA (Hsu et al., 1999), viruses (Sturesson et al., 1999) and bacteria-derived compounds (Ren et al., 2002).

Microencapsulation has been widely used in the design of controlled release dosage forms for the past few decades, since it can readily be adapted for various administration methods. Indeed, there have been significant developments in controlled release administration in the last three decades, from primitive delayed-release dosage forms in the 1960s to highly sophisticated self-regulated delivery systems in the 1990s (Park, 1997). These advances have produced many clinically useful controlled release dosage forms and provided better shelf-life for many existing drugs.

Controlled release systems can be described as formulations intended to provide temporal or spatial control of drug release in the body. The term "control" includes phenomena such as protection and masking, reduced of dissolution rate, facilitation of handling and spatial targeting of the active principle to the affected area in the body.

Conventional drug administration may provide an immediate release of drug concentration in the blood followed by a reduction of drug concentration, as shown in Figure I.2(a); whereas, controlled release formulations, illustrated in Figure I.2(b), can circumvent problems related to the conventional formulations by enhancing the durability and effectiveness of the drug in the body, because they provide a constant drug concentration in the body at some optimum level over the duration of therapy. As a consequence, these formulations have outstanding advantages compared to conventional pharmaceutical dosage forms: increased patient compliance and acceptance by reducing the frequency of administration; increased therapeutic benefit by minimizing the drug blood level fluctuations and potentially lowering the total administered amount of drug by reducing peaks and valleys; drug targeting to specific locations resulting in a higher efficiency; protection of labile compounds before and after administration and prior to appearance at the site of action (Berkland et al., 2002; Freiberg et al., 2004; Hickey et al., 2002a; Kim et al., 2002; King et al., 2000; Meinel et al., 2001). Although controlled release formulations are invariably more expensive than conventional formulations, the overall cost of treatment may be lower due to one or more therapeutic advantages, fewer side-effects and less time required of health care personnel to dispense and administer drugs and monitor patients. However, controlled release delivery systems may present some disadvantages, such as the loss of flexibility in adjusting the drug dose and/or dosage regimen and an increased risk of sudden and total drug release due to technological failure of the dosage unit.

(a)

(b)
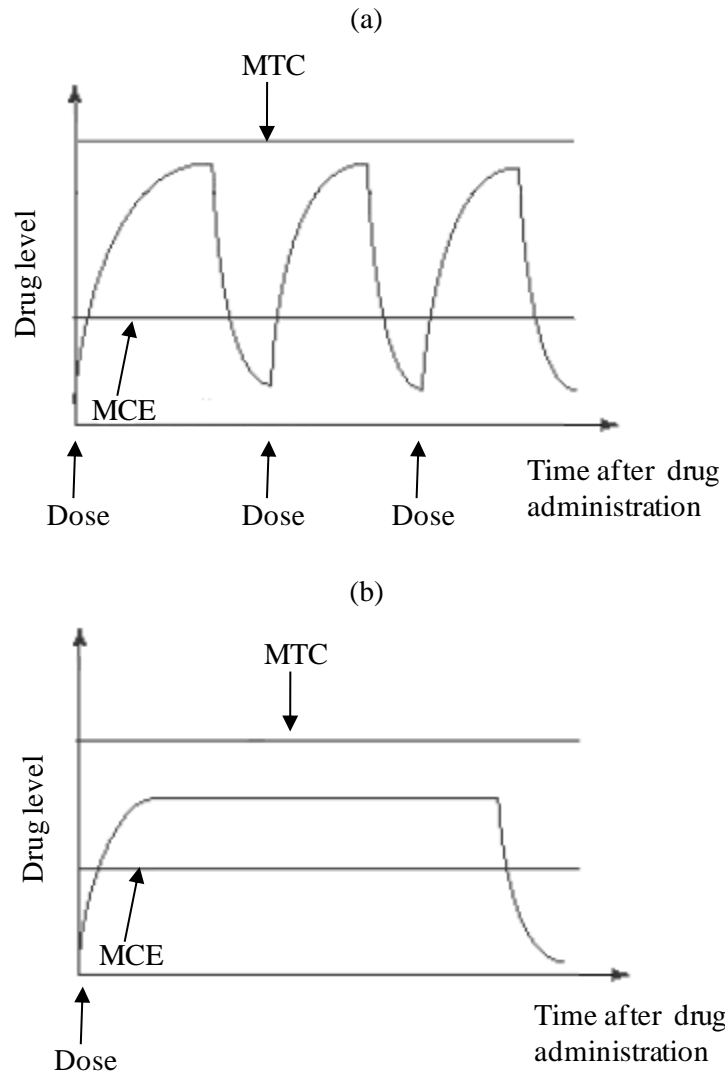
Figure I.2(a-b) *Comparison between (a) traditional dosing and (b) controlled delivery dosing (MEC = minimum effective concentration, MTC = minimum toxic concentration).*

Controlled release formulations are commonly prepared with the use of microparticles of drug-polymer composites, either as microspheres (or matrix system) or microcapsules (or core-and-shell system), both schematically illustrated in Figure I.3(a-b). The former are polymer microparticles in which the active agent is uniformly dispersed; the latter are structured microparticles composed by a core (the intrinsic part) of the active

substance surrounded by a polymer shell (the extrinsic part). Typically, the lowest particle size is 1 μm and the largest size is 1 mm.
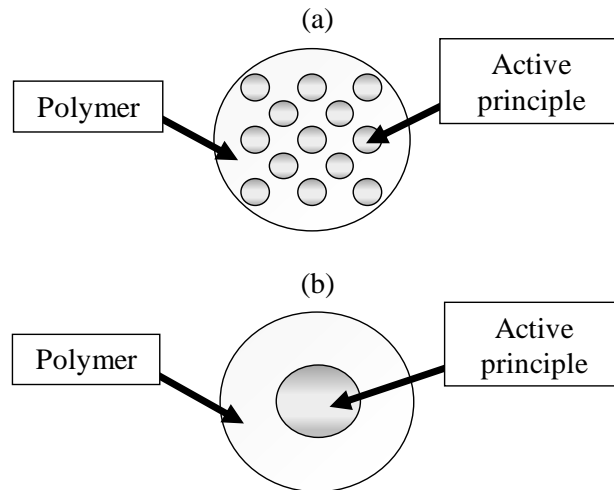
Figure I.3(a-b) *Classification of controlled release systems: (a) microsphere and (b) microcapsule.*

Biopolymer microspheres are the best devices for locally injectable controlled release formulations, providing a number of advantages over conventional parenteral formulations.

Investigations about drug incorporation and release are an important tool in the design and evaluation of a potential drug-carrier system (zur Mühlen et al., 1998). Biodegradable polymers have been successfully employed as drug carriers to design controlled drug delivery systems. In general, when biodegradable and bioerodible polymers are used in controlled release formulations, the polymers are degraded or eroded to non-toxic materials by body fluids over time. Thus, the removal of polymeric material from the body after the drug release is unnecessary.

Controlled drug release from biodegradable matrices is obtained by different mechanisms: polymer swelling, diffusion of drug through the polymer matrix, polymer degradation or a combination of these mechanisms (Washington, 1996). The design of a controlled release system is a complicated process due to the interdependency of several factors: particle size and surface morphology, as well as, drug and polymer physical chemistry are key factors governing release kinetics. Particularly, sphere size and distribution will determine the surface area/volume ratio and, thereby, the amount of surface available for drug release. Monodisperse microspheres may exhibit the most uniform drug release (Berkland et al., 2002, 2003). It was also observed that there is an ideal sphere size which provides a desired release rate; but, since the rate of drug release from microspheres dictates

their therapeutic action, sphere size and therapeutic action are related. Spheres that are ''too small'' exhibit poor sustained release efficiency, they also may migrate from the site of injection producing undesirable drug release; whereas, spheres that are ''too large'' may not easily pass through a syringe needle. Thus, the typically polydisperse samples generated by conventional fabrication techniques must be filtered or sieved to isolate particles within the desired size range. Precise size distributions may also allow the preparation of advanced delivery systems formulation that are not possible using polydisperse microspheres; for example, uniform microspheres approximately of 1-5 µm in diameter would be ideal for passive targeting of specific antigen-presenting cells (APCs) such as macrophages and dendritic cells (Evora et al., 1998). Similarly, microspheres of 10-20 µm in diameter could be used to target the tortuous capillary bed of tumor tissues by chemo-embolization (Dass and Burton, 1999).

I.2 Emulsions

Emulsions are mixtures consisting of at least two completely o partially immiscible liquid phases, one of which (i.e. the dispersed phase, oil phase) is dispersed as droplets of microscopic or ultramicroscopic size in the other liquid phase (i.e., the continuous phase, aqueous phase). Depending upon the nature of the dispersed phase, there are different kinds of emulsions. For example, a solution of hydrophobic active principle and polymer in an organic solvent (oil phase) is emulsified in an aqueous solution containing an emulsifying agent (water phase) to produce single *oil-in-water (o-w) emulsion*. This method can be successfully employed to encapsulate poorly water soluble active principles, but it is not suitable for the encapsulation of high hydrophilic active principles. There are two main reasons: 1) the hydrophilic active principle may not be dissolved in the organic solvent; 2) the active principle will diffuse into the continuous phase during emulsion, leading to a high loss of active principle. Therefore, depending on the solubility of active principle in water and encapsulating polymer, the emulsion kind can be varied from *water-in-oil-in-water* (w-o-w for encapsulation of water-soluble drug in water-insoluble polymer) or *water-in-oil-in-oil* (w-o-o for encapsulation of water-soluble drug in water-insoluble polymer) to *water-in-oil* (w-o for encapsulation of water-soluble drug in water-soluble polymer). Some examples of different kinds of emulsions are reported in a schematic representation in Figure I.4:

oil-in-water   water-in-oil   water-in-oil-in-water
(o-w)   (w-o)   (w-o-w)
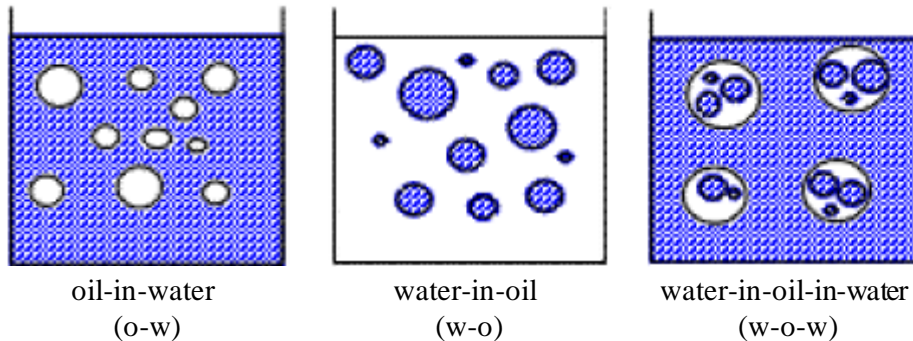
Figure I.4 *Schematic representation of oil-in-water (o-w), water-in-oil (w-o) and water-in-oil-in-water (w-o-w) emulsions.*

From a thermodynamic point of view, the emulsions are metastable systems which means they are prepared using an excess energy (mechanical in most cases, such as shaking, stirring, homogenizing or spraying). To achieve a thermodynamic equilibrium between the solvent in the emulsion droplets and the aqueous phase, the addition of an emulsifying agent, such as a surfactant, to the dispersed phase is required.

Surfactants are amphiphilic molecules which consist of a hydrophilic "head" group and a hydrophobic "tail" (Figure I.5). This means one part of the molecule has more affinity to polar solutes, such as water (hydrophilic), and the other part has more affinity to non-polar solutes, such as hydrocarbons (hydrophobic). Therefore, a surfactant molecule contains both a water insoluble (or oil soluble) component and a water soluble component. Due to their amphiphilic nature, surfactant molecules have a high affinity towards surfaces and interfaces, thereby the term "surfactant" which is an abbreviation for "surface active agent".

hydrophilic head   hydrophobic tail
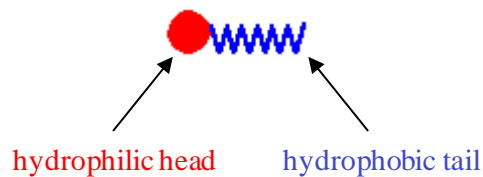
Figure I.5 *Schematization of surfactants.*

Surfactant molecules will diffuse in water and adsorb at the interface between oil and water. As shown in Figure I.6, the insoluble hydrophobic group may extend out of the bulk water phase, into the oil phase, while the water soluble head group remains in the water phase. This alignment of surfactant molecules at the surface modifies the surface properties of water

at the water/oil interface. Particularly, surfactants reduce the interfacial tension of the continuous phase and stabilize the droplets forming a film at the droplets surface that acts as protective layer and prevents droplets from coalescence and agglomeration.
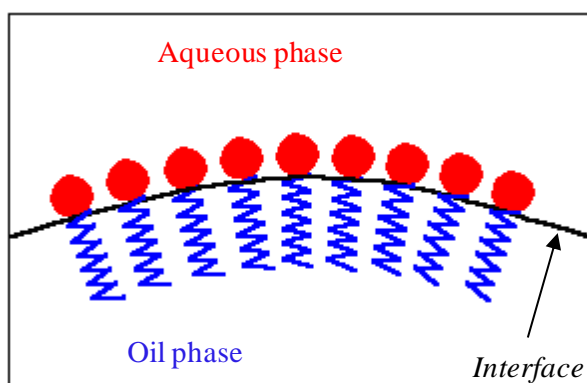
Figure I.6 *Schematization of the adsorption of surfactant at the interface between an aqueous phase and an oil phase.*

In aqueous solutions, the surfactants associate into aggregates called micelles, if the concentration is above the critical micelle concentration (CMC). If the concentration is increased even further or a polar additive is added, the surfactants self-assemble into liquid crystalline mesophases.

I.2.1 The theory of emulsification

Many theories have been proposed to account for the way by which the emulsion is stabilized by the emulsifier. At the present time no theory has been postulated that seems to apply universally to all emulsions. Probably, different factors play a role and the relative importance of each varies not only in different emulsions but in the same emulsion under different circumstances. The *"Adsorbed film and interfacial tension theory"* proposed by Bancroft (1913) is probably the most universally accepted for the formation of emulsions. It has been developed or rather extended from earlier theories. Particularly, Bancroft stated the underlying principles, basing them upon Donnan's early work of interfacial tension; but many others have extended the interpretations.

The emulsifier may be adsorbed by the water or by the oil, but it is usually adsorbed more in one liquid than in the other and thus lowers the interfacial tension of one liquid to a greater extent than that of the other. If the tension of the water is lowered more than that of the oil, the water has less tendency to form drops, flows to form a film more readily and becomes the continuous phase. Thus the kind of emulsion formed depends upon the nature of the

emulsifying agent: if the emulsifying agent is more soluble in water than in oil, the water becomes the continuous phase; if the emulsifying agent is more soluble in oil than in the water, the oil phase becomes the continuous phase (Figure I.7). When the tension on each side of the film or the emulsifying agent is the same, no emulsion is formed. This may occur when opposing emulsifying agents are in the mixture and the effect of each counterbalances that of the other.

w-o emulsion   *o-w emulsion*
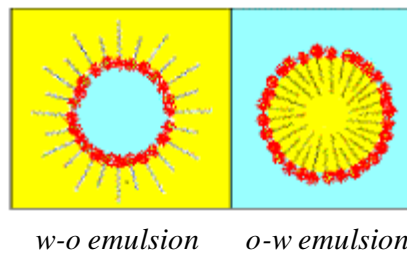
Figure I.7 *Films of surfactants at the water/oil interface of w-o and o-w emulsions.*

1.2.2 Physical instability of emulsions

Over the time (depending on the preparation method, the surfactant and the oil properties), emulsions eventually tend to revert to the stable state of the phases comprising the emulsion: a water plus surfactant phase and an organic phase; an example of this is observed in the separation of the oil and vinegar components of vinaigrette, an unstable emulsion that will quickly separate unless shaken continuously. There are different main types of physical instability in emulsions: creaming or sedimentation, flocculation, coalescence, phase inversion and Ostwald ripening (disproportionation). The physics of these instability processes is rather complex. They may occur simultaneously rather than consecutively. A schematic representation of these physical instability phenomena is given in Figure I.8:
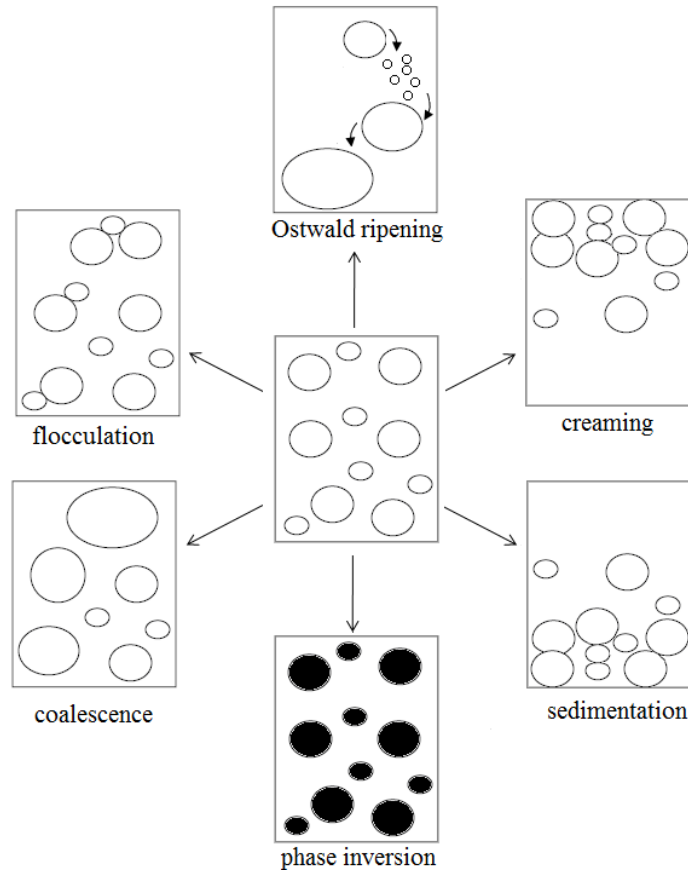
Figure I.8 *Schematic representation of the break-down processes in emulsions.*

Emulsions can undergo creaming or sedimentation under gravitational forces. Creaming refers to the migration of dispersed droplets to the top of the emulsion, under the influence of buoyancy, or under centripetal force when a centrifuge is used; whereas, sedimentation refers to the migration of dispersed droplets to the bottom of the emulsion. Sedimentation or creaming occurs depending on the relative densities of the solvent and the droplets. Creaming happens when the droplets density is lower than the solvent density (oil-in-water system) and sedimentation happens in the opposite case (water-in-oil system). In most cases, creaming rather than sedimentation occurs, since most oils have densities lower than the continuous aqueous phase. Creaming or sedimentation can be prevented by homogenization to reduce the dimensions of the droplets. Also by reducing the difference in density or by increasing the viscosity of the dispersed phase, creaming or sedimentation may be prevented.

Flocculation describes clustering of individual dispersed droplets together, whereby the individual droplets do not lose their identity. This phenomenon may occur when the van der Waals attractive energy between the droplets exceeds the repulsive energy. Flocculation is thus the initial step leading to further aging of the emulsion: droplet coalescence and ultimate separation of the phases. In the coalescence, droplets bump into each other and combine to form progressively larger droplets, losing their original identity. Coalescence is induced by thinning and disruption of the liquid film between the droplets. The final result is the breaking of the emulsion and the phase separation, that is an irreversible process. To come back to the original stage (emulsion), energy has to be furnished to the system. The characteristic time of coalescence can vary tremendously, depending upon the systems. In given cases, this time can be extremely long and no coalescence happens for years, making this kind of emulsions kinetically "stable". The mechanical strength of the interfacial film is important to prevent coalescence.

Phase inversion of an emulsion happens when the continuous phase becomes the dispersed phase and vice versa, i.e. the dispersed medium forms the droplets and the dispersed droplets form the continuous phase (e.g. an o-w emulsion reverting to a w-o emulsion and vice versa). An emulsion may be inverted by adding an electrolyte that can react with the emulsifying agent changing its characteristics; for example, an o-w emulsion formed by sodium stearate as emulsifier can be inverted to w-o emulsion by addition of $CaCl_2$.

Ostwald ripening (disproportionation) is a physical phenomenon in which the large particles grow at the expense of smaller ones which eventually disappear. It is caused by the difference in solubility between the small and large droplets. Indeed, it may occur when the small droplets, which have higher solubility than the larger ones, tend to dissolve on storage and become deposited on the larger ones.

Accelerated storage testing is needed for prediction of the long-term physical stability of the formulations as well as the change of consistency with time. Several procedures have been applied to predict such stability: (a) subjecting the formulation to temperature changes as well as temperature cycling; (b) application of high centrifugal forces to detect separation of the emulsion; (c) subjecting the emulsion to vibration and investigation of the resulting system by microscopy (Tadros, 2004).

I.3 Microencapsulation techniques from emulsions

A successful microencapsulation of drug should include the following requirements:

✓ the stability and biological activity of the encapsulated drug should be maintained during the encapsulation process or in the final microsphere product;

- ✓ the yield of the microspheres having a good entrapment efficiency, a desired particle size and an effectively sustained release property should be high;
- ✓ the microsphere quality and the drug release profile should be reproducible within specified limits;
- ✓ the microspheres should not exhibit aggregation or coalescence.

Moreover, technologies capable of producing larger amounts of microspheres in a safe, economic, robust and well-controlled manner are required.

Different methods of microencapsulation have been developed over the years for the production of biopolymer microspheres starting from emulsions. The selection of a particular technique depends on the nature of the polymer and the drug to be incorporated, the intended use and the duration of the therapy.

The following discussion is focused on the most investigated conventional technique of microencapsulation, and also provides a comprehensive description of a recently developed process based on the use of supercritical carbon dioxide.

I.3.1 Conventional techniques of microencapsulation

One of the earliest and most popular conventional methods used to produce biopolymer microspheres is the solvent evaporation/extraction of single or double emulsions. The technique of microencapsulation by solvent evaporation/extraction of emulsions is widely applied in pharmaceutical industries to obtain the controlled release of drug.

Single emulsion solvent evaporation/extraction method. This method has been primarily used to encapsulate insoluble or poorly water-soluble active substances through oil-in-water (*o-w*) emulsification process. The polymer is first dissolved in a water immiscible, volatile organic solvent (the oil phase). The drug is either dissolved or dispersed in this solution. The resultant mixture is then emulsified with large quantities of an aqueous continuous phase, containing a suitable emulsifier, to form discrete droplets. The emulsion formed is stirred until most of the organic solvent is removed by either evaporation or extraction process, resulting in phase separation of the polymer and the drug to produce solid microparticles, suspended in an aqueous phase (Arshady, 1991). In the former case, the emulsion is maintained at reduced or atmospheric pressure, with a low stirring rate to enable the volatile solvent to evaporate. In the latter case, a further continuous phase and/or additional extraction agents are added to the emulsion at an amount sufficient to absorb the entire solvent leaching from the solidifying microspheres (Freitas et al., 2005). The solid microspheres obtained from evaporation/extraction method are, then, washed and collected

by centrifugation and filtration or sieving. They are dried under appropriate conditions or lyophilized. A schematic diagram of this technique is shown in Figure I.9:
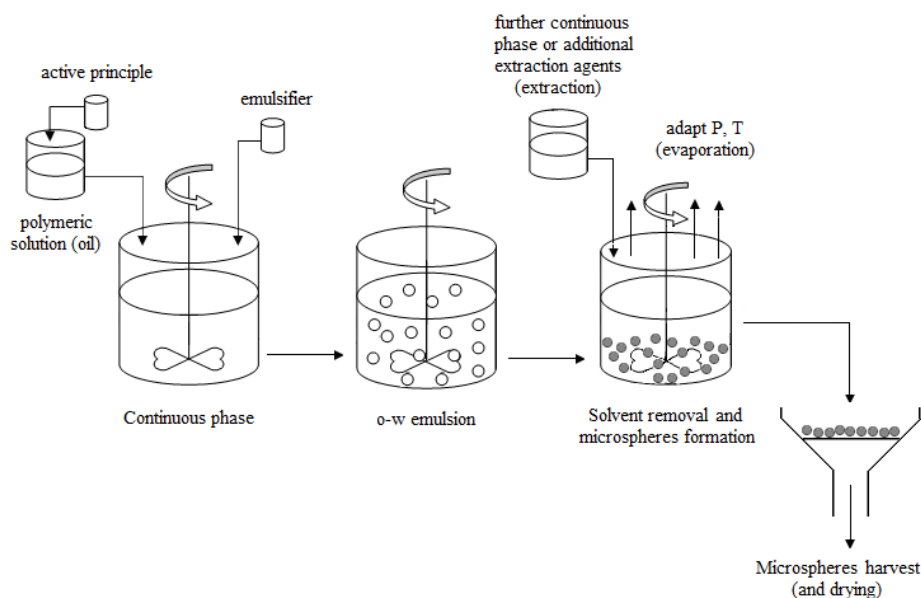
Figure I.9 *Schematic diagram showing the preparation of microparticles by o-w single emulsion solvent evaporation/extraction method.*

Double emulsion solvent evaporation/extraction method. Sensitive water-soluble drugs such as proteins, peptides and vaccines can be incorporated into microspheres using the double emulsion solvent evaporation/extraction (Herrmann and Bodmeier, 1995; Cohen et al., 1991). Briefly, the water soluble drug is initially dissolved in a small aqueous aliquot (sometimes containing a viscosity enhancer and/or stabilizer), which is then emulsified with the organic polymer solution to form a *w-o emulsion*. In a second emulsification, this emulsion is gently added into an aqueous solution containing an emulsifier and a double *w-o-w emulsion* is the result. The organic solvent is then removed by either evaporation or extraction process to leave an aqueous suspension of microspheres containing the drug. The solid microspheres obtained are washed and collected by centrifugation and filtration or sieving. These are then dried under appropriate conditions or lyophilized to give the final free flowing microsphere product. A schematic diagram of this technique is reported in Figure I.10:
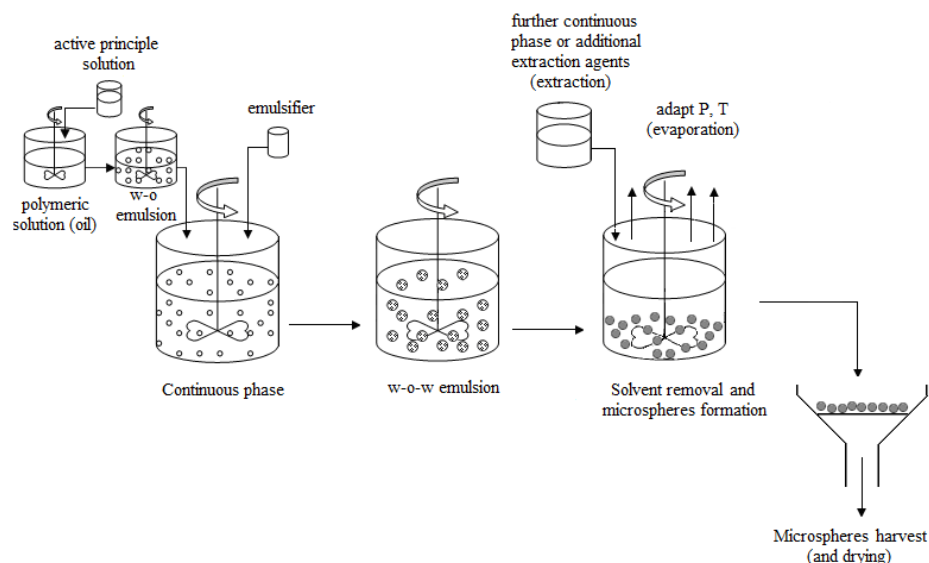
Figure I.10 *Schematic diagram showing the preparation of microparticles by the w-o-w double emulsion-solvent evaporation method.*

In solvent evaporation/extraction techniques, the solvent of the dispersed phase must be slightly soluble in the continuous phase, so that partitioning into the continuous phase can occur leading to precipitation of the polymer. In solvent evaporation, the capacity of the continuous phase is not sufficient to dissolve the entire volume of the dispersed phase solvent; therefore, the solvent has to evaporate from the surface of the dispersion (air-liquid interface) to yield sufficiently hardened microspheres. In solvent extraction, the amount and composition of the continuous phase are chosen so that the entire volume of the dispersed phase solvent can be dissolved.

The rate of solvent removal by evaporation method strongly depends on the temperature, pressure and the solubility parameters of polymer, solvent and dispersion medium. Very rapid solvent evaporation may cause local explosion inside the droplets and lead to the formation of porous structures on the microsphere surface. The rate of solvent removal by extraction method depends on the temperature of the additional continuous phase or extraction agents, the ratio of emulsion volume to continuous phase/medium volume and the solubility characteristics of polymer, solvent and dispersion medium. The solvent removal by extraction method is faster than the evaporation process and, hence, the microspheres obtained by the solvent extraction method are more porous in comparison to those produced from the solvent evaporation method under similar conditions (Arshady, 1991).

The solvent evaporation/extraction is widely used because it is easy to be implemented into a simple reactor/stirrer setup. However, solvent evaporation/extraction technology has several drawbacks. Solvent

evaporation requires relatively high temperatures because they facilitate the solvent evaporation from the continuous phase and thereby maintain a high concentration gradient for the solvent between the microspheres and the continuous phase. As an alternative to elevated temperature, reduced pressure is sometimes used to promote the evaporation of the solvent (Freitas et al., 2005); nevertheless, solvent evaporation, in several cases, can be inappropriate for producing large amounts of microspheres in a robust and well-controlled manner. Solvent extraction uses relatively large amounts of a second solvent and, consequently, involves expensive downstream processes to recover the solvents used.

Common drawbacks are the low encapsulation efficiency and the extremely slow rate that requires quite long processing times (several hours) and, as a consequence, aggregation phenomena occur between the droplets producing microspheres with a larger polidispersity than the starting emulsion (Yang et al., 2000). Both processes are also intrinsically discontinuous and, therefore, problems of batch-to-batch reproducibility (Li et al., 2008) are expected, as well as difficulties for process scale up to industrial scale. High batches reproducibility is particularly relevant for biomedical and pharmaceutical applications because the approval of a manufacturing process by Food and Drug Administration (FDA) requires the demonstration that all batches give a product with identical characteristics.

I.3.2 Supercritical Emulsion Extraction (SEE)

The limitations of the conventional techniques has been the focus of studies towards the potential replacement of traditional organic solvents with more environmentally friendly materials, such as supercritical fluids (SCFs).

The supercritical fluid is a substance above its critical temperature and critical pressure. Beyond the critical point, the liquid and gas phases become indistinguishable. SCFs are highly compressed gasses that possess several advantageous properties of both liquids and gases. The density of a SCF is generally closer to that of conventional liquids and several orders of magnitude higher than that of conventional gases, and accounts for the solvating capabilities of the SCFs. It is well known that near to the critical point, small changes in pressure or temperature can greatly modify the density and, hence, the solvating ability of the supercritical fluid. Thus the physicochemical properties of SFCs can be varied significantly without changing the molecular structure of the substance. This ability to change the properties of the supercritical fluid by changing the temperature and pressure in the vicinity of the critical point provides the equivalent of a series of different solvents, thus giving selective extraction properties. Like gases, SCFs possess high diffusivities (two orders of magnitude larger than those of liquids), improving the mass transfer which is often a limiting factor of conventional technologies.

15

Among all the possible SCFs, carbon dioxide (CO_2) is the most widely used for its readily accessible critical points on the industrial scale (T_c = 31.1°C; P_c = 73.8 bar), in addition to its nontoxic and nonflammable properties; it is also readily available, highly pure and cost-effective. Critical temperature is very near to the room temperature allowing the treatment of thermolabile compounds. The Pressure-Temperature diagram of pure CO_2 is reported in Figure I.11:
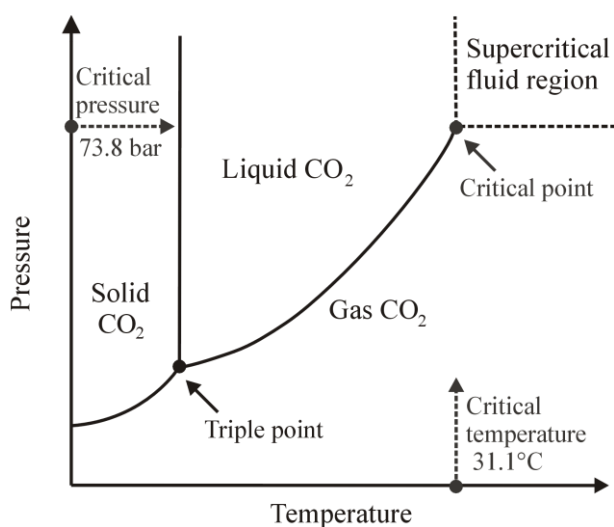
Figure I.11 *Pressure-Temperature diagram of pure CO_2.*

Due to the favorable properties, SCFs are currently proposed in a wide range of different processes for the production of biopolymer microparticles, since several processes can operate in the micronic domain depending on the operating conditions and on the process arrangement (Della Porta et al., 2005, 2006; Yeo and Kiran, 2005; Tandya et al., 2007).
As a major advantage, supercritical fluids processes lead to pure and solvent-free products while working at mild operating conditions. For this reasons, supercritical fluid-processed products can be extended to pharmaceutical applications. The application to pharmaceutical compounds has been developed far, mainly with the view of exploring processes that could give new characteristics to the compound itself either in the formulation or the delivery systems. The increasing interest in advanced controlled release formulations and the combination of their characteristics provide the increasing potential of supercritical fluids technology in the pharmaceutical industry. The preparation of controlled release formulations using supercritical fluid-assisted techniques offers several unique features such as the ability to perform the process in a single stage without any exposure of the products to the external environment, the ease solvent removal, the use

of high-grade stainless steel equipment and the inherent sterilizing effects, low handling and disposal expenses (York, 1999). Furthermore, the supercritical fluid technology may facilitate the development of significant improvements in the efficiency of both currently marketed drugs and new therapeutic entities.

Recently, Supercritical Emulsion Extraction (SEE) has been proposed in literature for the production of particles with controlled size and distribution, starting from *oil-in-water (o-w)* and *water-in-oil-in-water (w-o-w)* emulsions. In this process, SC-CO_2 has been proposed for the selective extraction of the oily phase of emulsions, obtaining the polymer hardening and microspheres formation.

The use of supercritical fluids as extraction media is a promising alternative for the formation of microparticles of active principles and pharmaceutical excipients. There are two main reasons for using this technique. Firstly, the selective solvating power of supercritical fluids makes it possible to extract the organic solvent from emulsions and produce microspheres. Secondly, the favorable mass transfer properties and high solubility of solvents in the supercritical fluid make the solvent removal rapid and efficient with low level of residual solvent as requested by the authorities. In a recent study, it was shown that SC-CO_2 can be used for inactivation of a wide variety of bacterial organisms. This means that the final product (microparticles) obtained by supercritical carbon dioxide is sterilized (Dillow et al., 1999).

The process layout of SEE has been first proposed by Chattopadhyay et al. (2004, 2006, 2007), obtaining particles of nanometric and micrometric size with narrow particle size distribution. Particularly, they used SC-CO_2 to eliminate the organic solvent from *o-w emulsions* for the preparation of drug microparticles of megestrol acetate, griseofulvin and cholesterol acetate, or for the formation of biopolymer particles charged with ketoprofen and indometacin. It has been reported that the mean diameter of the particles ranged between 0.1 and 2 μm and the residual solvent was less than 50 ppm. A schematic representation of the apparatus used by Chattopadhyay et al. for the precipitation of particles is shown in Figure I.12. The extraction of the solvent from emulsions was carried out in an electrically heated stainless-steel extraction column. The SCF fluid delivery system consisted of a liquid CO_2 pump which provided SC-CO_2 to the bottom of the extraction column through a frit. The emulsion was delivered from the top countercurrently, using an HPLC pump, and was injected through a capillary nozzle, which broke the emulsion into droplets, thereby increasing its surface area of contact with SC-CO_2. After the contact with SC-CO_2, an aqueous particles suspension was formed at the bottom of the column and removed through a needle valve. The effluent SC-CO_2 was vented from the top of the column. The pressure inside the column was maintained constant using a backpressure regulator valve.
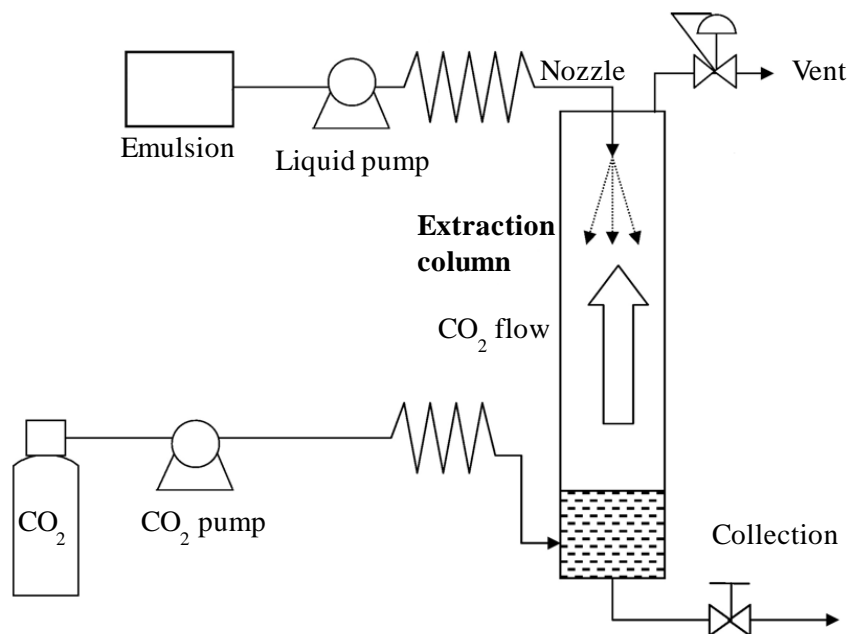
Figure I.12 *Schematic representation of the SEE experimental system proposed by Chattopadhyay et al.*

A different process layout for the extraction of the emulsion organic phase using SC-CO_2 was also proposed by Della Porta and Reverchon (Della Porta and Reverchon, 2008b; Della Porta et al., 2010). They gave some indications on the mechanism of solvent extraction by SC-CO_2 of *o-w* and *w-o-w emulsions* for the production of polymer (PLGA) microspheres loaded with different anti-inflammatory drugs (Piroxicam and Diclofenac Sodium), controlling their size, distribution and drug loading by varying both emulsion and SC-CO_2 process conditions. PLGA microspheres with mean sizes ranging between 1 to 3 μm and solvent residue smaller than 40 ppm were successfully obtained at optimized operating conditions.

A schematic representation of the apparatus proposed by Della Porta and Reverchon for the precipitation of particles in the supercritical fluid extraction, in batch mode, is reported in Figure I.13. The emulsion was placed into a cylindrical stainless steel vessel. SC-CO_2, delivered using a high pressure diaphragm pump, was bubbled into the extraction vessel, through a cylindrical stainless steel porous dispenser located at the bottom of the extractor. The dispenser maximizes the contact between the two phases during the extraction. Temperature was controlled using an air-heated thermostated oven. The pressure inside the reactor was controlled by a micrometric valve located downstream the extractor. A separator located downstream the extractor was used to recover the liquid solvent extracted

and the pressure in the separator was regulated by a backpressure valve. At the exit of the separator, a rotameter and a dry test meter were used to measure the CO_2 flow rate and the total quantity of CO_2 delivered, respectively. When the extraction process was complete, the microspheres suspension produced was removed from the bottom of the extractor vessel for analysis and further processing.
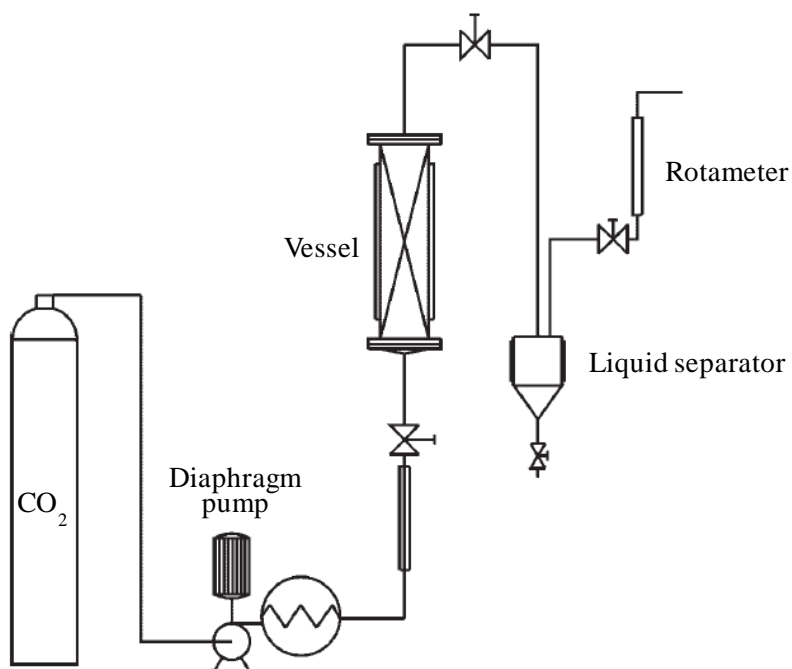
Figure I.13 *Schematic representation of the SEE apparatus proposed by Della Porta and Reverchon.*

Mazzotti and co-workers (Kluge et al., 2009a, 2009b) also proposed the use of SC-CO_2 for the production of particles of pure PLGA and PLGA loaded with lysozyme or ketoprofen through supercritical fluid extraction of emulsions. Particles with average sizes ranging between 0.1 μm and a few μm with very narrow size distributions were produced. A schematic representation of the experimental setup used by Mazzotti and co-workers for supercritical fluid extraction of emulsions is shown in Figure I.14. CO_2 was drawn from a dip tube cylinder and pre-cooled in a pressure module before being delivered to the reactor by a piston pump. The stream then passed a backpressure regulator above the desired reactor pressure, to reduce stream fluctuations generated by the piston pump. The emulsion was delivered to the reactor by an HPLC pump. Both streams were mixed at the inlet of the reactor in a two substance nozzle. The reactor was kept at the

operating temperature by a thermostat. The particles were formed by solvent extraction from the organic emulsion droplets and remained suspended in the continuous water phase throughout the whole process. The product suspension accumulated at the bottom of the reactor was withdrawn through an outlet at the bottom of the reactor. The off-gas stream left the reactor through an outlet at the top. The pressure inside the reactor was controlled by a backpressure regulator located downstream, through which the off-gas stream was expanded to atmospheric pressure and was vented.
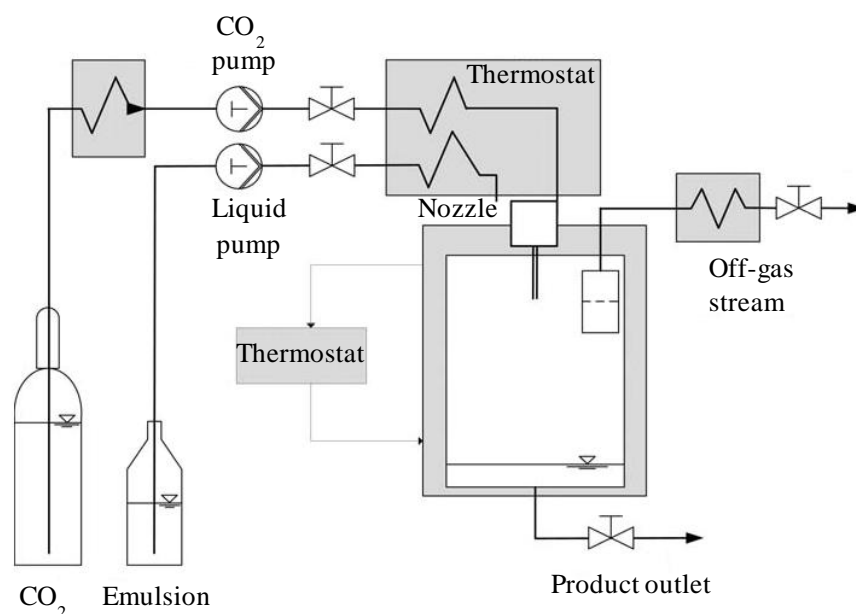
Figure I.14 *Schematic representation of the SEE setup proposed by Mazzotti and co-workers for solvent extraction experiments.*

It has been shown that the average size of particles is clearly related to the average size of droplets in the original emulsion. The size of the emulsion droplets mainly depends on the mixing rate or the degree of homogenization and the concentration of surfactant or polymer. Generally, a high degree of homogenization, higher concentrations of surfactant and lower concentrations of polymer tend to produce smaller droplets (Chattopadhyay et al., 2004; Della Porta and Reverchon, 2008b; Kluge et a., 2009a). Therefore, precipitation of particles with different sizes can be accomplished by varying the emulsion formulations and by optimization of the solvent-surfactant system.

Moreover, SC-CO_2 is known to produce porous structures with plasticized amorphous polymers such as PLGA. This phenomenon is related to the expansion of CO_2 bubbles within the polymer during decompression. The

20

number and the sizes of these pores are dependent upon the rate of decompression, the operating conditions such as pressure and temperature, and the size of polymer particles (Chattopadhyay et al., 2006).

The SCF-based emulsion extraction is beneficial compared to the traditional emulsion evaporation/extraction. Indeed, SEE process combines the advantages of traditional emulsion based technology, namely control of particle size and surface properties, with the advantages of supercritical fluid extraction process, such as higher product purity and shorter processing times. Due to the enhanced mass transfer of SC-CO_2, this process has a relatively faster extraction rate compared to other conventional techniques (processing in minutes instead of several hours) and, thus, adds to the formation of relatively smaller particles with narrow size distributions (Della Porta et al., 2010). In the SEE process, PLGA microparticles aggregation phenomena are not observed, due to the presence of the external water phase, immiscible with SC-CO_2, which prevents their aggregation (Kluge et al., 2009a). High product purity and low content of residual solvents may be achieved at the same time, at moderate operating temperatures and with reasonable CO_2 consumption.

One of the major limitation of the SEE process is that the process remains intrinsically discontinuous, sharing this inconvenient with traditional solvent evaporation/extraction processes. Indeed, a batch of emulsion can be treated for each run with problems of repeatability of the batches and reduction of the process yield, due to the material lost (Della Porta and Reverchon, 2008b).

I.4 Factors influencing the properties of microspheres

The formation of microspheres is affected by a number of factors. The main variables influencing the microencapsulation process and the final microsphere product are summarized in Figure I.15 (Li et al., 2008). Particularly, the characteristics of microspheres containing drug should be correlated with the required therapeutic action and are strongly dependent on the nature of materials and also on the parameters during the manufacturing of microspheres (André-Abrant et al., 2001; O'Donnell and McGinity, 1997).
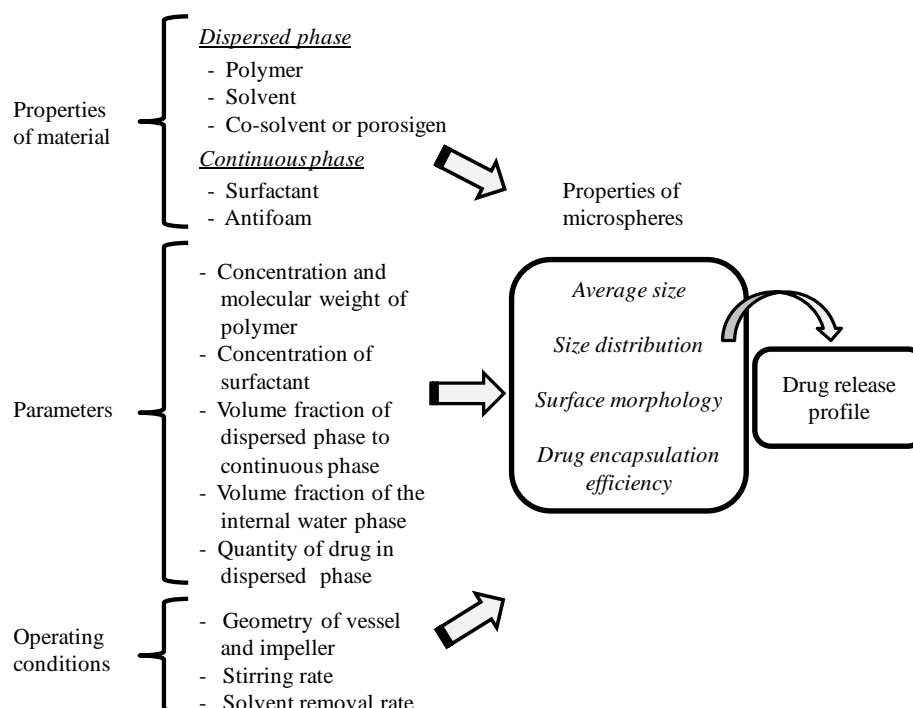
Figure I.15 *Scheme of the factors influencing the properties of microspheres.*

The most important physico-chemical characteristics that may be controlled in microsphere manufacture are:

- ✓ nature and solubility of the drug being encapsulated;
- ✓ polymer concentration, composition and molecular weight;
- ✓ drug/polymer ratio;
- ✓ organic solvents used;
- ✓ concentration and nature of the emulsifier used;
- ✓ stirring/agitation rate of the emulsification process;
- ✓ viscosities and volume ratio of the dispersed and continuous phases (Lewis, 1990).

Each of these can be related to the manufacture and the rate of drug release from the system.

I.4.1 Choice of materials

I.4.1.1 Dispersed phase

Polymer. The biodegradability or biocompatibility is an essential property for the polymer used for pharmaceutical applications.

'Biodegradability' means that the components are degraded into harmless by-products which are either metabolized or excreted, avoiding the removal of empty remnants upon drug exhaust. 'Biocompatibility' means that the component should be physiologically tolerable and should not cause an adverse local or systemic response after administration.

Polymers and copolymers of lactic and glycolic acids are the most commonly used to develop drug delivery systems due to their safe and FDA (Food and Drug Administration) approved applications in humans (Chulia e al., 1994; Langer, 2000). They can ultimately degrade by hydrolysis of their constituents, which are usual metabolic products. Other biodegradable polymers, such as bacterial storage polyesters, have been studied for pharmaceutical and medical applications (Amass et al., 1998). Poly-3-hydroxybutyrate and its copolymers with hydroxyvalerate are members of this biopolymer group. They are produced biosynthetically by bacteria from natural raw materials and indeed can be readily broken down by microorganisms under different conditions.

The choice of polymer used as drug carrier depends also on the desired drug release rate, which is essentially determined by the polymer's physical properties. If one polymer cannot offer a satisfying drug release, a single polymer, called co-polymer, can be synthesized from two different polymers. The properties of the co-polymer are improved since it has two segments on the chain. For example, a co-polymer (PEG/PLA) was synthesized from polyethylene glycol (PEG) and polylactic acid homopolymers (PLA) to increase the degradation rate (Huang et al., 1997). Hydrophilic PEG segments in the PLA copolymers enhance the diffusion of water or drug in the polymer carriers (Zhu et al., 1990). As a result, drug release is faster with PEG/PLA than with PLA.

Solvent. A suitable solvent should meet the following criteria to be used in microencapsulation:

- ✓ being able to dissolve the chosen polymer;
- ✓ being poorly soluble in the continuous phase;
- ✓ having a high volatility and a low boiling point;
- ✓ having low toxicity.

Although moderate conditions are used, potentially toxic solvents are indispensable to dissolve lipophilic polymers (Bitz and Doelker, 1996).

Chloroform was frequently used before, but due to its toxicity and low vapor pressure, it was gradually replaced by methylene chloride.

Methylene chloride is the most common solvent for the encapsulation using solvent evaporation technique because of its high volatility, low boiling point and high immiscibility with water. Its high saturated vapor pressure compared to other solvents promises a high solvent evaporation rate, which shortens the duration of fabrication of microspheres.

23

Furthermore, the use of methylene chloride may also impose a problem in obtaining product approval by regulatory agencies because this solvent is confirmed carcinogenic according to EPA (Environmental Protection Agency) data and may be retained in the microsphere as a residual organic volatile impurity (O'Donnell and McGinity, 1997). As evidenced by Lupron Depot®, a small amount of methylene chloride remaining in a microsphere product is acceptable by the FDA, but only if the product's therapeutic benefits clearly outweigh a safety concern over the residual solvent. However, its use is not recommended for manufacturing process.

In recognition of this issue, the researchers are making great efforts to find less toxic replacements. Among them, ethyl acetate is considered one of the most preferable solvents because it shows promising potential as a less toxic substitute of methylene chloride. But due to the partial miscibility of ethyl acetate in water (4.5 times higher than that of methylene chloride), microspheres cannot form if the dispersed phase is introduced directly into the continuous phase. The sudden extraction of a big quantity of ethyl acetate from the dispersed phase makes the polymer precipitate into fibre-like agglomerates (Freytag et al., 2000). To resolve this problem created by the miscibility of solvent with water, the aqueous solution can be pre-saturated with solvent (Bahl and Sah, 2000). However, according to Herrmann and Bodmeier (1995), the drug encapsulation efficiency reduces significantly compared to the microspheres made by methylene chloride. This behavior can be due to the higher solubility of ethyl acetate in water (83 g/100 mL at room temperature), leading to the loss of drug, with respect to the more largely used methylene chloride that has a considerable lower solubility in water (1.32 g/100 mL at room temperature). Based on this assumption, Li et al. (2008) proposed a further explanation that is due to two main causes: (1) more drug is entrained into the continuous phase by the higher mass flux of solvent, which is driven by the diffusion from the dispersed phase into the continuous phase; (2) the large amount of solvent present in the continuous phase increases the solubility of drug in the continuous phase, facilitating its diffusion into the continuous phase. In addition, the reduced encapsulation efficiency is also affected by the increased porous nature of the microspheres produced using ethyl acetate instead of methylene chloride as organic solvent (O'Donnell and McGinity, 1997).

Ethyl formate shows also interesting results. Sah (2000) observed that the solvent removal rate of ethyl formate in water was 2.1 times faster than that of methylene chloride although ethyl formate possesses a lower vapor pressure and a higher boiling point. This phenomenon is explained by the fact that more molecules of ethyl formate are exposed to the air-liquid interface because of its higher water solubility. His work proved that water immiscibility of a solvent is not an absolute prerequisite for making an emulsion.

Moreover, Matsumoto et al. (2008) tried to establish a new preparation method of microencapsulation using acetone as the solvent for the dispersed phase. Acetone presents a low toxic potential to humans. It is a water-miscible solvent with a higher boiling point than methylene chloride, which allows its easy removal from formulations by washing.

Alternatives components. In given cases, other constituents are added to the dispersed phase such as co-solvent and porosity generator.

Co-solvent is used to dissolve the drug that is not totally soluble in the solvent of the dispersed phase (Luan et al., 2006). Organic solvents miscible with water, such as methanol or ethanol, are the common choices.

Porosity generator, called also porosigen or porogen, is used to generate the pores inside the microspheres, which consequently increases the degradation rate of polymer and improves drug release rate. For example, Incorporating Sephadex (cross-linked dextran gel) into Insulin-PLA microspheres significantly increases microsphere porosity (Watts et al., 1990).

I.4.1.2 Continuous phase

For the microencapsulation of an active principle it is favorable to have a continuous phase that is a non-solvent for the active principle. While for lipophilic compounds aqueous solutions may be comfortably chosen, the use of hydrophobic, organic liquids as continuous phase for the encapsulation of hydrophilic compounds (Viswanathan et al., 1999) is more delicate because hydrophobic extraction fluids may not be readily removed from the final product, potentially causing undesired residues. Therefore, aqueous solutions are usually used as continuous phase, even for the microencapsulation of hydrophilic compounds.

Surfactants. A suitable surfactant should be able to give microspheres a regular size and a small size distribution, guaranteeing a more predictable and stable drug release. Surfactants must exhibit the following characteristics to be effective as emulsifiers:

- ✓ good surface activity;
- ✓ ability to form a condensed interfacial film;
- ✓ diffusion rates to interface comparable to emulsion forming time.

Before choosing the type of surfactant and its concentration, it is important to know the polarity of the two immiscible phases, the desired size of microspheres and the demand on the sphericity of microspheres.

There are four different types of surfactant classified by the nature of the hydrophilic part of molecule: anionic, cationic, amphoteric and non-ionic.
The anionic surfactants (sodium dodecyl sulphate, SDS) release a negative charge in the aqueous solution. They have a relatively high HLB

(hydrophile-lipophile balance) level because they have prone to be hydrophilic.

The cationic surfactants (cetyltrimethyl ammonium bromide, CTAB) on the contrary release a positive charge in aqueous solution.

The amphoteric surfactants behave as anionic in alkali pH and as cationic in acid pH.

Non-ionic surfactants (partially hydrolyzed PVA (polyvinyl alcohol), methylcellulose, tween and span) have no charge.

Among different surfactants, partially hydrolyzed PVA is mostly used because it gives the smallest microspheres. The addition of surfactant reduces the surface tension of the continuous phase and the diminution of the latter one decreases the size of microspheres (Carrio et al., 1995; Yang et al., 2001). However, due to the critical micelle concentration (CMC), the surface tension cannot decrease infinitively. When surfactants concentration reaches a certain level, the solution surface is completely loaded. Any further additions of surfactant will arrange as micelles and the surface tension of the aqueous phase will not decrease any more (Li et al., 2008).

Alternative components. Besides the surfactant, the antifoam is sometimes added into aqueous phase in the case of strong agitation because the foaming problem will disturb the formation of microspheres. When the stirring rate increase, more air is entrained and foam forms. So anti-foams of silicon and non-silicon constituents are used to increase the rate at which air bubbles are dissipated (Berchane et al., 2006).

Recent studies showed that it is possible to prepare microspheres without surfactant by replacing it with an amphiphilic biodegradable polymer. The advantage is to avoid the potential harm of surfactant residual on the surface or inside the final microspheres (Carrio et al., 1995).

CHAPTER II
Aim of the work

Biodegradable microspheres for controlled release formulations can be prepared by various conventional methods, but the most thoroughly investigated method is the emulsion solvent evaporation. However, several processes are currently being studied to design composite microparticles and SCF-based technologies are able to overcome many drawbacks present in conventional methods. Among these SCF processes, Supercritical Emulsion Extraction (SEE) appears to be fast and selective, allowing the production of composite microparticles with better particle size control and good encapsulation efficiencies; but it shows problems related to the intrinsically discontinuous operation. Therefore, the PhD thesis is focused on an innovative SEE process layout operating in continuous mode, named SEE-C (*Continuous Supercritical Emulsion Extraction*), for the production of controlled-size biopolymer microparticles intended for controlled release formulations. Particularly, the aim of this work is the optimization and characterization of the SEE-C process to investigate its capabilities and performances in the production of PLGA microparticles with engineered size and distribution and charged with different active principles.

PLGA has been chosen as biopolymer, due to its safety in biomedical preparations and its approval for human use by the FDA. The extraction experiments have been performed using both single and double emulsions; different active principle/PLGA systems have been tested. Particularly, anti-inflammatory drugs (such as Piroxicam and Diclofenac Sodium), corticosteroids (such as Hydrocortisone acetate) and proteins (such as Insulin) have been selected as active principles to be entrapped within microspheres.

This work has been developed in the following steps:

- ✓ process parameters optimization:
    - thermodynamic study of the selected system (ethyl acetate+CO_2) over a temperature range from 295 to 340 K at pressures up to 32 MPa; indeed, information on the volumetric properties of fluid

mixtures at high pressures is important for the operation of processes involving supercritical fluids.

- analysis of SEE-C operating parameters to select the conditions for the maximum extraction of the oily dispersed phase of the emulsion.

- fluidodynamic characterization of the packed tower. Indeed, the hydrodynamic behavior strongly depends on parameters such as, density difference of the phases, kind of the internal packing and the relative amounts of phases flowing in the tower.

✓ investigation of the effect of emulsion formulation parameters (such as polymer concentration and emulsion stirring rate) and of different emulsion approaches on the droplets and, therefore, on the produced microspheres.

✓ detailed characterization of the produced microspheres in terms of size distribution, morphology, encapsulation efficiency and physico-chemical properties (solid state, solvent residue) of the different products obtained using the SEE-C technology.

✓ comparison of SEE-C process performance with the one of the corresponding batch operating mode processes (supercritical and conventional evaporation) in terms of process yield, particle size distributions, morphology, encapsulation efficiency and physico-chemical properties.

✓ study of the PLGA microparticles degradation to monitor any morphological differences in time of the biodegradable devices produced by SEE-C.

✓ study of the influence of active principle loading, particle size and emulsion kind on drug release profiles from microspheres produced by SEE-C technology, to obtain further information about the microspheres structure and their efficiency to achieve sustained release.

Microparticles characterization and drug release analyses have required the use of several analytical methods such as laser scattering, scanning electron microscopy, HLPC analysis, UV-vis spectrophotometry, differential scanning calorimetry and X-Ray diffractometry.

The most significative results have been reported in the next chapters, related to some examples of the materials tested and thought to be the most interesting for better understanding the potentialities of the SEE-C process.

CHAPTER III
Continuous Supercritical Emulsion Extraction (SEE-C)

III.1 SEE-C apparatus description

Process equipment consists of a high pressure packed column where gas and liquid phases (SC-CO_2 and emulsion) are contacted counter currently and mass transfer between the two phases is improved by the internal packing elements.

The SEE-C apparatus mainly consists of a 1680 mm long column with an internal diameter of 13.11 mm. The column is packed with stainless steel packings 4 mm nominal size with 1889 m^{-1} specific surface and 0.94 voidage (0.16-inch Pro-Pak, Scientific Development Company, State College, PA, USA), and is formed by five AISI 316 cylindrical sections connected by 4-port elements. The extraction stages are three. The apparatus is thermally insulated by ceramic cloths and its temperature is controlled by six controllers (Series 93, Watlow, Milan, Italy) inserted at different heights of the column. SC-CO_2 is fed at the bottom of the column by a high-pressure diaphragm pump (mod. Milroyal B, Milton Roy, Pont Saint-Pierre, France) at a constant flow rate. The emulsion is taken from a reservoir and delivered from the top of the column, using a high pressure piston pump (mod. 305; Gilson, Villiers-le-Bel, France), at a constant flow rate. Particles formation in emulsion is achieved by removal of the internal organic oil phase from the emulsion droplets by extraction using SC-CO_2. A separator located downstream the top of the column is used to recover the extracted "oily" solvent and the pressure in the separator is regulated by a backpressure valve (26-1700 Series, Tescom, Selmsdorf, Germany). At the exit of the separator, a rotameter (mod. N5-2500, ASA, Sesto San Giovanni, Italy) and a dry test meter (mod. LPN/S80AL class G2.5, Sacofgas, Milan, Italy) are used to measure the CO_2 flow rate and the total amount of CO_2 delivered, respectively. The microspheres suspension is continuously removed from the bottom of the extraction column by decompression, using a needle valve

(mod. SS-31RS4, Swagelok, Brescia, Italy). A detailed representation of the SEE-C process layout is reported in Figure III.1:
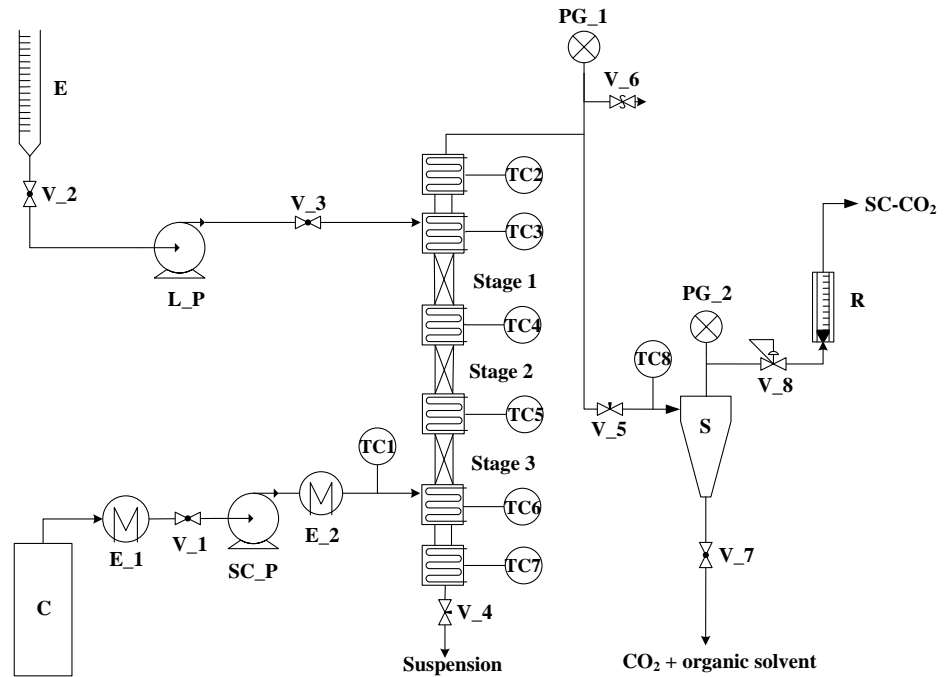
Figure III.1 *Continuous tower diagram: C, CO_2 supply; E, emulsion supply; PG_1 and PG_2, pressure gauges; SC_P, diaphragm pump used for high pressure SC-CO_2; L_P, piston pump used for the emulsion; TC1…TC8, thermocouples; S, separator; R, rotameter; E_1 and E_2, heat exchangers; V_1…V_8, valves.*

The start-up of the extraction process begins delivering SC-CO_2 from the bottom of the column until the operating pressure is reached. Then, the emulsion delivery is started at the top of the column. At the end of each run, the column is washed with distilled water to eliminate any processing residue from the packing surface.

After the SEE-C experiment, particles are recovered from the suspension and separated from the surfactant by centrifugation with a large volume of distilled water at a rotation speed of 4500 rpm for 45 min. Then, the supernatant is discharged and particles are re-suspended in pure water, recovered by membrane filtration and dried at air for further processing.

A schematic representation of SEE-C process is illustrated in Figure III.2:
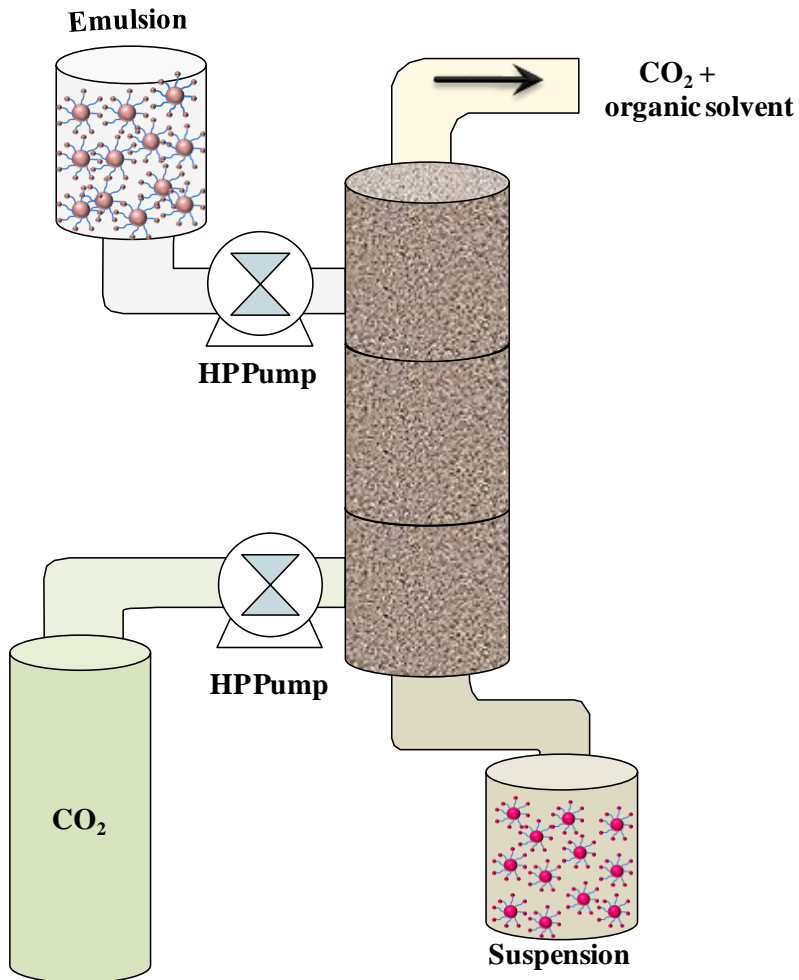
Figure III.2 *Schematic representation of SEE-C process.*

The laboratory apparatus used is located at the University of Salerno (Italy) and a picture is shown in Figure III.3:

Figure III.3 *Laboratory SEE-C apparatus located at the University of Salerno (Italy).*

III.2 SEE-C process description

The continuous packed tower takes advantage from the similarities of this process with the classical absorption/stripping procedure, in which mass transfer between the liquid and the gaseous phase can be obtained in a continuous packed column. The major difference with the traditional "stripping" process is the progressive formation of a solid phase into the tower. The use of packed towers is commonly not recommended for processes involving the presence of a solid phase; indeed, it is expected that the solid precipitates from the liquid phase and deposits on the packing surface, producing a progressive reduction of the mass transfer and,

subsequently, the blockage of the process. However, in the SEE-C, this limitation is not observed. There are two good conditions to justify why this phenomenon does not significantly interfere with the continuous solvent elimination process. As the dimensions of the microspheres produced (related to droplet diameters) are always in the range 0.2-50 µm, they remain suspended in the falling liquid film (i.e., the emulsion external phase) inside the column (i.e., particles residence time in the column is expected to be shorter than their sedimentation time); moreover, the presence of the surfactant on the particle surfaces allows their easy slipping on the packing surfaces. The presence of surfactant around the microspheres suspension is also useful for their recovery at the bottom of the column, since it avoids any other particle collapsing or aggregation. Moreover, the Joule-Thomson effect that follows the CO_2 lamination induces a strong cooling effect on the microparticles suspension (2-4°C are normally reached), improving drug/polymer particles stability during their recovery (Della Porta et al., 2011).

In the classical interpretation of a liquid extraction process, mass transfer is concentrated at the interface between the two films formed by liquid and gas phase (Richardson et al., 2002). This schematization can also be applied to SEE-C process, therefore, mass transfer between the liquid and the gas can be hypothesized to take place at the interface between the film of liquid moving downwards the surface of the packing and the film of SC-CO_2 moving upward in the column. During the continuous operation, due to the interactions between the two countercurrent flow rates, mass transfer between the two phases is activated, but, variations in the top and bottom product compositions can be observed until steady state conditions have been obtained. As a consequence, another relevant process parameter in the continuous operation is the time required to obtain steady state conditions in the column. In preliminary experiments performed, using an empty *o-w emulsion* (ratio 20:80), it was observed that after 30 min, the solvent residue in the water recovered at the bottom of the column became almost constant. Following these indications, the SEE-C experiments were always performed after the attainment of the steady state conditions using an empty emulsion.

III.3 SEE-C process mechanism

Precipitation of PLGA inside the droplets is induced by SC-CO_2 extraction of the organic solvent of the oily dispersed phase. Although the detailed behavior of this process has not yet been defined, a possible mechanism can be described as follows (Della Porta et al., 2011); when emulsion and SC-CO_2 come in contact, the mass transfer of the organic solvent proceeds by two parallel pathways: (A) the diffusion of the organic solvent into water followed by subsequent extraction of the solvent from the aqueous phase into SC-CO_2; (B) the direct extraction upon contact between

SC-CO_2 and the organic phase inside the droplet (Figure III.4). The path (A) is the only one used to describe the conventional SE because, in that case, the quantity of solvent evaporated at the liquid air interface is compensated by the solvent diffusing into the continuous phase from the droplet (Li et al., 1995). This path can be justified also in the supercritical emulsion extraction process by the fact that a thermodynamic equilibrium occurs into the solvent-rich and aqueous-rich phases. Moreover, at selected operating conditions, very large solubility of the oily phase is assured in SC-CO_2; therefore, it may extract the solvent of the dispersed oily phase from the external water phase of the emulsion causing the subsequent diffusion of the solvent from the droplets to the continuous phase, to restore the thermodynamic equilibrium. This phenomenon may prevail, for example, in the case of ethyl acetate because its solubility in water is particularly great (8.7% w/w at ambient conditions (Meng et al,. 2004)). However, the co-existence of the path (B) in the supercritical emulsion extraction process should be confirmed by the process of water-in-oil emulsion reactions assisted by SC-CO_2 for the production of metal oxides (Chattopadhyay and Gupta, 2003; Reverchon et al., 2010). In that case, the CO_2 was used not only as extracting agent of the organic external phase, but also as a reagent that, reacting with the solute in the internal water phase, forms metal oxides nanoparticles. In this particular application, the SC-CO_2 diffusion into the droplet is necessary for the reaction evolution and the results reported in the literature indicated a very fast reaction rate after SC-CO_2 diffusion into the droplets, through the surfactant shell. Mattea et al. (2010) also observed the behavior of a dichloromethane drop (covered by surfactant) in water after its contact with SC-CO_2 at a given pressure, temperature and CO_2 molar fraction and reported possible swelling of the drops, after SC-CO_2 diffusion in it (that may suggest the direct extraction of the solvent), suddenly overcame by a rapidly drop shrinking, probably due to the dichloromethane diffusion out of the drop into the external water phase (that may also suggest the indirect solvent extraction). Both mass transfer paths, namely ''direct solvent extraction'' and ''indirect solvent extraction'' from the external phase, may concur in generating the drug/polymer supersaturation inside the droplet and its fast precipitation. An hypothesis about the possible prevailing mechanism in the SEE-C process cannot be attempted at the moment due to lack of experimental data in the literature.
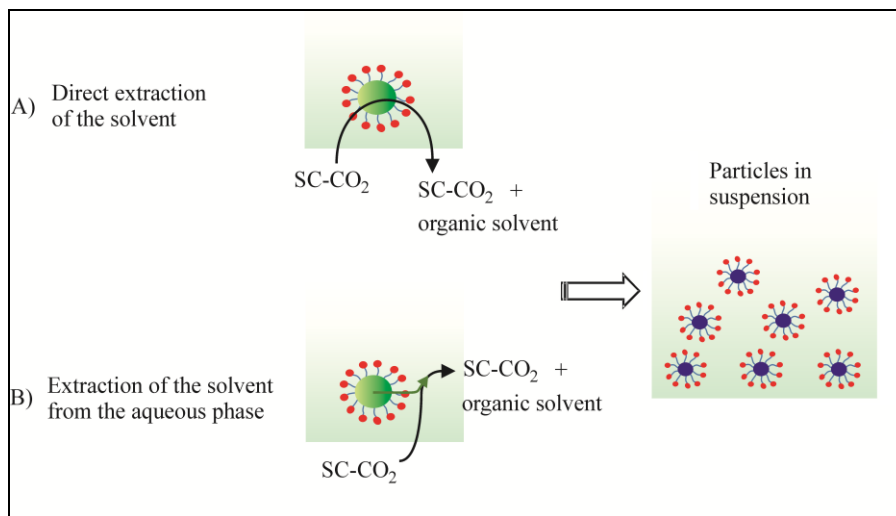
Figure III.4 *Schematic representation of the possible mass transfer pathways of the oily phase during the SEE process. Two parallel pathways: (A) diffusion of the organic solvent into water followed by subsequent supercritical extraction of the solvent from the aqueous phase; (B) direct supercritical extraction upon contact between SC-CO$_2$ and the organic phase into the droplet.*

Chapter IV
Materials and methods

IV.1 Materials

IV.1.1 Biopolymer: Poly (lactic-co-glycolic acid) (PLGA)

Poly (lactic-*co*-glycolic acid) (PLGA) is a Food and Drug Administration (FDA) approved copolymer, used for controlled release devices production (Jain, 2000; Mundargi et al., 2008), owing to its biodegradability and biocompatibility (Anderson and Shive, 1997). The list of some FDA approved controlled release products available in the market is given in Table IV.1:

Table IV.1 *PLGA-based microparticles available in the market.*

Product name	Active principle	Company	Application
Lupron Depot®	Leuprolide acetate	TAP	Prostate cancer
Nutropin Depot®	Growth hormone	Genetech	Pediatric growth hormone deficiency
Decapeptyl®	Triptorelin pamoate	Ferring	Prostate cancer
Sandostatin LAR® Depot	Octreotide acetate	Novartis	Acromegaly
Trelstar™ Depot	Triptorelin pamoate	Pfizer	Prostate cancer
Risperidal® Consta™	Risperidone	Johnson & Johnson	Antipsychotic

PLGA is synthesized by means of random ring-opening co-polymerization of two different monomers, the cyclic dimers (1,4-dioxane-

2,5-diones) of glycolic acid and lactic acid. During polymerization, successive monomeric units (of glycolic or lactic acid) are linked together in PLGA by ester linkages, thus yielding a linear, aliphatic polyester as a product.

PLGA has been successful as a biodegradable polymer because it degrades by non-enzymatic hydrolysis of its ester linkages into non-toxic and non-harmful by-products, lactic and glycolic acid, which are metabolized primarily via the Krebs cycle (Anderson and Shive, 1997).

Depending on the ratio of lactide to glycolide (PLA/PGA) used for the polymerization, different forms of PLGA can be obtained; these are usually identified with respect to the monomers ratio used (e.g. PLGA 75:25 identifies a copolymer whose composition is 75% lactic acid and 25% glycolic acid). The time required for degradation of PLGA within an organism is related to the monomers ratio, as shown in Figure IV.1 (Miller et al., 1977): the higher the content of glycolide units, the lower the time required for degradation. An exception to this rule is the copolymer with 50:50 monomers ratio, which exhibits the faster biodegradation rate of the lactide/glycolide polymers (about 50-60 days). Other combinations, i.e. 65:35, 75:25 and 80:20, have progressively longer in vivo life-times.
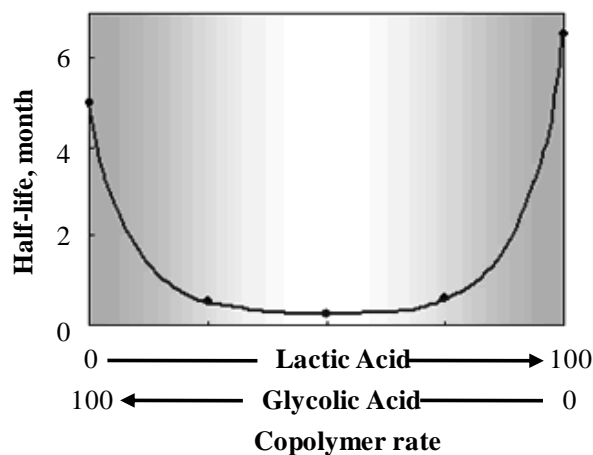
Figure IV.1 *Half life of various lactic acid and glycolic acid as copolymers implanted in rat tissue.*

PLGA ($[C_3H_4O_2]_m$ $[C_2H_2O_2]_n$) copolymers with different lactide/glycolide ratios have been used in this work. PLGA 75:25 with molecular weight in the range 66000-107000 was supplied by Sigma Aldrich (Milan, Italy) and it appears as light yellow granules, whereas PLGA 50:50 RESOMER® RG 504H with molecular weight ranging between 38,000-54,000 was received from Boehringer Ingelheim (Ingelheim, Germany) and it appears as white powder. All PLGAs are amorphous and show a glass transition temperature

in the range of 40-50°C. Unlike the homopolymers of lactic acid and glycolic acid which show poor solubilities, PLGA can be dissolved by a wide range of common solvents, including chlorinated solvents, tetrahydrofuran, acetone or ethyl acetate. The chemical structure of PLGA is shown in Figure IV.2:
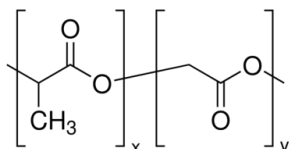
Figure IV.2 *Chemical structure of PLGA.*

IV.1.2 Pharmaceutical compounds

NSAIDs. Piroxicam and Diclofenac Sodium are nonsteroidal anti-inflammatory drugs (NSAIDs), i.e. agents that possess analgesic and antipyretic (fever-reducing) effects and, in higher doses, anti-inflammatory effect. Indeed, Piroxicam and Diclofenac Sodium are widely used for the treatment of inflammatory disorders and painful conditions such as rheumatoid arthritis, gout, bursitis, painful menstruation and headache; but, they are also effective in the relief of pain and fever. Research continues into their potential for prevention of colorectal cancer and treatment of other conditions, such as cancer and cardiovascular disease.

Piroxicam (PX, $C_{15}H_{13}N_3O_4S$, purity $\geq$ 98% (TLC)) with molecular weight of 331.348 g/mol, and Diclofenac Sodium (DS, $C_{14}H_{10}C_{l2}NNaO_2$, purity 99% (TLC)) with molecular weight of 318.13 g/mol were supplied from Sigma-Aldrich (Milan, Italy). Both of them appear as a yellowish hygroscopic crystalline powder. The approximate solubility of Piroxicam in water is 23 mg/L at room temperature and the melting point is 198-200°C. The solubility of Diclofenac Sodium in water is approximately 50 mg/mL at room temperature; moreover, it is soluble in alcohols (PBS pH 7.2, in EtOH, DMF) and insoluble in chloroform and in dilute acid. The melting point is 288-290°C. The chemical structure of Piroxicam and Diclofenac Sodium are shown in Figure IV.3:

Piroxicam   Diclofenac Sodium
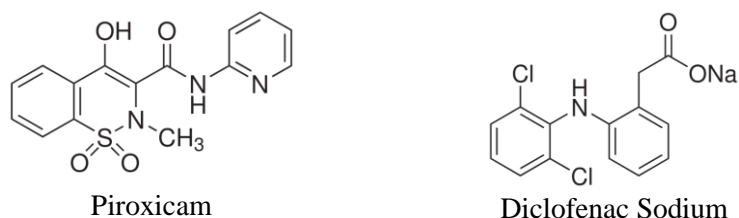
Figure IV.3 *Chemical structures of Piroxicam and Diclofenac Sodium.*

Corticosteroids. Hydrocortisone Acetate is classified as a steroid hormone which is used primarily for its anti-inflammatory, anti-allergic and antipruriginisa action. It is more specifically a glucocorticoid, produced by the adrenal gland. Hydrocortisone Acetate stimulates gluconeogenesis (the breakdown of protein and fat to provide metabolites that can be converted to glucose in the liver) and activates anti-stress and anti-inflammatory pathways. It is used in oral administration, intravenous injection or topical application.

Hydrocortisone Acetate (HA, $C_{23}H_{32}O_6$, purity $\geq$ 98 (HPLC)) with a molecular weight of 404.5 g/mol was received from Sigma-Aldrich (Milan, Italy). Untreated Hydrocortisone Acetate is a white powder. It is stable, but may be light or moisture sensitive. The solubility in water is 1.08×10^{-3} M and the melting point is 223°C. The chemical structure is shown in Figure IV.4:
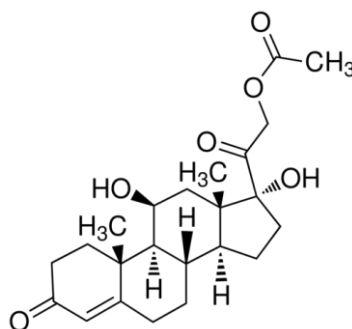
Figure IV.4 *Chemical structure of Hydrocortisone Acetate.*

Proteins. Insulin is a hormone (and like many hormones, it is a protein), produced in vivo by β-cells from inside the pancreas, which is required to regulate carbohydrate and fat metabolism in the body. It is a peptide composed of 51 amino acids shared between two intramolecular chains, A and B, linked together by two disulfide bonds. In most species, the A chain consists of 21 amino acids and the B chain of 30 amino acids.

Insulin is medically used to treat some forms of diabetes mellitus. Indeed, diabetes is a chronic disease which is characterized by high blood glucose (sugar) levels resulting from the body not producing Insulin or using it properly. Insulin must be injected into the fat under the skin in order for it to reach into the blood. There are many different types of Insulin for many different situations and lifestyles. Each Insulin differs in how it is made, how it works in the body, and in price. There are 4 types of Insulin mainly used:

- ✓ **Rapid-acting Insulin** – it begins to work immediately after injection and reaches the peak time in an hour. Its duration lasts for about 2-4 hours.
- ✓ **Regular or Short-acting insulin** – this type of Insulin reaches the bloodstream within 30 minutes after injection. It reaches the peak time anywhere from 2-3 hours after injection and stays effective for about 3-6 hours.
- ✓ **Intermediate Acting Insulin** – this type of Insulin reaches the bloodstream within 2-4 hours after injection, hits peak time around 4-12 hours after, and then stays effective for about 12-18 hours.
- ✓ **Long Acting Insulin** – this type of Insulin reaches the bloodstream at a much slower rate, usually 6-10 hours after injection. Its duration is about 20-24 hours.

Insulin from bovine pancreas (INS, $C_{254}H_{377}N_{65}O_{75}S_6$, purity 99%) with a molecular weight of 5733.5 g/mol was obtained from Sigma-Aldrich (Milan, Italy). Untreated Insulin is a white powder. The isoelectric point for the native protein is pI=5.3. Insulin is sparingly soluble in water and insoluble in organic solvents. It has low solubility at neutral pH. It can be solubilized (1-10 mg/ml) at 2 mg/mL in dilute acetic or dilute hydrochloric acid, pH 2-3. Typically, it is used as a medium supplement for cell culture. The concentration range is 1-10 mg/mL, depending on the cell type. The chemical structure of Insulin is shown in Figure IV.5:
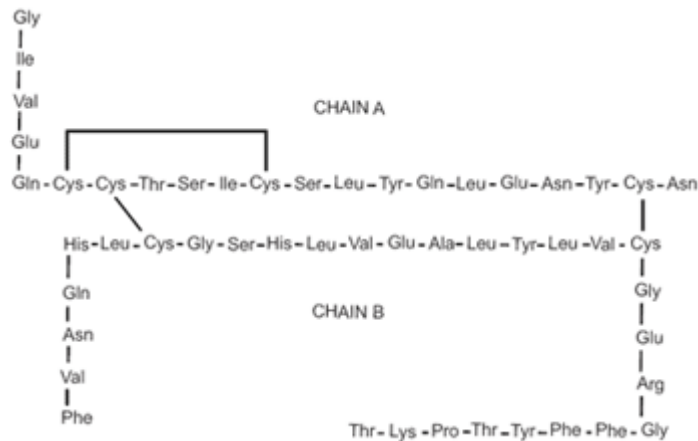
Figure IV.5 *Chemical structure of Insulin.*

IV.1.3 Surfactant: Polyvinyl alcohol (PVA)

Polyvinyl alcohol (PVA) has been used as surfactant to stabilize the emulsions. It is a synthetic polymer produced by hydrolysis of polyvinyl

acetate. The physical characteristics and its specific functional uses depend on the degree of polymerization and the degree of hydrolysis. Polyvinyl alcohol has excellent film forming, emulsifying and adhesive properties. It has high tensile strength and flexibility, as well as high oxygen and aroma barrier properties. PVA is fully degradable and dissolves quickly.

PVA with an hydrolization grade of 98-99% and molecular weight of 31000-50000 g/mol was supplied by Sigma-Aldrich (Milan, Italy). Untreated PVA is a white fine powder formed of irregular particles with size ranging from about 50 to 250 μm. Polyvinyl alcohol is soluble in water, slightly soluble in ethanol, but insoluble in other organic solvents. It has a melting point of 180-190°C and decomposes rapidly above 200°C. The chemical structure of the monomer is given in Figure IV.6:
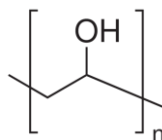
Figure IV.6 *Chemical structure of PVA.*

IV.1.4 Liquid solvents

Ethyl acetate (EA, purity 99.9%), supplied by Carlo Erba Reagents (Milan, Italy), was used as organic solvent in the preparation of the oily phase of emulsions. This solvent is classified by the International Conference on Harmonization (ICH) as Class 3 solvent with residual solvent limit in drug substances fixed at 5000 ppm (Federal Register, 1997).

Dimethyl sulfoxide (DMSO, purity 99.9%, Carlo Erba Reagents, Milan, Italy), ethanol (EtOH, purity 99.9%, Carlo Erba Reagents, Milan, Italy) and distilled water were used as solvents of the internal water phase of w-o-w emulsions.

Trifluoroacetic acid (TFA, purity 99%) (supplied by Sigma-Aldrich, Milan, Italy), HPLC grade Acetonitrile (ACN, purity 99.8%) (purchased from Carlo Erba Reagents, Milan, Italy) and Sodium hydroxide (NaOH) 0.25 M (supplied by Sigma-Aldrich, Milan, Italy) were used in the analyses.

IV.1.5 Other materials

Carbon dioxide (CO_2) purchased from SON (Napoli, Italy) was used in the SEE-C process for the extraction of the organic solvent from the emulsions in supercritical conditions. Sodium chloride (NaCl, purity 99%), Dibasic sodium phosphate (Na_2HPO_4, purity 99%), Monobasic sodium phosphate dihydrate ($NaH_2PO_4 \cdot 2H_2O$, purity 99%), Tween-80 and Glycerol

(GLY, purity 99%) obtained by Sigma-Aldrich (Milan, Italy) were used in the analyses.

IV.2 Methods

IV.2.1 Emulsion Preparation

For the encapsulation of the mentioned active principles into PLGA, different possible emulsion kinds (*o-w*, *w-o-w* and *s-o-w*) have been tested, generically described below. Empty emulsions have also been prepared.
The emulsions have been produced varying the active principle or PLGA concentrations in the emulsion droplets or the emulsion stirring rate.

o-w emulsion. Oily phase was prepared dissolving fixed amounts of AP and PLGA into an organic solvent. Water phase was prepared dissolving PVA into an aqueous solution. The oily phase was added into the water phase using a high-speed stirrer (model L4RT, Silverson Machines Ltd., Waterside, Chesham Bucks, United Kingdom).

w_1-o-w_2 emulsion. A known amount of AP was pre-suspended or dissolved into a solution containing PVA and used as the inner water phase (w_1); a known amount of PLGA was dissolved into an organic solvent, which was used as the oil phase (*o*). The water phase (w_1) was emulsified with the oily phase (*o*) to form a primary w_1-o emulsion upon sonication by a digital ultrasonic probe at 50% of amplitude (mod. S-450D, Branson Ultrasonics Corporation, Danbury, CT, USA) or an ultrasonic bath (mod. VCX130, Vibra Cell, Sonics & Materials, Inc., Newtown, CT, USA). Sonication, in particular, is an exothermic operation; this is why using an ice bath during the different steps can be beneficial. Then, the resulting primary emulsion was immediately poured into a known amount of an aqueous PVA solution, which was used as the outer water phase (w_2), and homogenized to form the secondary emulsion by high-speed stirring.

s-o-w suspension emulsion. A fixed amount of AP was mixed with a solution of a known amount of PLGA in an organic solvent to form a suspension, which was then added into a known amount of an aqueous PVA solution to form a s-o-w suspension emulsion by high-speed homogenization.

Emulsions composition and conditions used in this work are described in details in Table IV.2:

Table IV.2 *Emulsions composition and conditions used.*

AP	Emulsions composition and conditions
Drug free	***o-w emulsion*** (20:80 w/w). **- *oil phase***: 5-10% w/w PLGA 50:50 (of the oil phase) into EA **- *water phase***: EA-saturated aqueous solution with 0.8% w/w PVA **Emulsion conditions**: high-speed homogenization operating at 2800 rpm for 3 min. ***w-o-w emulsion*** (1:19:80 w/w/w). **- *inner water phase***: water solution with 0.04% w/w PVA **- *oil phase***: 10% w/w PLGA 50:50 (of the oil phase) into EA **- *outer water phase***: EA-saturated aqueous solution with 0.8% w/w PVA **Primary emulsion conditions**: 60-second sonication by digital ultrasonic probe at 50% of amplitude. **Secondary emulsion conditions**: high-speed stirring at 2800 rpm for 6 min.
PX	***o-w emulsion*** (20:80 w/w) **- *oil phase***: 5-7.5% w/w PLGA 75:25 (of the oil phase) and 10% w/w PX (of the PLGA) into EA **- *water phase***: EA-saturated aqueous solution with 0.8% w/w PVA **Emulsion conditions**: high-speed homogenization operating at 2800 rpm for 3 min.
DS	***w-o-w emulsion*** (2:18:80 w/w) **- *inner water phase***: 10% w/w DS (of the polymer) in water solution with 0.04% w/w PVA **- *oil phase***: 2.5-5% w/w PLGA 75:25 (of the oil phase) into EA **- *outer water phase***: EA-saturated aqueous solution with 0.8% w/w PVA **Primary emulsion conditions**: sonication by ultrasonic bath for 2 min. **Secondary emulsion conditions**: high-speed stirring at 2800 rpm for 6 min.

AP	Emulsions composition and conditions
HA	*w₁-o-w₂ emulsion* (1:19:80 w/w/w). - *inner water phase*: 2.3-9% w/w HA (of the polymer) in EtOH or DMSO with 0.04% w/w PVA - *oil phase*: 5-10% w/w PLGA 50:50 (of the oil phase) into EA - *outer water phase*: EA-saturated aqueous solution with 0.8% w/w PVA **Primary emulsion conditions**: 60-second sonication by digital ultrasonic probe at 50% of amplitude. **Secondary emulsion conditions**: high-speed stirring at 2800 rpm for 6 min. *s-o-w suspension emulsion* (20:80 w/w). - *solid phase*: 4.5-9% w/w HA (of the polymer) in EA - *oil phase*: 10% w/w PLGA 50:50 (of the oil phase) into EA - *water phase*: EA-saturated aqueous solution with 0.8% w/w PVA **Emulsion conditions**: high-speed homogenization operating at 2800 rpm for 3 min.
INS	*w₁-o-w₂ emulsion* (1:19:80 w/w) - *inner water phase*: 0.5-1% w/w INS (of the polymer) an aqueous/TFA GLY solution (250 µl of GLY and 750 µl of water with 0.1% TFA) with 0.04% w/w PVA - *oil phase*: 10% w/w PLGA 50:50 (of the oil phase) into EA - *outer water phase*: EA-saturated aqueous solution with 0.8% w/w PVA **Primary emulsion conditions**: 90-second sonication by digital ultrasonic probe at 50% of amplitude. **Secondary emulsion conditions**: high-speed stirring at 1000-2800 rpm and 10°C in an ice bath for 3 min.

IV.2.2 Droplets and microspheres morphology

The droplets formed in the emulsions were observed using an optical microscope (mod. BX 50 Olympus, Tokyo, Japan) equipped with a phase contrast condenser.

Microspheres shape and morphology were analyzed by Field Emission-Scanning Electron Microscope (FE-SEM mod. LEO 1525, Carl Zeiss SMT AG, Oberkochen, Germany). Powders were dispersed over an adhesive

carbon tab, previously stuck to an aluminum stub. Samples were coated with a thin gold film (layer thickness 250 Å) using a sputter coater (mod.108 A, Agar Scientific, Stansted, United Kingdom).

IV.2.3 Droplets and microspheres size and distribution

Droplet Size Distributions (DSDs) and Particle Size Distributions (PSDs) were measured by dynamic light scattering (DLS, mod. Mastersizer S, Malvern Instruments Ltd., Worcherstershire, United Kingdom). The Mastersizer S software uses Mie theory to produce an optimal analysis of the light energy distribution and to obtain the size distribution of the particles. Analyses were performed immediately after the preparation of the emulsion and of the microspheres suspension, using several milligrams of sample appropriately diluted with distilled water. The distributions proposed are the mean of several DLS analysis. Droplets and particle size are expressed as volume mean diameter (in μm) ± SD of values collected. Droplet Size Distributions (DSDs) and Particle Size Distributions (PSDs) are also described through the values of D_{10}, D_{50} and D_{90} of the volumetric distribution.

IV.2.4 Solvent residue analysis

Ethyl acetate content in the final suspensions was analyzed, to determine the efficiency of solvent removal from the emulsion during SC-CO_2 extraction. The solvent residue was evaluated using a head space sampler (mod. 50 Scan, Hewlett & Packard, Palo Alto, CA, USA) coupled to a gas chromatograph interfaced with a flame ionization detector (GC-FID, mod. 6890 Agilent Series, Agilent Technologies Inc., Wilmington, DE). Ethyl acetate was separated using a fused-silica capillary column 30 m length, 0.25 mm internal diameter, 0.25 μm film thickness (mod. DB-1, J&W, Folsom, CA, USA). GC conditions were: oven temperature at 40°C for 8 min. The injector was maintained at 180°C (split mode, ratio 1:1) and Helium was used as the carrier gas (7 mL/min). Head space conditions were: equilibration time 60 min at 100 °C, pressurization time 2 min, loop fill time 1 min. Head space samples were prepared in 10 mL vials filled with 3 mL of suspension. Analyses were performed on each sample in three replicates. Calculation of the concentration of ethyl acetate in microsphere samples was based on the standard calibration curve obtained using different EA/water solutions at fixed concentration (8-80-800 ppm).

IV.2.5 Solid state characterization

Diffraction patterns (XRD) of precipitated powders were obtained using an X-ray diffractometer (mod. D8 Discover, Bruker AXS, Inc., Madison,

WI) with a Cu sealed tube source. Samples were placed in the holder and flattened with a glass slide to assure a good surface texture. The measuring conditions were as follows: Ni-filtered CuK radiation, $\lambda=1.54$ Å, 2θ angle ranging between 20° and 70° with a scan rate of 3 seconds/step and a step size of 0.2°.

Thermograms of powder samples were obtained using a differential scanning calorimeter (DSC mod. TC11, Mettler Toledo, Inc., Columbus, OH). Fusion temperature and enthalpy were calibrated with an indium standard material (melting point 156.6°C). The samples (±5 mg) were accurately weighed, crimped in an aluminum pan and heated from to 25 to 400°C at 10°C/min, under a nitrogen purge of 50 mL/min.

X-ray and DSC analyses were performed in three replicates for each batch of material.

IV.2.6 Active principle loading

The amount of active principle loaded into the microspheres was determined by HPLC analyses (mod. 1200 series, Agilent Technologies Inc., Italy) or UV-vis spectrophotometry (mod. Cary 50, Varian, PA, CA, USA). The methods adopted for the determination of the AP loading are described in details below, for each AP charged into the microspheres.

PX and DS loadings were measured by dissolving 2.5 mg of microspheres in 1 mL of 0.25 M sodium hydroxide. Samples were stirred for at least 24 h at 10 rpm to ensure the complete dissolution of the polymer. Pure PX and DS were treated identically to verify their stability in the polymer degradation medium; no drug degradation was observed. The concentration of drug in the resulting solution was determined by UV-Vis, measuring the absorbance at 276 nm (both for PX and DS) in a quartz cuvette and then subtracting absorbance values obtained for the blank microspheres treated identically.

HA loading was determined by UV-Vis method at 254 nm, measuring the absorbance value obtained in the release medium at the end of the drug release performed, i.e. when all the HA was diffused from the microspheres to the outer water phase.

The amount of INS loaded into the microspheres was measured using the procedure described by Bilati et al. (2005). Briefly, accurately weighed 10 mg aliquots of dried microspheres were dissolved in 0.6 mL of acetonitrile in centrifuge tubes and sonicated until complete transparency. Then, 1.4 mL of water containing 0.1% TFA were added to the sonicated mixture to dissolve Insulin completely. The remaining undissolved PLGA was separated by centrifugation at 2000 rpm for 2 min. The clear supernatant was then withdrawn and the protein concentration in the resulting clear solution was directly analyzed at room temperature by HPLC equipped with a C18 column (LiCrosphere 250x4.6 mm, particles size 5 μm, pore size 100 Å).

47

Elution was performed with a mobile phase of acetonitrile:water mixture (32:68 v/v) containing 0.1% v/v TFA. The flow rate was 0.9 mL/min, the injection volume was 20 μL and the detecting wavelength was 214 nm. Pure INS was also tested to verify its stability in water with 0.1% TFA; no protein degradation was observed.

The measurements were performed in three replicates and a good reproducibility was observed. The amount of measured AP, calculated from a calibration curve, was then converted in the effective AP loaded into microspheres. The encapsulation efficiency (EE) is the ratio of the final amount of AP effectively loaded to the nominal (starting) one:

$$EE\% = \frac{effective\ AP\ loading}{theoretical\ AP\ loading} \times 100 \qquad (IV.1)$$

IV.2.7 Active principle release

Active principles release rates were determined using the UV-Vis spectrophotometer or monitored by HPLC. The percentage of released AP is defined as the mass of released AP divided by the total mass of AP in the microspheres. The methods used for the determination of the AP released from the microspheres are described below. Each sample was assayed in triplicate and the proposed curves are the mean profiles obtained.

PX and DS release profiles were determined in 200 mL of release medium, phosphate-buffered saline solution (PBS, pH 7.4) in the case of PX and physiological solution in the case of DS, continuously stirred at 100 rpm in a 37°C incubator to maintain adequate sink conditions. For each test, 100 mg of microspheres containing the drug were suspended in 2 mL of release medium and charged into a dialysis sack. In the case of PX release, the addition of 0.5% Tween-80 into the phosphate-buffered solution was necessary to enhance PX solubility in the release medium. Indeed, PX solubility in pure water is 0.03 mg/mL at 37°C; whereas, in the used release medium is 1.00 mg/mL (Berkland et al., 2003). PX and DS release rates were both measured using an on-line UV-Vis probe at 276 nm.

For each HA release test, since solubility of HA in water is about 0.01 mg/mL, approximately 50 or 100 mg of microspheres containing HA (depending on the theoretical HA loading) were suspended in 2 mL of distilled water with 0.5% of Tween-80 and placed into a dialysis sack. This sack was then incubated in 200 mL of distilled water continuously stirred at 100 rpm and 37°C to maintain adequate sink conditions. The concentration of the HA released in the external medium was continuously detected by an on-line UV-Vis spectrophotometer, measuring the absorbance at 254 nm.

In vitro release kinetics of INS from microsphere formulations were evaluated by suspending accurately weighed 20 mg of dried microspheres in

2 mL of Phosphate-Buffered Saline (PBS, 100 mM, pH 7.4) or 2 mL of Dulbecco's Modified Eagle Medium (DMEM) used for cell culture, in a centrifuge tube. Then, the tubes were placed in an incubator-shaker at 37°C and stirred continuously at 50 rpm. At defined time intervals, the samples were centrifuged at 4000 rpm for 15 min and the supernatant was completely withdrawn and replaced with fresh media to maintain sink conditions. The amount of released protein was determined by measuring the protein concentration in the supernatant using HPLC method.

IV.2.8 Microspheres degradation

100 mg of PLGA microspheres were suspended in 20 mL of water, agitated at 50 rpm and 37°C. 10 mL of suspension were sampled every 7 days, dried and mounted on an aluminum stub for the morphological analysis by FE-SEM. The suspension pH was measured by a pHmeter (mod. pH 210, HANNA Instruments, Italy).

Chapter V
Process optimization

V.1 Volumetric properties of ethyl acetate+carbon dioxide binary

mixtures at high pressures

Information on the volumetric properties of fluids and fluid mixtures at high pressures is important for the design and operation of processes involving dense or supercritical fluids. Density and its dependence on pressure, temperature and fluid composition are particularly important because many properties of supercritical fluids, such as their solvating power, viscosity, diffusivity (which depend on several parameters such as temperature, pressure and composition) can be correlated and scale best with density.

Several publications have already appeared on thermodynamics and phase behavior of ethyl acetate+CO_2 mixtures. Critical loci have been reported (Ting et al., 1993; Chester and Haynes, 1997). Even though publications on vapor-liquid equilibrium for these mixtures have been published (Wagner and Pavlíček, 1994; da Silva et al., 2000; Byun et al., 2006), their reliability has been questioned in a recent publication (Wyczesany, 2007). Limited density information has been published, but at pressures below 20 MPa and temperatures below 313 K (Aida et al., 2010; Smith et al., 1998). Even though density (Vargaftik, 1975; Gardas et al., 2007) and volumetric property data are available for ethyl acetate (Gardas et al., 2007), there is no information on the higher pressure/temperature volumetric properties such as density, compressibility, expansivity or pressure coefficient for its mixtures with carbon dioxide.

In this work, therefore, the density and related volumetric properties of ethyl acetate+CO_2 mixtures containing 0, 27.7, 42.6, 52.9, 67.3 and 100 wt % CO_2 have been determined over a wider range of temperatures up to 340 K for mixtures and up to 380 K for pure components at pressures up to 32 MPa. These measurements have been carried out in a variable-volume view-cell employing a unique measurement technique. The methodology allows

real-time recording of the piston position which permits generation of essentially continuous density-pressure data (Falco and Kiran, 2012).

V.1.1 System description

Figure V.1 shows a schematic diagram of the experimental system used. It is based on a system that had been reported earlier (Zhuang and Kiran, 1996), which now incorporates a modified computer interface and data acquisition software. It consists of a high-pressure variable-volume cell (VC/VVP) with an internal movable piston, a special linear variable differential transformer (LVDT) to monitor in-real time the position of the movable piston, a pressure generator (PGN), two sapphire windows (SW) for visual or optical observations, an optical sensor to monitor the transmitted light intensity from a laser source (L), and a data acquisition board (DAQ) for the real time computerized recording of the pressure, temperature, transmitted light intensity and position of the piston while pressure is changed. The cell body and the variable volume part of the cell are each heated with four cartridge heaters controlled with a Omega (Model-CN76000) temperature controller. Temperature of the fluid inside the cell is monitored with a J-type thermocouple directly mounted on the cell. Temperature is maintained within ± 0.5 K of the set value. The cell pressure is measured with a flush-mount pressure transducer (Dynisco PT467E-15M) mounted on the recirculation loop near the inlet port of the cell. It permits monitoring the pressure with an accuracy of ± 0.06 MPa.

The far end of the variable volume part (VVP) of the cell is extended with a stainless steel tube (30.5 cm long) which houses an extension rod. The extension rod is connected to the movable piston at one end, while the other end is connected to a long ferromagnetic core. A special, large diameter (5 cm) and 30 cm long LVDT unit (Lucas-Schaevitz 2003 XS-A) positioned around the stainless steel tube (housing the extension rod) is used to monitor the position of the ferromagnetic core and with it the position of the piston. The signal from this long-stroke LVDT is directly recorded by the computer in real time and converted to actual position using a calibration curve. In the pressure generator (High Pressure Equipment Co., mod. 50-60-15), ethanol is used as the pressurizing fluid to bring about the changes in the position of the movable piston at a given temperature.
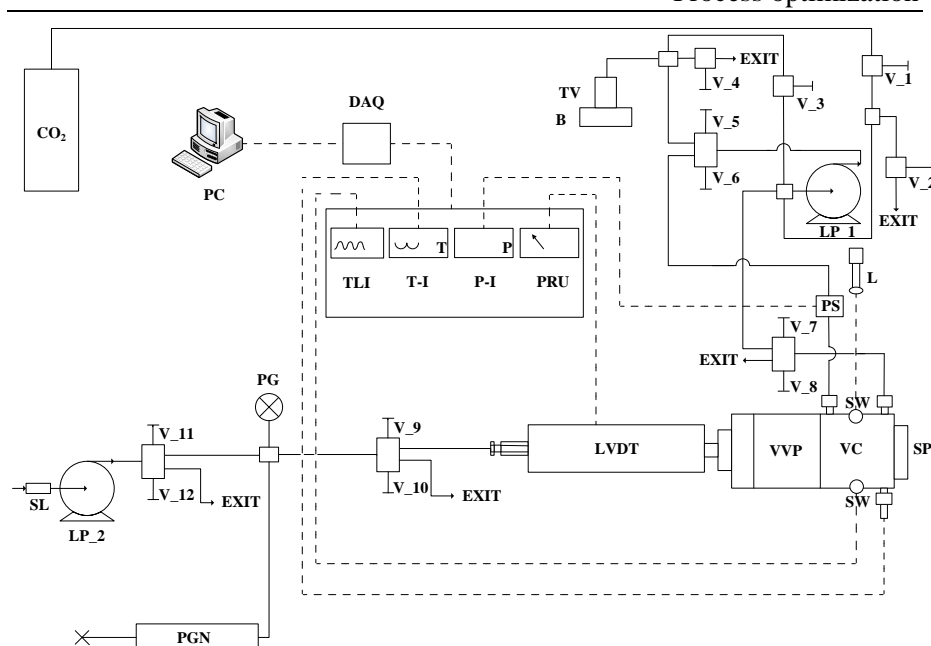
Figure V.1 *Schematic diagram of the experimental system: SL, solvent line; PG, pressure gauge; PGN, pressure generator; LP_1 and LP_2, liquid pumps; LVDT, linear variable differential transformer; VC, view cell; VVP, variable-volume part of the view cell; SW, sapphire window; SP, sample port; PS, pressure sensor; L, laser; PRU, position readout unit; PI, pressure indicator; TI, temperature indicator; TC, thermocouple; DAQ, computerized control and data acquisition units; TLI, transmitted light intensity; TV, transfer vessel; B, balance; V_1...V_12, valves.*

The maximum internal volume of the cell is 19.27 cm^3, corresponding to the all the way out position of the piston. The density of the fluid is then determined from the following equation:

$$\rho = M / (19.27 - 1.98\,L) \tag{V.1}$$

where ρ is the density (in g/cm^3), M is the total mass (in grams) initially loaded to the cell and L is the piston position (expressed in mm). The factor 1.98 incorporates the cross-sectional area of the piston and the conversion factor for unit consistency.

The experimental system used is located at Virginia Polytechnic Institute and State University (Virginia, USA), and a picture is shown in Figure V.2:
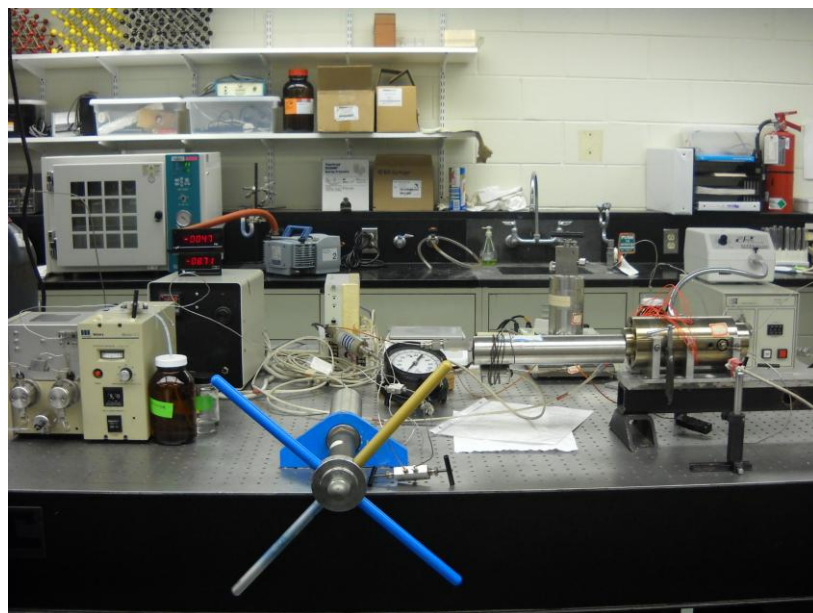
Figure V.2 *Experimental system used, located at Virginia Polytechnic Institute and State University (USA).*

V.1.2 Operational procedures

Prior to loading the fluid of interest, the cell was cleaned and purged by flushing it through the solvent delivery line with CO_2. This procedure was repeated 3-5 times to ensure that the cell was free of air or any residual solvent. Then, a known amount of the fluid to be tested was charged into the cell at room temperature using an HPLC pump (SSI, mod. 200) from a fluid transfer vessel that had been previously filled with the fluid. The transfer vessel for ethyl acetate was simply a glass bottle. The transfer vessel for CO_2 was a high pressure vessel. It was filled with carbon dioxide from a tank with an educator tube. The exact amount of each fluid charged during pumping was determined by direct reading of the weight change of the transfer vessels (containing ethyl acetate, or carbon dioxide) using a balance with 0.01 g accuracy (Mettler, mod. PM 6100). In a typical experiment, ethyl acetate was firstly charged, followed by CO_2 charge. The range of ethyl acetate mass charged was from 14.0 g for pure ethyl acetate to 4.93 g for the mixture with 67.3 wt % carbon dioxide content.

After the system was loaded, the cell was heated to the target temperature and held for about 1 h for equilibration before measurements were carried

out. After thermal equilibration was achieved, the piston was moved by applying pressure from the pressure generator. Pressure was continually changed slowly up to a desired high pressure (32 MPa in the present study) and then lowered back. After the pressure scan was completed, the system temperature was changed to a new value and the up-and-down pressure scans were carried out at each temperature.

During each scan, pressure, temperature, piston position and transmitted light intensity are recorded in real time with the dedicated computer. Under a continuous and slow pressure change, the fluid experiences a smooth expansion or compression. The pressure changes being brought about very slowly, the temperature control unit of the system compensates for any thermal changes associated with expansion or compression of the fluid. The experiments are thus conducted under quasi equilibrium state conditions.

Figure V.3(a-c) shows the real-time recording of pressure (a), piston position (b) and the internal volume (c) as a function of time during a pressure increase (compression) and pressure reduction (decompression) cycle for CO_2 at 340 K. The internal volume was changed from 18.6 to 13.7 cm^3 over a 2100 s (35 min) time-interval by increasing the pressure from 16 to 32 MPa, and then reducing it back by manipulation of the pressure generator by hand. This particular data set corresponds to about 7000 data points with data being recorded every 0.3 s during the scans. The resulting pressure-density curve from this experiment is shown in Figure V.3(d). The solid curve is a cubic polynomial fit to the data. The relatively high degree of reproducibility of the data in the up and down direction of the pressure change should be noted at this rate of pressure change employed. As shown in Figure V.3(a), relatively smooth pressure change is not too difficult to achieve by manipulating the pressure generator by hand if patience is exercised. The differences in the up and down pressure scans observed in Figure V.3(d) can be minimized further by reducing the rate of pressure increase or decrease. In this particular data set, the rate of pressure change employed was about 0.015 MPa/s. Of course, one can change the pressure to a new value, hold it there for a while to ensure full equilibration, and then move to a new equilibrium state and generate the pressure-position and thus pressure-density curves. However, the slow scanning procedure employed provides high degree of flexibility in the efficiency of generating data that are still reliable. Much smoother variations at desired rates are achievable by using a motorized version of the pressure generator.
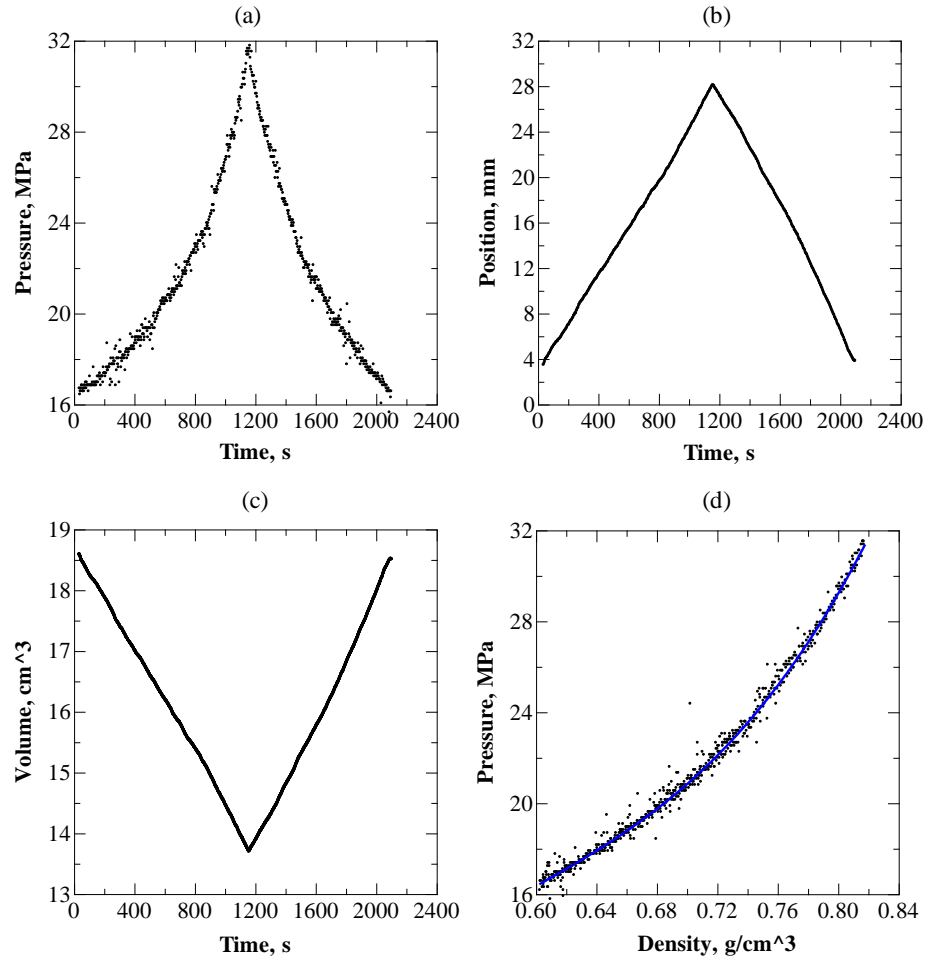
Figure V.3(a-d) *Real-time recording of pressure (a), piston position (b), cell volume (c) during a up-and-down pressure scan of CO_2 at 340 K, and the resulting pressure-density plot along with a polynomial fit (d).*

Figure V.4(a-d) show the real-time recording of pressure, position, volume and density during compression and decompression cycles for the binary mixture containing 67.3% by mass CO_2 at 313 K. The internal volume was changed from 18.7 to 16 cm^3 over a 850 s (14 min) time-interval by increasing the pressure from 14 to 30 MPa and then reducing it back. This particular data set corresponds to about 2700 data points with readings having again been taken every about 0.3 s during the experiment. Here the rate of pressure change employed was faster, being about 0.085 MPa/s. At this higher rate of pressure change, which is nearly 6 times faster than the case shown in Figure V.3(a), the density values in Figure V.4(d) show a

small hysteresis in the pressure increase or decrease direction, reflecting the small frictional differences arising from the O-ring of the piston.

Figure V.4(d) illustrates a unique feature of the present density determination procedure in that the demarcation pressure (or density) from the homogeneous one-phase to two-phase region (where the pressure remains unchanged -- strictly true for pure compounds-- while the density is altered) is distinctly displayed. In the absence of continuous recording of density (or volume) with continually changing pressure, the experimental identification of the exact point of this demarcation from one-phase to two-phase region would not be easy, as numerous single point measurements would be required, and even then would likely involve extrapolations.
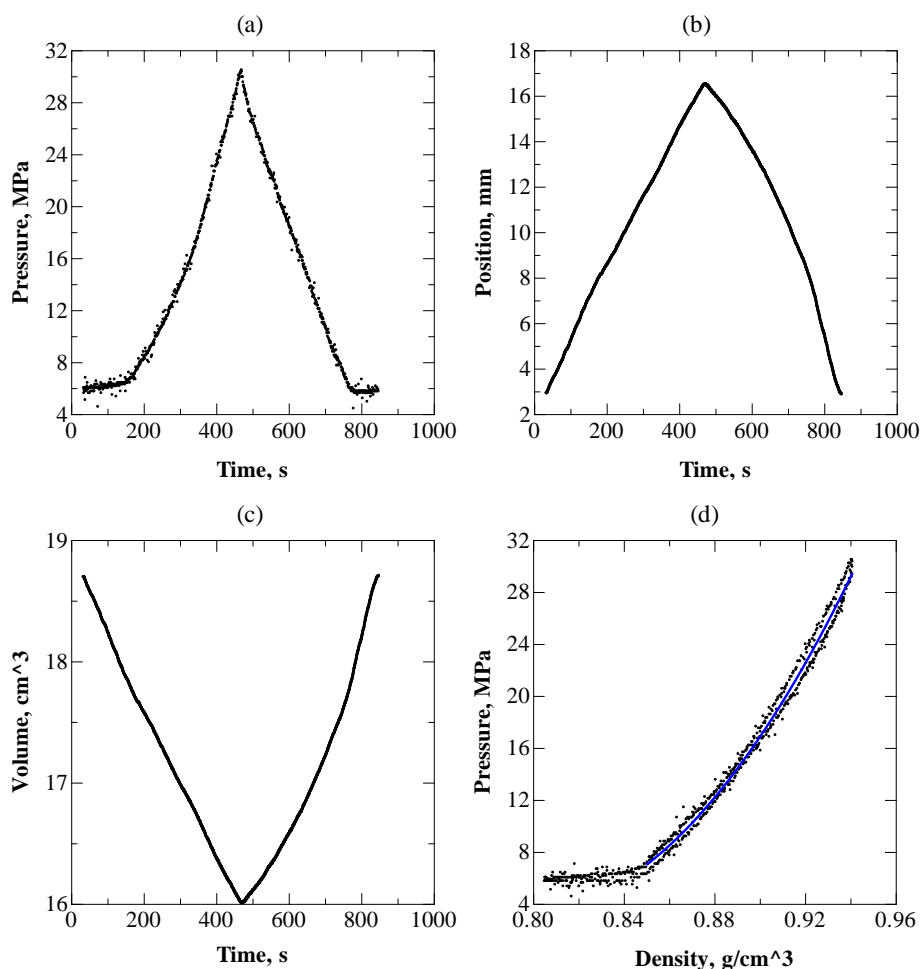
Figure V.4(a-d) *Real-time recording of pressure (a), piston position (b), cell volume (c) during a up-and-down pressure scan of the binary fluid mixture (ethyl acetate+CO_2) containing 67.3% by mass CO_2 at 313 K, and the resulting pressure-density plot along with a polynomial fit (d).*

The primary sources of error in the determination of density are linked to the uncertainties on the exact amount of fluid charged to the cell and the errors associated with the LVDT reading and its relation to the position of the piston. The balance was accurate to 0.01 g. The nonlinearity of the LVDT sensor was ± 0.30%. As will be discussed in the following sections, comparisons with NIST data base for CO_2 shows that the overall combined average error is less than 1%. To compensate for any errors that may arise from the pressure change rate, the density data were correlated by using all the values generated in both the pressure increase and decrease direction. The near continuous density data permits fitting the data with smooth polynomial functions representing the average values, as shown in Figure V.3(d) and Figure V.4(d). Experiments that were conducted by changing the pressure in step-wise manner and equilibration in between indicate that the equilibrium values indeed lie in between the up-and-down pressure-scan values, however, in the vicinity of the entrance to the two-phase region, they are closer to the values obtained in the pressure reduction direction.

V.1.3 Carbon dioxide

V.1.3.1 Density

Even though density of CO_2 is well documented in the literature and there are extensive data bases, such as those available through NIST (National Institute of Standards and Technology (NIST) - http://webbook.nist.gov/chemistry/fluid), for internal consistency and use in the comparisons with mixtures with ethyl acetate explored in the present study, the density of CO_2 at 295, 300, 320, 340 and 360 K over a pressure range from 5 to 32 MPa was measured. The results are shown in Figure V.5. The average rates of pressure increase and decrease employed were 0.027 and 0.034 MPa/s, respectively. The average piston velocities during pressure increase and decrease stages were 0.028 mm/s and 0.024 mm/s, respectively. Densities cover a range from about 0.60 to 0.98 g/cm^3.
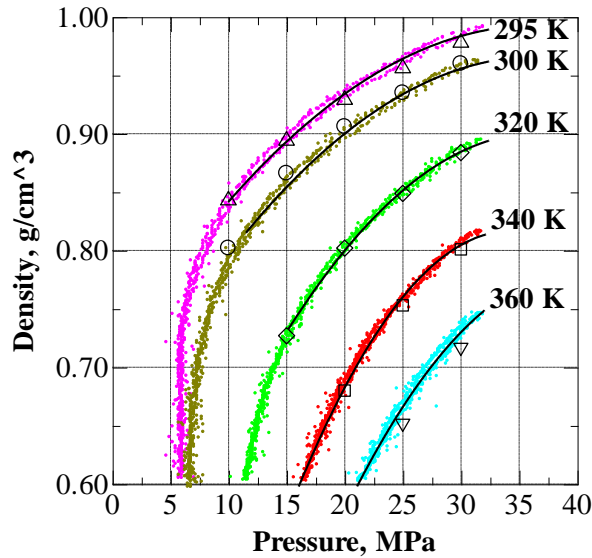
Figure V.5 *Variation of density with pressure of CO_2 at different temperatures. The filled symbols are the present experimental data at the indicated temperatures, the black solid curves are the polynomial fits to the data, and the open symbols are values from the NIST data base at the corresponding temperatures.*

At 295 K, CO_2 is subcritical (T_c = 304.1 K) and the density-pressure curve in Figure V.5 shows distinctly the two phase (V-L) region where density (volume) can change at constant pressure, and a smooth curved region corresponding to the homogeneous dense fluid domain where density increases monotonically with pressure. As indicated earlier, the near continuous recording of the density facilitates differentiation of the V-L two phase region from the homogeneous one-phase region. At higher temperatures, where the fluid is supercritical, the variation of density with pressure is smooth as there is no phase transition.

The density-pressure isotherms were fitted to quadratic equation of the form $\rho = a + bP + cP^2$ in the homogeneous domains. These equations are given in Table V.1 and shown also in Figure V.5. The data has been compared with the values from the NIST data base at selected pressures. They are shown in Table V.2 and also in Figure V.5. The average error is less than 1%. Overall, the agreement is excellent considering the rapidity with which such data are generated. The error increases at the higher temperatures. This, as will be discussed later also, stems from small leaks that develop in the system at higher temperatures, which leads to slightly higher values for densities.

Table V.1 *Density (g/cm^3)-Pressure (MPa) and Density-Temperature (K) correlations for CO$_2$.*

	Density (g/cm^3)-Pressure (MPa) correlations	T (K)	P range (MPa)
CO$_2$	$\rho = 0.7066 + 1.565 \cdot 10^{-2} P - 2.140 \cdot 10^{-4} P^2$	295K	10MPa<P<32MPa
	$\rho = 0.6452 + 1.753 \cdot 10^{-2} P - 2.393 \cdot 10^{-4} P^2$	300K	11MPa<P<32MPa
	$\rho = 0.4117 + 2.671 \cdot 10^{-2} P - 3.651 \cdot 10^{-4} P^2$	320K	15MPa<P<32MPa
	$\rho = 0.0421 + 4.523 \cdot 10^{-2} P - 6.604 \cdot 10^{-4} P^2$	340K	16MPa<P<32MPa
	$\rho = -0.0328 + 4.059 \cdot 10^{-2} P - 5.056 \cdot 10^{-4} P^2$	360K	21MPa<P<32MPa
	Density(g/cm^3)-Temperature (K) correlations	P (MPa)	T range (K)
CO$_2$	$\rho = 3.3756 - 8.5152 \cdot 10^{-3} T$	12 MPa	295 K<T<300 K
	$\rho = 2.8738 - 6.6822 \cdot 10^{-3} T$	16 MPa	295 K<T<340 K
	$\rho = 2.5533 - 5.4952 \cdot 10^{-3} T$	20 MPa	295 K<T<340 K
	$\rho = 2.3388 - 4.6856 \cdot 10^{-3} T$	24 MPa	295 K<T<360 K
	$\rho = 2.1789 - 4.0849 \cdot 10^{-3} T$	28 MPa	295 K<T<360 K
	$\rho = 2.5533 - 5.4952 \cdot 10^{-3} T$	32 MPa	295 K<T<360 K

Table V.2 *Comparison of CO$_2$ densities with literature values from NIST data base.*

	T (K)									
	295		300		320		340		360	
P (MPa)	ρ_{lit} (g/cm^3)	ρ_{exp} (g/cm^3)	ρ_{lit} (g/cm^3)	ρ_{exp} (g/cm^3)	ρ_{lit} (g/cm^3)	ρ_{exp} (g/cm^3)	ρ_{lit} (g/cm^3)	ρ_{exp} (g/cm^3)	ρ_{lit} (g/cm^3)	ρ_{exp} (g/cm^3)
10	0.8427	0.8417	0.8016	0.7966	0.4483	-	0.2586	-	0.2083	-
15	0.8940	0.8932	0.8658	0.8543	0.7268	0.7302	0.5356	-	0.3871	-
20	0.9287	0.9340	0.9056	0.9001	0.8023	0.7999	0.6797	0.6825	0.5515	-
25	0.9557	0.9641	0.9354	0.9339	0.8487	0.8513	0.7527	0.7601	0.6517	0.6660
30	0.9780	0.9835	0.9597	0.9557	0.8830	0.8844	0.8012	0.8046	0.7166	0.7299

Figure V.6 shows the variation of density with temperature at selected pressures from 12 to 32 MPa. In this temperature interval, density shows linear decrease with temperature given by the equations in Table V.1.
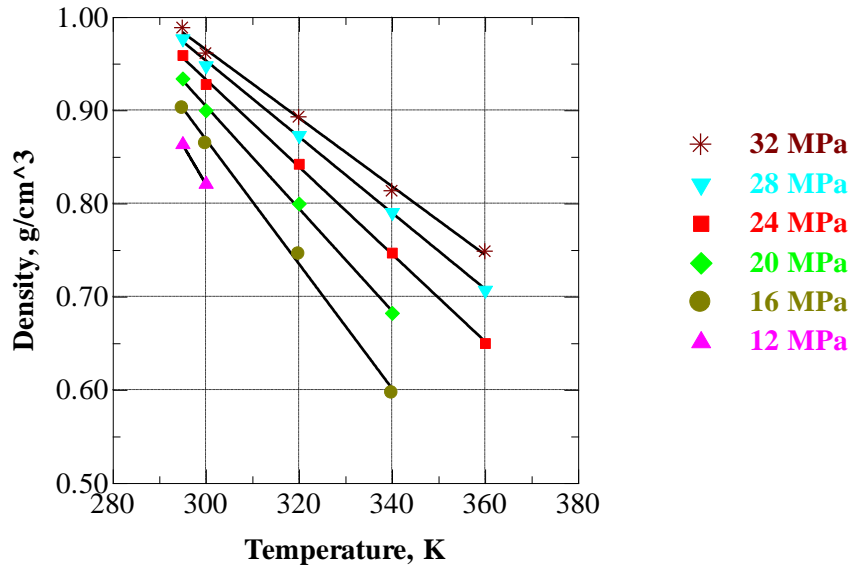
Figure V.6 *Temperature dependence of density of CO_2 at selected pressures.*

V.1.3.2 Isothermal compressibility, isobaric expansivity, and isochoric pressure coefficients

Using the equations describing the variation of density with pressure and temperature given in Table V.1, isothermal compressibility k_T, isobaric expansivity α_P and isochoric thermal pressure coefficient γ_ρ for carbon dioxide have been evaluated using the following relationships:

$$k_T = -\frac{1}{V_m}\left(\frac{\partial V_m}{\partial P}\right)_T = \frac{1}{\rho}\left(\frac{\partial \rho}{\partial P}\right)_T \tag{V.2}$$

$$\alpha_P = \frac{1}{V_m}\left(\frac{\partial V_m}{\partial T}\right)_P = -\frac{1}{\rho}\left(\frac{\partial \rho}{\partial T}\right)_P \tag{V.3}$$

$$\gamma_\rho = \left(\frac{\partial P}{\partial T}\right)_\rho = \frac{\alpha_P}{k_T} \tag{V.4}$$

The results are shown in Figures V.7-9. Isothermal compressibility and isobaric expansivity values increase with temperature, but decrease with pressure. Both of these coefficients show a greater change with the temperature at the lower pressures. Compressibility values are in the range from 0.002 to 0.04 MPa^{-1}. Expansivity values are in the range from 3.7 to

$11x10^{-3}$ K^{-1}. At a fixed pressure, the thermal pressure coefficient decreases with the increasing temperature. At a given temperature, it increases with pressure. The values are in the range from 0.3 to 1.9 MPa/K (Falco and Kiran, 2012).
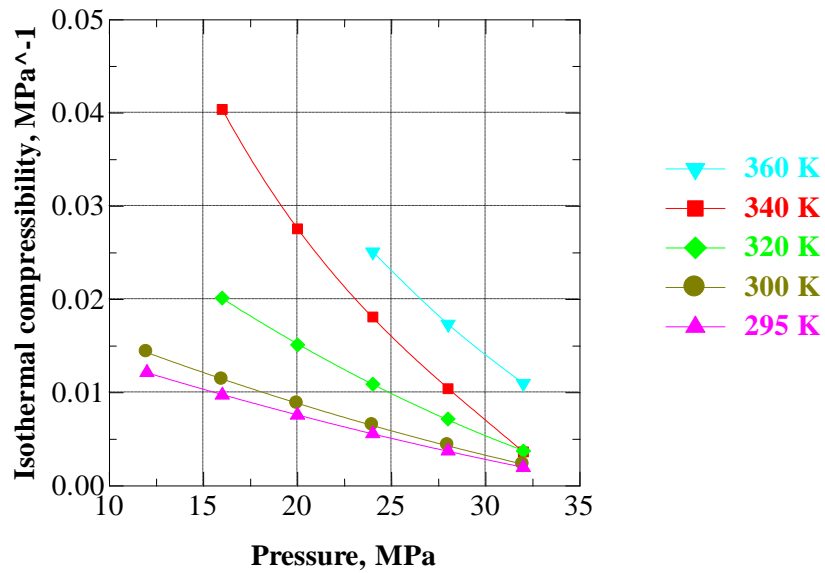
Figure V.7 *Isothermal compressibility k_T of CO_2 at selected temperatures.*
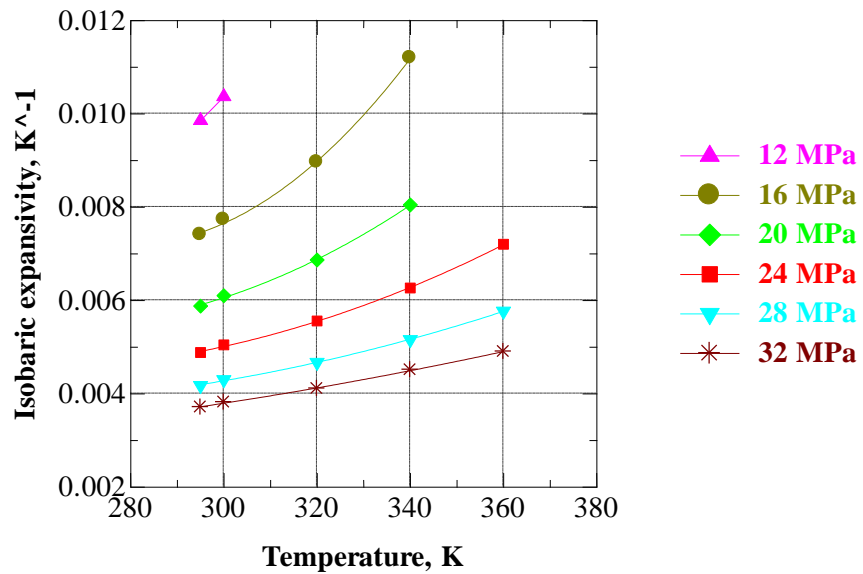
Figure V.8 *Isobaric expansivity α_P of CO_2 at selected pressures.*
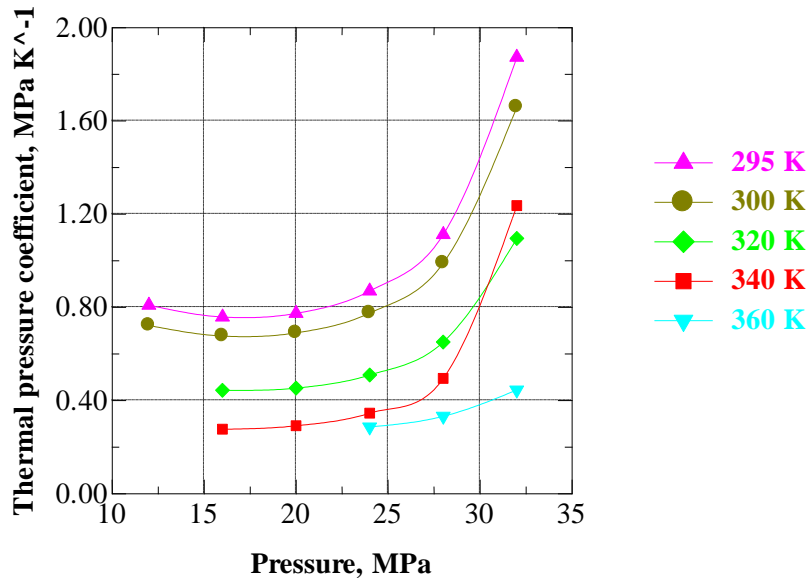
Figure V.9 *Thermal pressure coefficient γ_ρ of CO_2 at selected temperatures.*

Isothermal compressibility values for CO_2 were reported earlier in the literature at 298, 323 and 348 K (Zhuang and Kiran, 1996). At 298 K, the literature values are in the range 0.06 to 0.005 MPa^{-1} in going from 5 to 20 MPa; at 323 K, they are in the range 0.07 to 0.005 MPa^{-1} in going from 10 to 30 MPa, and at 348 K in the range 0.08 to 0.01 MPa^{-1} in going from 15 to 30 MPa. The present values are in a similar range. A recent article provides isothermal compressibility data for mixtures of carbon dioxide with dimethyl carbonate (Hou et al., 2010) in the temperature range from 308 to 337 K, but at a lower pressure range from 6 to 17 MPa. Even though k_T values are not given for pure carbon dioxide at these conditions, for a mixture containing 0.98 mole percent of CO_2, the values are reported to be below 0.05 MPa^{-1} for pressures in the range 10-15 MPa.

V.1.4 Ethyl acetate

V.1.4.1 Density

Figure V.10 shows the density data for ethyl acetate at 295, 320, 340, 360 and 380 K. The pressures ranges investigated were up to 28 MPa at 295 K, 320 K and 340 K; up to 20 MPa at 360 K, and up to 13 MPa for 380 K. The density values in the pressure increase and decrease directions were almost identical with some minor hysteresis observed at 320 and 340 K. In these experiments, the average rates of compression and decompressions were

0.140 MPa/s and 0.154 MPa/s, respectively. Piston velocities were about 0.017 mm/s.

These temperatures are all below the critical temperature of ethyl acetate (T_c = 523.1 K). A density range from about 0.80 to 0.92 g/cm^3 has been covered. Linear equations of the form $\rho = a + bP$ were used to correlate the density at each temperature. These equations are given in Table V.3 and are included in Figure V.10.
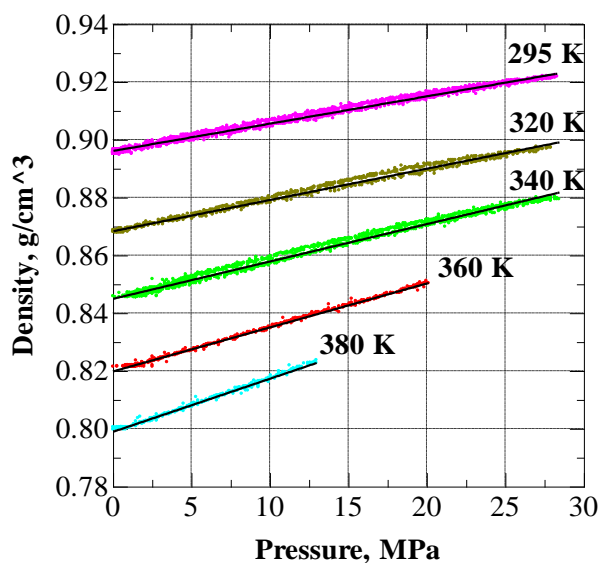
Figure V.10 *Pressure dependence of density of EA at selected temperatures. The solid lines are the linear fits to the data.*

Figure V.11 shows the variation of density with temperature for ethyl acetate at selected pressures from 4 to 28 MPa. These again could be represented by linear equations which are shown in the figure and are given in Table V.3.
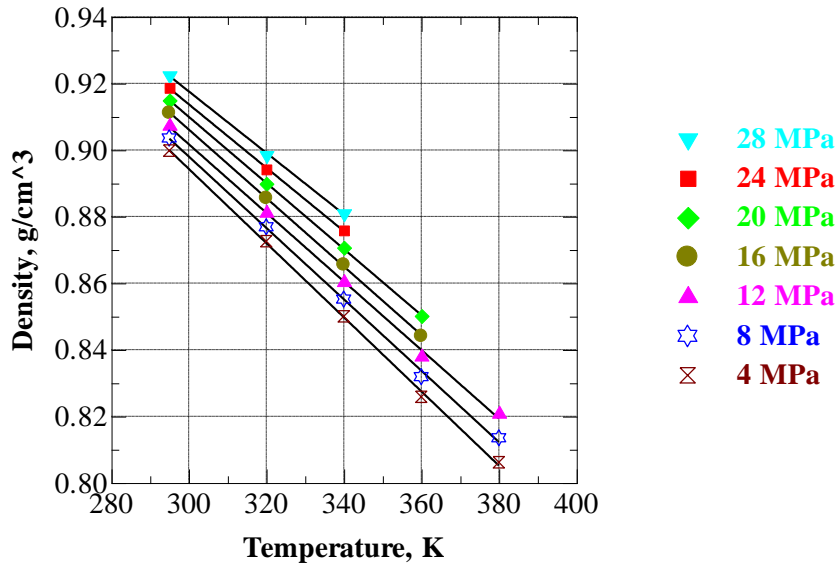
Figure V.11 *Variation of density of EA with temperature at selected pressures.*

Table V.3 *Density (g/cm³)-Pressure (MPa) and Density-Temperature (K) correlations for ethyl acetate.*

	Density (g/cm³)-Pressure (MPa) correlations	T (K)	P range (MPa)
	$\rho = 0.8960 + 0.946 \cdot 10^{-3} P$	295K	0.05MPa<P<28MPa
	$\rho = 0.8683 + 1.081 \cdot 10^{-3} P$	320K	0.05MPa<P<28MPa
EA	$\rho = 0.8448 + 1.293 \cdot 10^{-3} P$	340K	0.05MPa<P<28MPa
	$\rho = 0.8197 + 1.522 \cdot 10^{-3} P$	360K	0.05MPa<P<20MPa
	$\rho = 0.7988 + 1.837 \cdot 10^{-3} P$	380K	0.05MPa<P<13MPa
	Density(g/cm³)-Temperature (K) correlations	P (MPa)	T range (K)
	$\rho = 1.229 - 1.114 \cdot 10^{-3} T$	4 MPa	295 K<T<380 K
	$\rho = 1.220 - 1.072 \cdot 10^{-3} T$	8 MPa	295 K<T<380 K
	$\rho = 1.211 - 1.030 \cdot 10^{-3} T$	12 MPa	295 K<T<380 K
EA	$\rho = 1.215 - 1.029 \cdot 10^{-3} T$	16 MPa	295 K<T<360 K
	$\rho = 1.208 - 0.9928 \cdot 10^{-3} T$	20 MPa	295 K<T<360 K
	$\rho = 1.200 - 0.9528 \cdot 10^{-3} T$	24 MPa	295 K<T<340 K
	$\rho = 1.194 - 0.9223 \cdot 10^{-3} T$	28 MPa	295 K<T<340 K

The density data for saturated ethyl acetate are available at atmospheric pressure over the temperature range from 273 to 523 K (Vargaftik, 1975). As shown in Figure V.12, the values obtained in the present study are in very close agreement with the literature values.
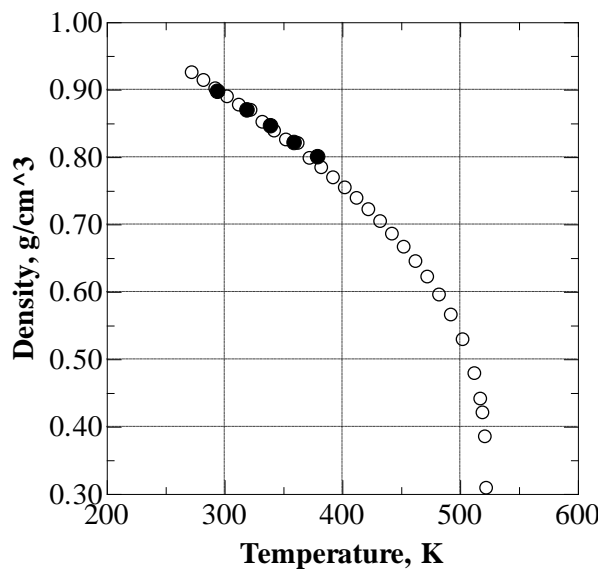
Figure V.12 *Comparison of density data of EA (filled symbols) at atmospheric pressure at different temperatures with literature values (open symbols) from Vargaftik (1975).*

Density values for ethyl acetate at high pressures have also been previously reported. One data set is at 313 K in the pressures range from 0.1 to 21 MPa (Smith et al., 1998). A more recent publication (Gardas et al., 2007) provides density data over a wider range of temperatures (from 298 to 393 K) at pressures up to 35 MPa. Table V.4 illustrates a comparison of the densities at 20 MPa reported by Gardas et al. (2007) with the values from the present study using the density-temperature correlations at this pressure given in Table V.3. They are in close agreement with deviations being in the range from 0.19 to 0.92%. The higher deviations at high temperatures, which were also observed in carbon dioxide density measurements, most likely arise from small leaks in the system over time as measurements are carried out on a given loading starting with low temperatures.

Table V.4 *Comparison of EA density values at 20 MPa with literature (Gardas et al., 2007).*

	T (K)							
	313	**313**	**323**	**323**	**343**	**343**	**363**	**363**
	lit	*exp*	*lit*	*exp*	*lit*	*exp*	*lit*	*exp*
ρ (g/cm³)	0.8954	0.8971	0.8843	0.8871	0.8630	0.8673	0.8397	0.8474
% difference		0.19		0.32		0.50		0.92

V.1.4.2 Isothermal compressibility, isobaric expansivity, and isochoric pressure coefficients

From the density *vs* pressure and temperature correlations, the parameters k_T, α_P, γ_ρ for pure ethyl acetate have also been determined.

Figure V.13 shows the pressure dependence of the isothermal compressibility at selected temperatures. The isothermal compressibility displays the expected decrease with pressure and increase with temperature. The values are in the range from about 1.0 to 2.3×10^{-3} MPa^{-1}, which are much lower (by a factor of about 10-30) than the compressibility values for carbon dioxide over the same P/T range.
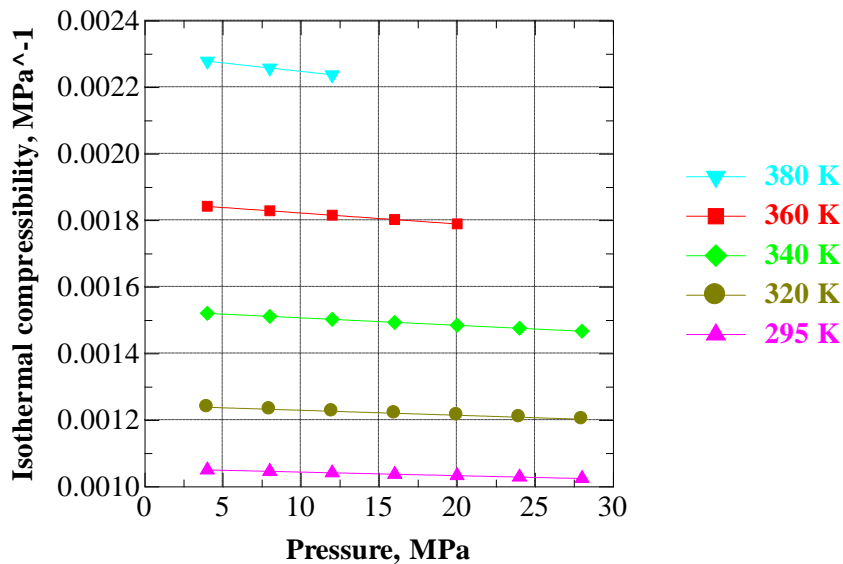
Figure V.13 *Variation of isothermal compressibility k_T of EA at selected temperatures.*

Figure V.14 shows the variation of the isobaric expansivity with temperature at selected pressures. Isobaric expansivity increases with temperature and decreases with pressure. The rate of increase with temperature is noted to be slightly higher at lower pressures. The expansivity values are in the range 1.0 to 1.4×10^{-3} K^{-1}, which are less than the values for CO_2 (by a factor of about 5-8).
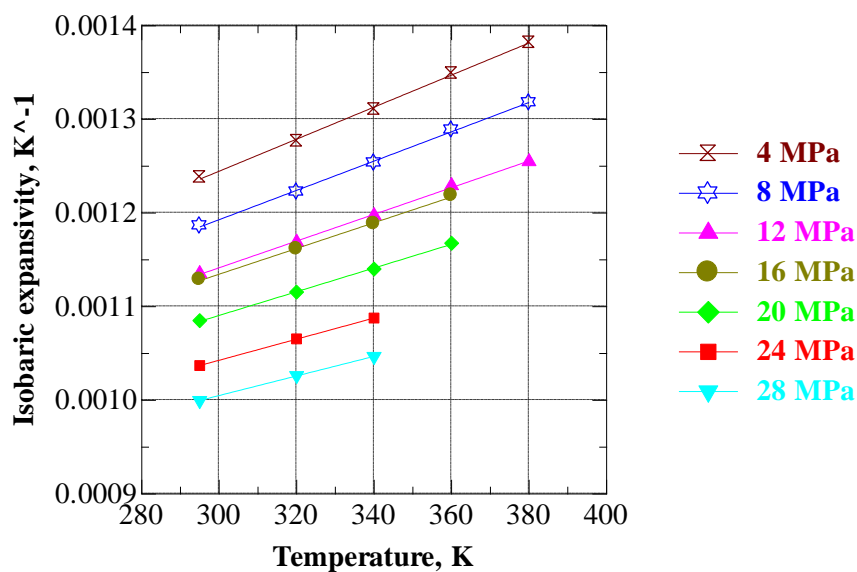
Figure V.14 *Isobaric expansivity α_P of EA at selected pressures.*

The thermal pressure coefficient γ_ρ for ethyl acetate is shown in Figure V.15. As expected, the thermal pressure coefficient decreases with increasing temperature. Along each isotherm, it decreases with pressure. Thermal pressure coefficients are in the range from 0.55 to 1.2 MPa/K, which are higher than that for CO_2 by a factor of about 2.
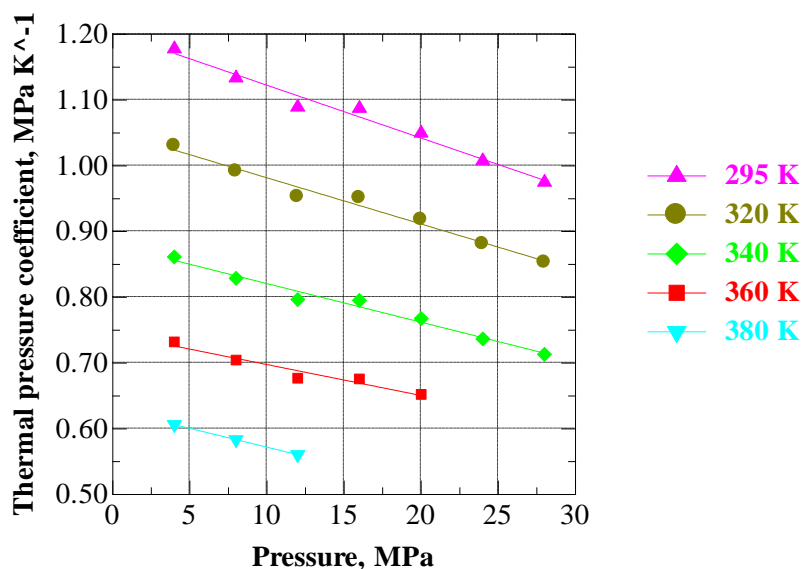
Figure V.15 *Thermal pressure coefficient γ_ρ of EA at selected temperatures.*

There is one earlier study in the literature that has reported on the compressibility, expansivity and the thermal pressure coefficients for ethyl acetate (Gardas et al., 2007). The values and the trends are in very close agreement with the present observations. In the 10-30 MPa range, depending on the temperature, compressibility values reported in the literature are in the range $1.0\text{-}2.5 \times 10^{-3}$ MPa^{-1}; expansivity values are in the range $1.1\text{-}1.6 \times 10^{-3}$ K^{-1}, and pressure coefficients are in the range 0.6-1.3 MPa/K. In the present study, the thermal pressure coefficients are decreasing with pressure, as shown in Figure V.15 at all temperatures investigated. However, in the literature, a similar decreasing trend is noted only at temperatures above 380 K.

It should be pointed out that a recent publication reports on these coefficients for other esters, such as ethyl propionate, ethyl butyrate and ethyl pentanoate, from 298 to 393 K and up to 35 MPa (Costa et al., 2009). For ethyl propionate, compressibility values are reported, which are in the range $1.0\text{-}2.5 \times 10^{-3}$ MPa^{-1}, while for ethyl butyrate expansivity values are reported, which are in the range $1.0\text{-}1.6 \times 10^{-3}$ K^{-1}, both of which are similar to the values for ethyl acetate. For ethyl propionate, thermal pressure coefficients that are reported are in the range 0.77-1.05 MPa/K, which are somewhat lower than that for ethyl acetate. However, for ethyl propionate pressure coefficients are reported to increase with pressure, which is a trend opposite to that observed with carbon dioxide or ethyl acetate.

V.1.5 Ethyl acetate+carbon dioxide mixtures

V.1.5.1 Density

The densities for ethyl acetate+CO_2 mixtures have been determined for solutions containing 27.7, 42.6, 52.9 and 67.3% by mass CO_2 at selected temperatures in the range 295-340 K at pressures up to 30 MPa. The results are shown in Figures V.16-19. Along each isotherm, the two-phase, vapor-liquid region where large density changes occur with small variations in pressure, and the homogeneous liquid region where the density changes monotonously with pressure are easily noted. In these experiments, the average rates of pressure increase and decrease were 0.137 MPa/s and 0.134 MPa/s, respectively. Piston velocities were around 0.03 mm/s during the pressure increase and around 0.02 mm/s during pressure decrease stages.

The pressure dependence of the experimental densities in the one-phase region was correlated using quadratic equations of the form $\rho = a + bP + cP^2$. The equations are given in Table V.5. They are also included in Figures V.16-19. These correlations provide the average values of the densities obtained during pressure scans in both the pressure-increase and decrease-directions. The hysteresis is more apparent in these binary mixtures where the density values obtained tend to be higher (volumes that are recorded tend to be smaller) in the pressure-reduction direction then the pressure-increase direction.
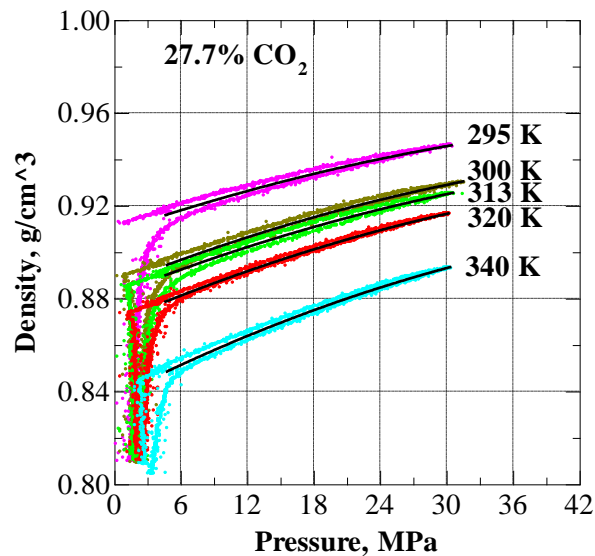
Figure V.16 *Pressure dependence of density of EA+CO_2 mixture with 27.7 wt % CO_2 at 295, 300, 313, 320 and 340 K.*
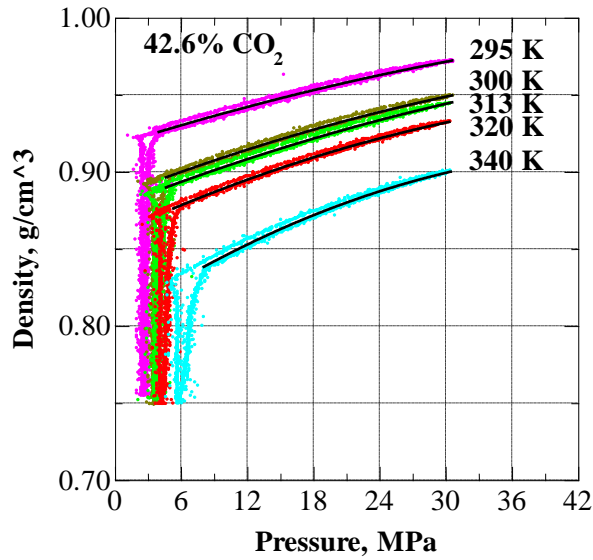
Figure V.17 *Pressure dependence of density of EA+CO$_2$ mixture with 42.6 wt % CO$_2$ at 295, 300, 313, 320 and 340 K .*
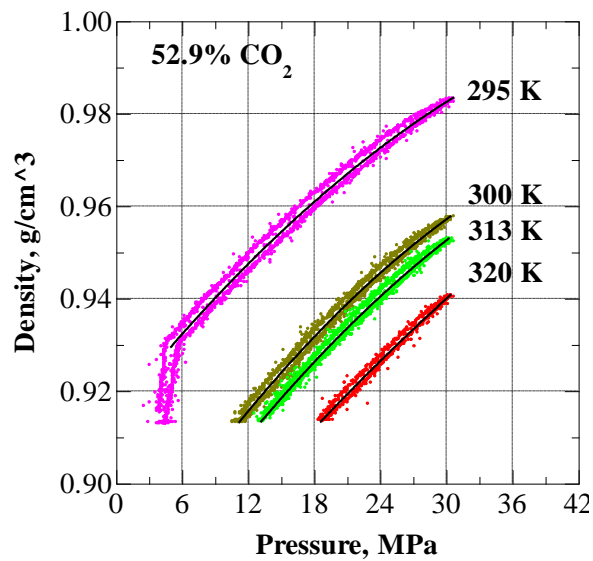
Figure V.18 *Pressure dependence of density of EA+CO$_2$ mixture with 52.9 wt % CO$_2$ at 295, 300, 313, 320 and 340 K.*
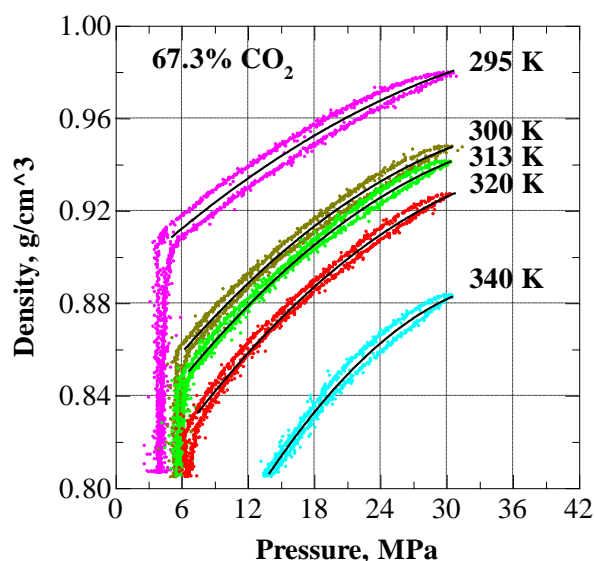
Figure V.19 *Pressure dependence of density of EA+CO$_2$ mixture with 67.3 wt % CO$_2$ at 295, 300, 313, 320 and 340 K.*

Figures V.20-23 show comparative plots for the different mixtures at 295, 300, 320 and 340 K. These figures include also the density data for pure CO$_2$ and ethyl acetate. As shown, ethyl acetate has a relatively low compressibility as displayed by the steep increase in pressure required to bring about changes in density. For example, in Figure V.20, at 295 K, the density of ethyl acetate changes only from about 0.90 to 0.93 g/cm^3 when the pressure is changed from about 6 to 30 MPa, while in the same interval the density of carbon dioxide increases from 0.60 to 0.98 g/cm^3. With increasing pressure, the density of carbon dioxide becomes greater than that of ethyl acetate at around 17 MPa.

As shown in Figure V.20, the mixtures are all more compressible than pure ethyl acetate (densities of the binary mixture are higher than the density of pure ethyl acetate), and each mixture shows a density crossover (i.e., the density of the mixture becomes greater than that of pure ethyl acetate) at a characteristic pressure. At a given pressure, density goes through a maximum with increasing CO$_2$ mass fraction in the mixture. For example, at 15 MPa density increases with increasing CO$_2$ content up to 52.9 mass %. The density of the mixture containing 67.3% CO$_2$ is however lower than that of the mixture containing 52.9% CO$_2$ at the same pressure condition. As will be discussed later, excess volume becomes less negative for mixtures with carbon dioxide content higher than about 50 wt %. As the CO$_2$ content is increased, the slope of the mixture density *vs* pressure becomes less steep, as it should gradually fold over to attain the shape of the isotherm for pure CO$_2$. Similar trends are observed at the other temperatures (Figures V.21-23),

which show the variation of density with pressure at 300, 320 and 340 K. The densities of the mixtures at these temperatures are mostly higher than the density of pure CO_2.

Table V.5 *Density (g/cm^3)-Pressure (MPa) correlations for EA+CO_2 mixtures.*

	Density (g/cm^3)-Pressure (MPa) correlations	T (K)	P range (MPa)
27.7% CO₂	$\rho = 0.9087 + 1.620 \cdot 10^{-3} P - 1.297 \cdot 10^{-5} P^2$	295K	5MPa<P<30MPa
	$\rho = 0.8857 + 1.897 \cdot 10^{-3} P - 1.523 \cdot 10^{-5} P^2$	300K	5MPa<P<30MPa
	$\rho = 0.8816 + 1.885 \cdot 10^{-3} P - 1.468 \cdot 10^{-5} P^2$	313K	5MPa<P<30MPa
	$\rho = 0.8695 + 2.034 \cdot 10^{-3} P - 1.562 \cdot 10^{-5} P^2$	320K	5MPa<P<30MPa
	$\rho = 0.8374 + 2.417 \cdot 10^{-3} P - 1.876 \cdot 10^{-5} P^2$	340K	5MPa<P<30MPa
42.6 % CO₂	$\rho = 0.9169 + 2.265 \cdot 10^{-3} P - 1.517 \cdot 10^{-5} P^2$	295K	4MPa<P<30MPa
	$\rho = 0.8838 + 2.783 \cdot 10^{-3} P - 2.081 \cdot 10^{-5} P^2$	300K	5MPa<P<30MPa
	$\rho = 0.8772 + 2.799 \cdot 10^{-3} P - 1.909 \cdot 10^{-5} P^2$	313K	5MPa<P<30MPa
	$\rho = 0.8594 + 3.287 \cdot 10^{-3} P - 2.920 \cdot 10^{-5} P^2$	320K	5MPa<P<30MPa
	$\rho = 0.8039 + 4.647 \cdot 10^{-3} P - 4.902 \cdot 10^{-5} P^2$	340K	8MPa<P<30MPa
52.9 % CO₂	$\rho = 0.9153 + 2.965 \cdot 10^{-3} P - 2.423 \cdot 10^{-5} P^2$	295K	5MPa<P<30MPa
	$\rho = 0.8759 + 3.684 \cdot 10^{-3} P - 3.266 \cdot 10^{-5} P^2$	300K	13MPa<P<30MPa
	$\rho = 0.8714 + 3.550 \cdot 10^{-3} P - 2.825 \cdot 10^{-5} P^2$	313K	13MPa<P<30MPa
	$\rho = 0.8614 + 3.076 \cdot 10^{-3} P - 1.533 \cdot 10^{-5} P^2$	320K	19MPa<P<30MPa
67.3 % CO₂	$\rho = 0.8869 + 4.454 \cdot 10^{-3} P - 4.577 \cdot 10^{-5} P^2$	295K	5MPa<P<30MPa
	$\rho = 0.8232 + 6.306 \cdot 10^{-3} P - 7.309 \cdot 10^{-5} P^2$	300K	6MPa<P<30MPa
	$\rho = 0.8089 + 6.753 \cdot 10^{-3} P - 7.901 \cdot 10^{-5} P^2$	313K	7MPa<P<30MPa
	$\rho = 0.7825 + 7.316 \cdot 10^{-3} P - 8.468 \cdot 10^{-5} P^2$	320K	8MPa<P<30MPa
	$\rho = 0.677 + 11.30 \cdot 10^{-3} P - 15.03 \cdot 10^{-5} P^2$	340K	14MPa<P<30MPa
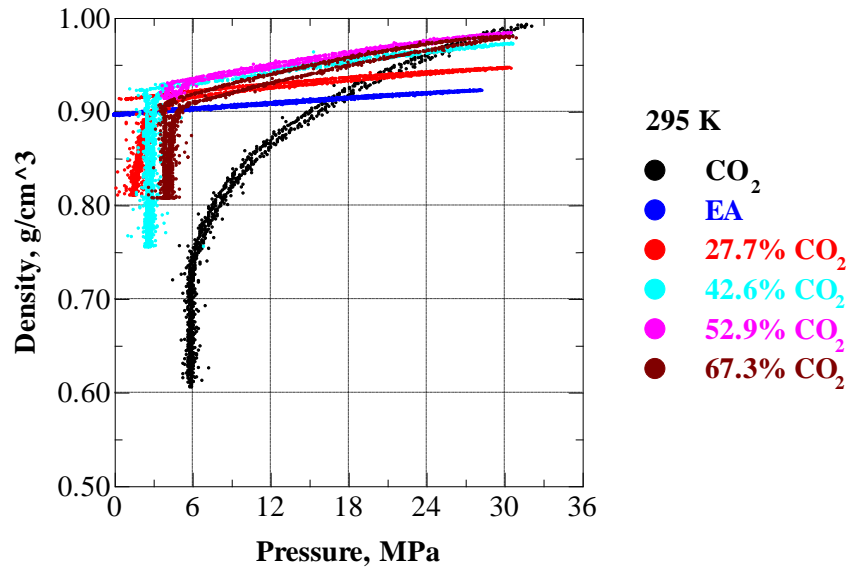
Figure V.20 *Pressure dependence of density of EA+CO₂ mixtures at 295 K (compositions are in mass percent). At 15 MPa, order of curves from higher to lower density: 52.9; 42.6; 67.3; 27.7 % CO₂; pure EA; pure CO₂.*
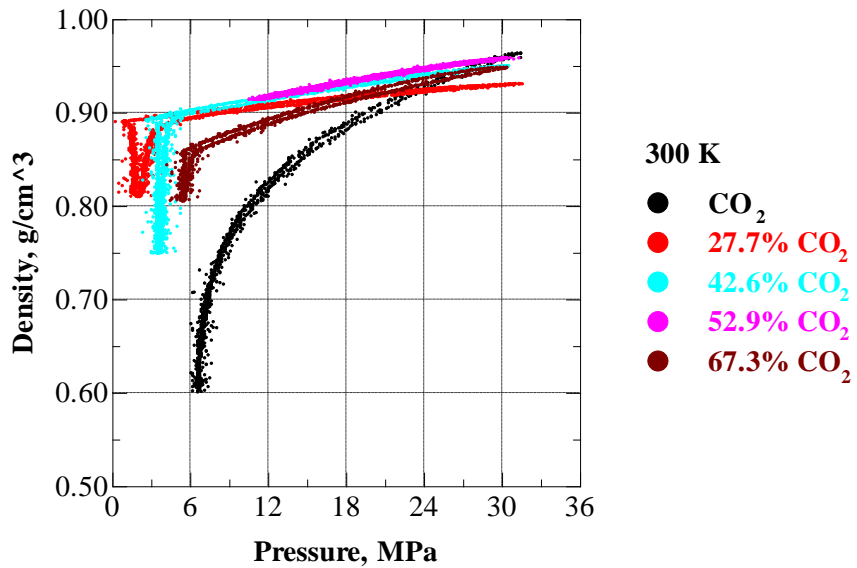
Figure V.21 *Pressure dependence of density of EA+CO₂ mixtures at 300 K (compositions in mass percent). At 15 MPa, order of curves from higher to lower density: 52.9; 42.6; 27.7; 67.3 % CO₂; pure CO₂.*
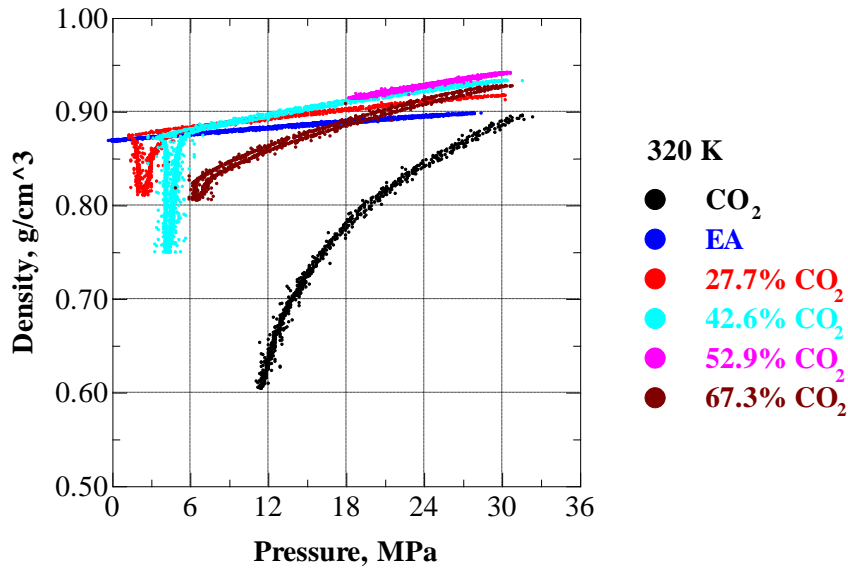
Figure V.22 *Pressure dependence of density of EA+CO$_2$ mixtures at 320 K (compositions in mass percent). At 20 MPa, order of curves from higher to lower density: 52.9; 42.6; 27.7; 67.3 % CO$_2$; pure EA; pure CO$_2$.*
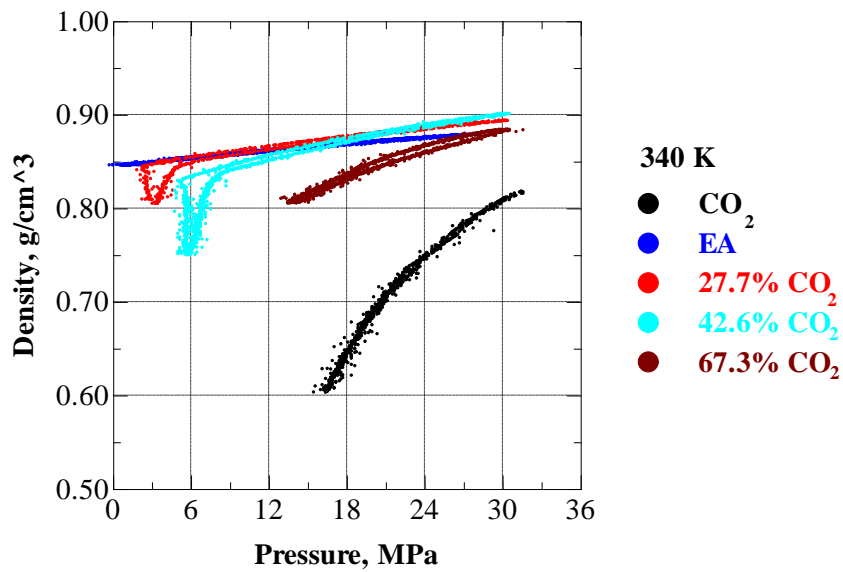
Figure V.23 *Pressure dependence of density of EA+CO$_2$ mixtures at 340 K (compositions in mass percent). At 25 MPa, order of curves from higher to lower density: 42.6; 27.7 % CO$_2$; pure EA; 67.3 % CO$_2$; pure CO$_2$.*

There is only one prior publication that reports densities for ethyl acetate+CO_2 mixtures containing 25, 42.9 and 66.6 wt % CO_2 (Smith et al., 1998). Data are however only at 313 K and at pressures below 20 MPa. Even though not identical with the compositions reported in the literature, for comparisons, density determinations were carried on the mixtures explored in the present study (which contain 27.7, 42.6 and 67.3 % CO_2) at 313 K as well. As shown in Figure V.24, the results are in good relative agreement in the homogeneous regions.
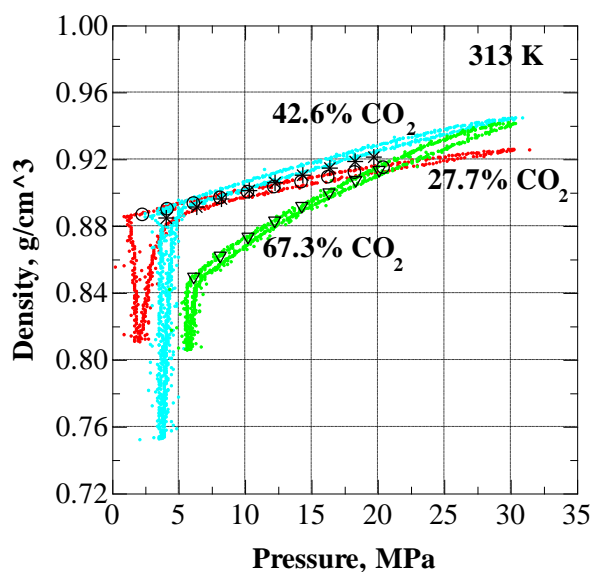
Figure V.24 *Comparisons of density of EA+CO$_2$ mixtures at 313 K with literature data from Smith et al., (1998) (open symbols). At 15 MPa, order of curves from higher to lower density: 42.6; 27.7; 67.3 % CO$_2$.*

Figures V.25-28 show the variation of density of the mixtures with temperature at different pressures from 8 to 30 MPa. The data were fitted to linear equations which are given in Table V.6.
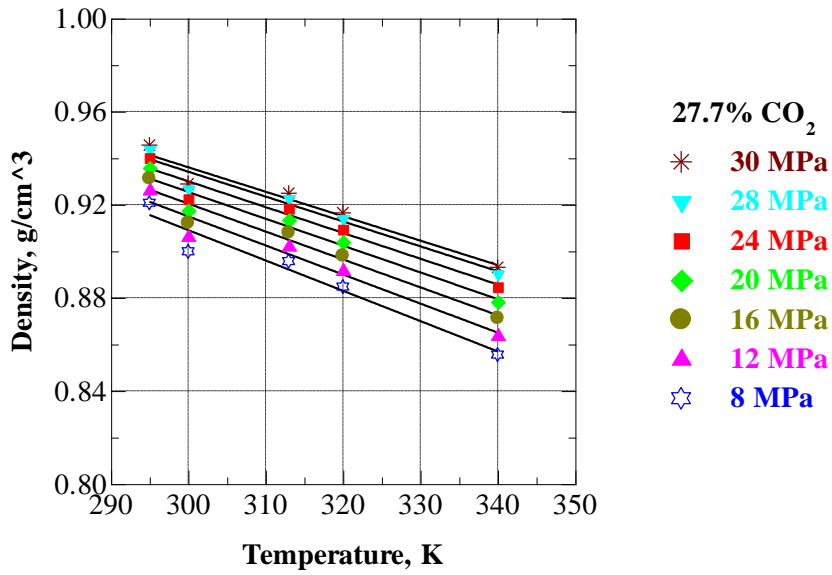
Figure V.25 *Temperature dependence of the density of EA+CO$_2$ mixture containing 27.7 wt % CO$_2$ at selected pressures.*
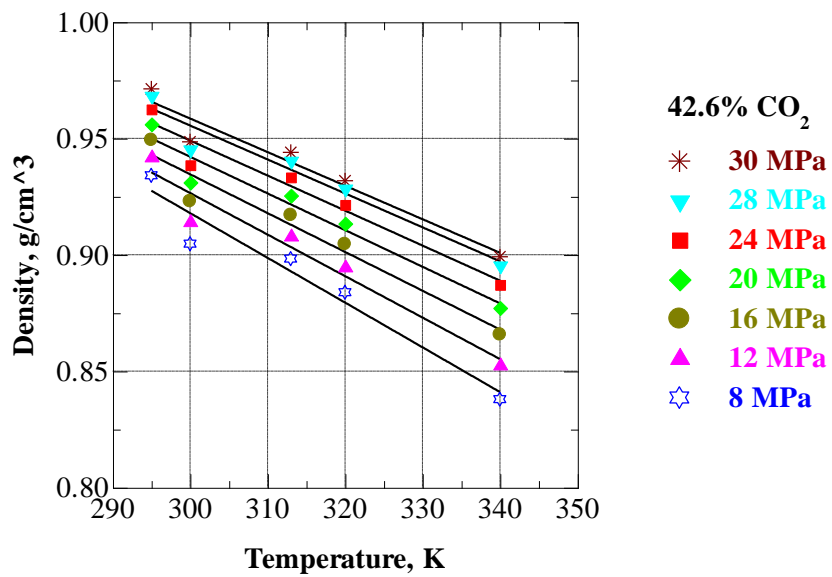
Figure V.26 *Temperature dependence of the density of EA+CO$_2$ mixture containing 42.6 wt % CO$_2$ at selected pressures.*
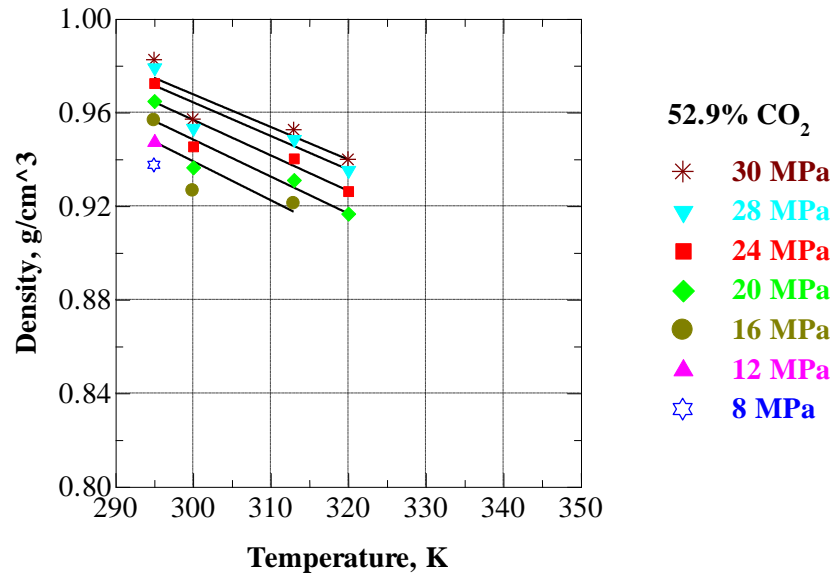
Figure V.27 *Temperature dependence of the density of EA+CO₂ mixture containing 52.9 wt % CO₂ at selected pressures.*
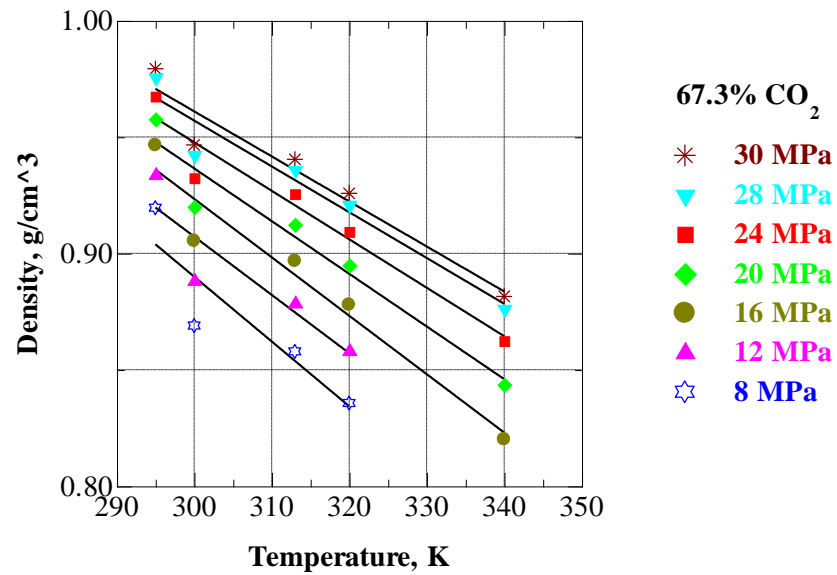
Figure V.28 *Temperature dependence of the density of EA+CO₂ mixture containing 67.3 wt % CO₂ at selected pressures.*

Table V.6 *Density (g/cm^3)-Temperature (K) correlations for EA+CO$_2$ mixtures.*

	Density (g/cm^3)-Temperature (K) correlations	P (MPa)	T range (K)
27.7% CO$_2$	$\rho = 1.300 - 1.303 \cdot 10^{-3} T$	8 MPa	295K<T<340K
	$\rho = 1.290 - 1.249 \cdot 10^{-3} T$	12 MPa	295K<T<340K
	$\rho = 1.280 - 1.199 \cdot 10^{-3} T$	16 MPa	295K<T<340K
	$\rho = 1.271 - 1.152 \cdot 10^{-3} T$	20 MPa	295K<T<340K
	$\rho = 1.263 - 1.109 \cdot 10^{-3} T$	24 MPa	295K<T<340K
	$\rho = 1.255 - 1.069 \cdot 10^{-3} T$	28 MPa	295K<T<340K
	$\rho = 1.251 - 1.051 \cdot 10^{-3} T$	30 MPa	295K<T<340K
42.6 % CO$_2$	$\rho = 1.495 - 1.922 \cdot 10^{-3} T$	8 MPa	295K<T<340K
	$\rho = 1.462 - 1.783 \cdot 10^{-3} T$	12 MPa	295K<T<340K
	$\rho = 1.435 - 1.668 \cdot 10^{-3} T$	16 MPa	295K<T<340K
	$\rho = 1.415 - 1.575 \cdot 10^{-3} T$	20 MPa	295K<T<340K
	$\rho = 1.400 - 1.505 \cdot 10^{-3} T$	24 MPa	295K<T<340K
	$\rho = 1.393 - 1.457 \cdot 10^{-3} T$	28 MPa	295K<T<340K
	$\rho = 1.391 - 1.442 \cdot 10^{-3} T$	30 MPa	295K<T<340K
52.9 % CO$_2$	$\rho = 1.438 - 1.663 \cdot 10^{-3} T$	16 MPa	295K<T<313K
	$\rho = 1.423 - 1.582 \cdot 10^{-3} T$	20 MPa	295K<T<320K
	$\rho = 1.412 - 1.516 \cdot 10^{-3} T$	24 MPa	295K<T<320K
	$\rho = 1.396 - 1.438 \cdot 10^{-3} T$	28 MPa	295K<T<320K
	$\rho = 1.386 - 1.395 \cdot 10^{-3} T$	30 MPa	295K<T<320K
67.3 % CO$_2$	$\rho = 1.725 - 2.782 \cdot 10^{-3} T$	8 MPa	295K<T<320K
	$\rho = 1.658 - 2.503 \cdot 10^{-3} T$	12 MPa	295K<T<320K
	$\rho = 1.677 - 2.510 \cdot 10^{-3} T$	16 MPa	295K<T<340K
	$\rho = 1.616 - 2.263 \cdot 10^{-3} T$	20 MPa	295K<T<340K
	$\rho = 1.572 - 2.082 \cdot 10^{-3} T$	24 MPa	295K<T<340K
	$\rho = 1.547 - 1.967 \cdot 10^{-3} T$	28 MPa	295K<T<340K
	$\rho = 1.541 - 1.935 \cdot 10^{-3} T$	30 MPa	295K<T<340K

V.1.5.2 Isothermal compressibility, isobaric expansivity, and isochoric pressure coefficients

For each ethyl acetate+CO_2 mixture, isothermal compressibility, isobaric expansivity and isochoric thermal pressure coefficients were determined from the density *vs* pressure data shown in Figures V.16-19 and the correlations given in Table V.5 and Table V.6.

Figures V.29-31 show the results for the mixture containing 27.7% by mass CO_2. The compressibility values for this mixture vary in the range from about 0.90 to 2.5×10^{-3} MPa^{-1}. They decrease with increasing pressure or decreasing temperatures. The isobaric expansivity increases with temperature and decreases with pressure. They are in the range from 1.1 to 1.5×10^{-3} K^{-1}. The thermal pressure coefficient decreases with temperature and increases with pressure. The values are in the range of 0.6-1.25 MPa/K.

Figure V.32(a-c) show the isothermal compressibility, Figure V.33(a-c) the isobaric expansivity and Figure V.34(a-c) the isochoric thermal pressure coefficient as a function of temperature and pressure for the other mixtures containing 42.6, 52.9 and 67.3% by mass of CO_2 respectively.

Figure V.35(a-c) shows these quantities at 20 MPa as a function of CO_2 content of the mixture. As illustrated, at a given temperature, compressibility and expansivity values increase with increasing carbon dioxide content in the mixture. This increase becomes more significant at CO_2 levels above 50 wt %. Thermal pressure coefficients show a decrease with CO_2 content.
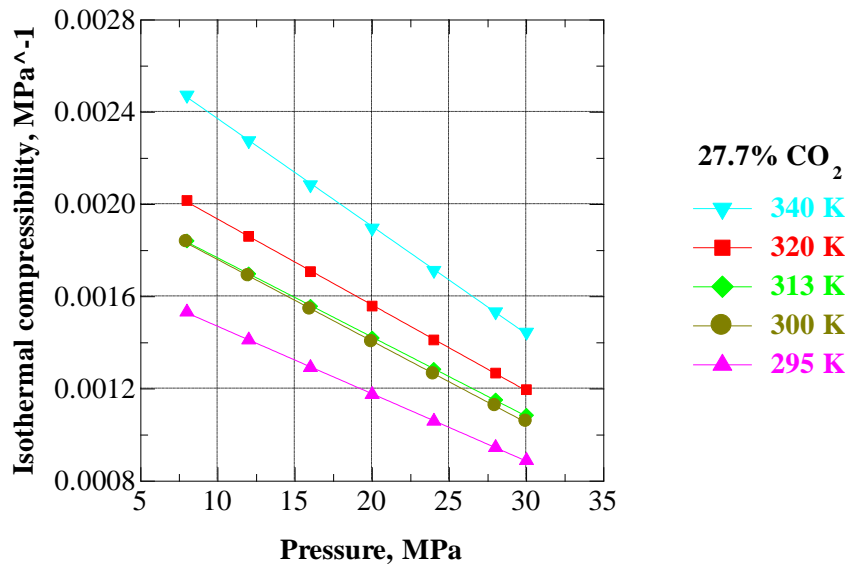
Figure V.29 *Pressure dependence of the isothermal compressibility of EA+CO_2 mixture containing 27.7 wt % CO_2 at selected temperatures.*
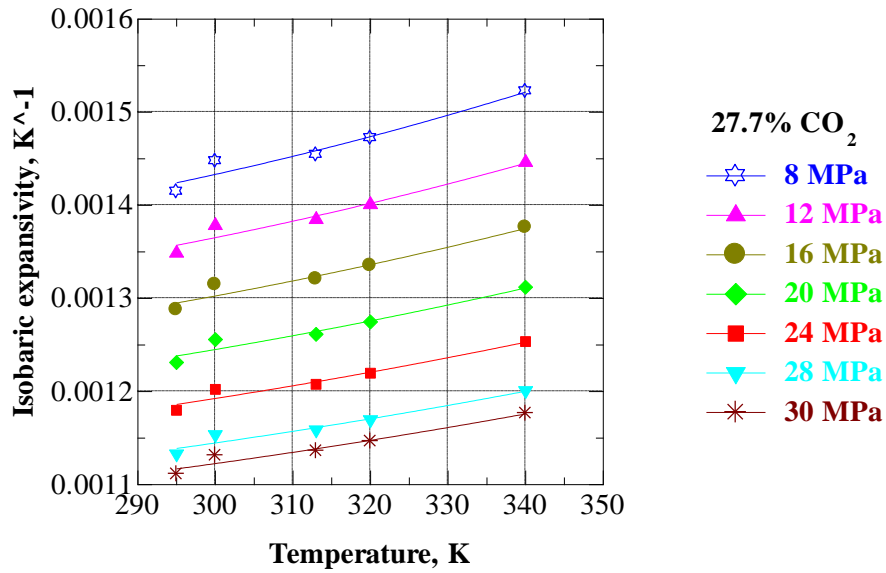
Figure V.30 *Temperature dependence of the isobaric expansivity of EA+CO₂ mixture containing 27.7 wt % CO₂ at selected pressures.*
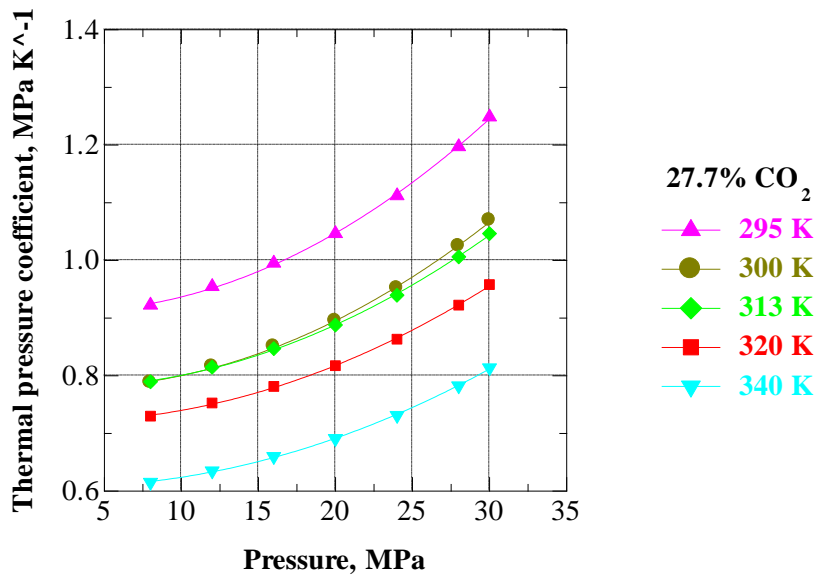
Figure V.31 *Pressure dependence of the thermal pressure coefficient of EA+CO₂ mixture containing 27.7 wt % CO₂ at selected temperatures.*
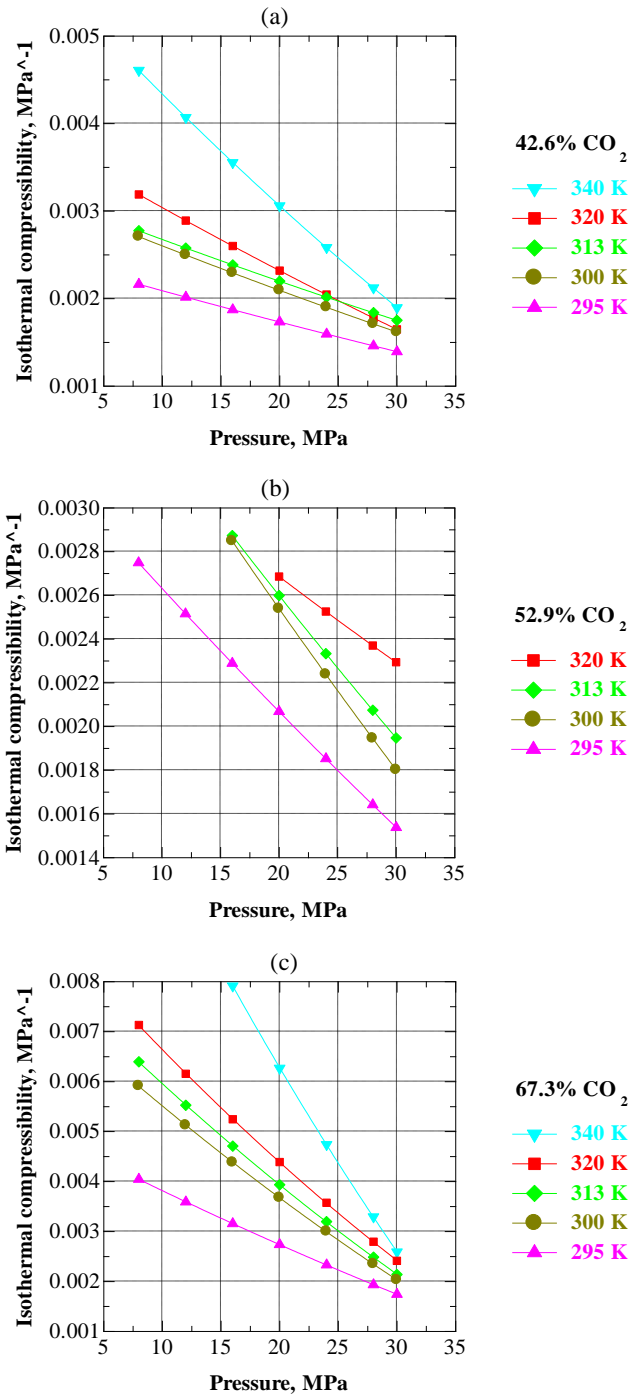
Figure V.32(a-c) *Pressure dependence of the isothermal compressibility of EA+CO₂ mixtures containing (a) 42.6, (b) 52.9, (c) 67.3 wt % CO₂ at selected temperatures.*
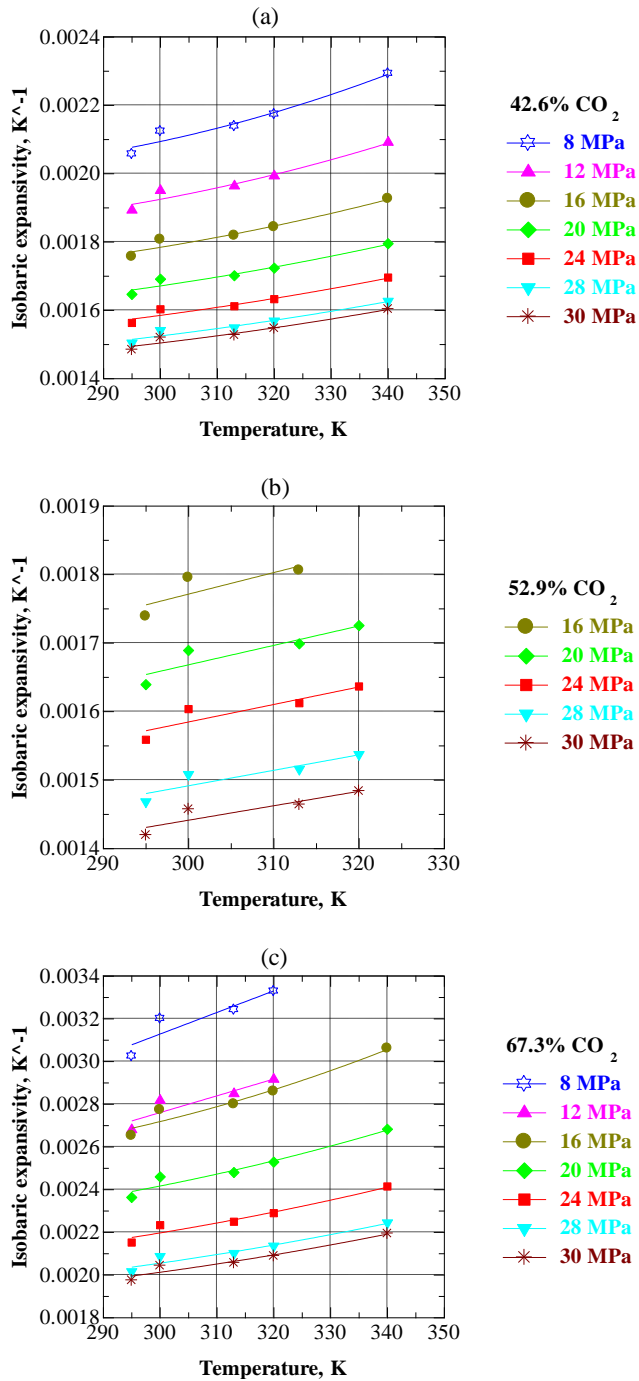
Figure V.33(a-c) *Temperature dependence of the isobaric expansivity of EA+CO₂ mixtures containing (a) 42.6, (b) 52.9, (c) 67.3 wt % CO₂ at selected pressures.*

83
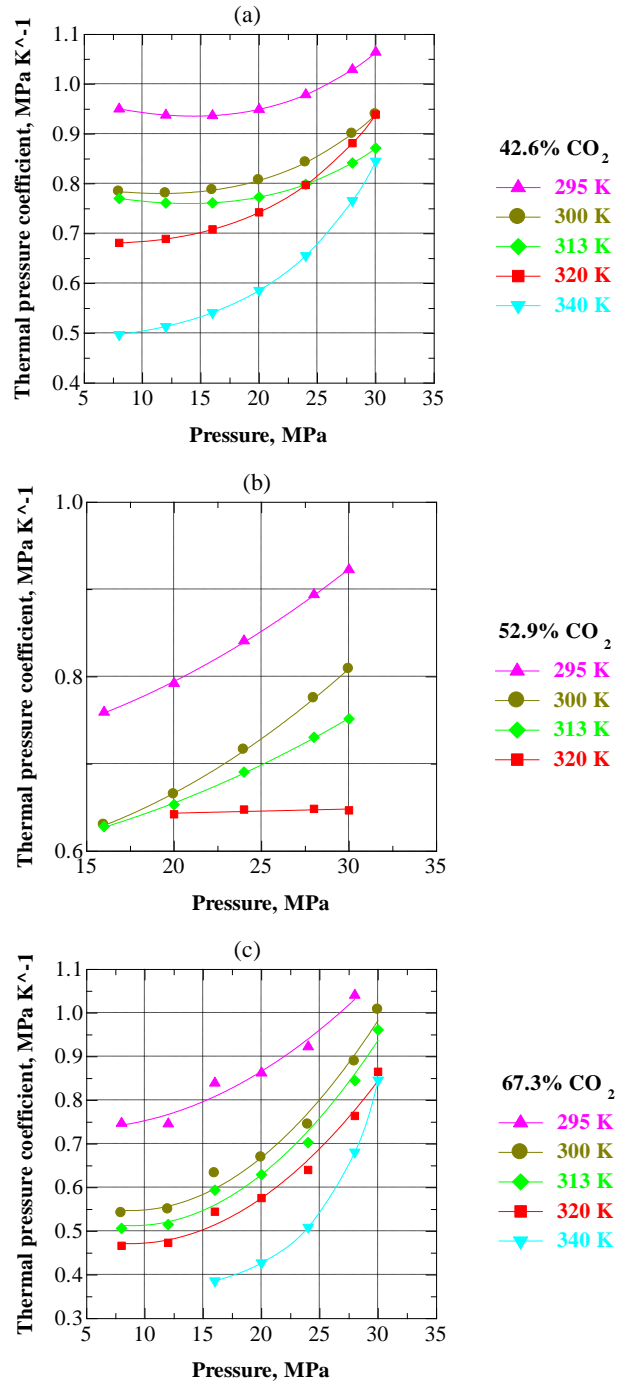
Figure V.34(a-c) *Pressure dependence of the thermal pressure coefficient of EA+CO$_2$ mixtures containing (a) 42.6, (b) 52.9, (c) 67.3 wt % CO$_2$ at selected temperatures.*
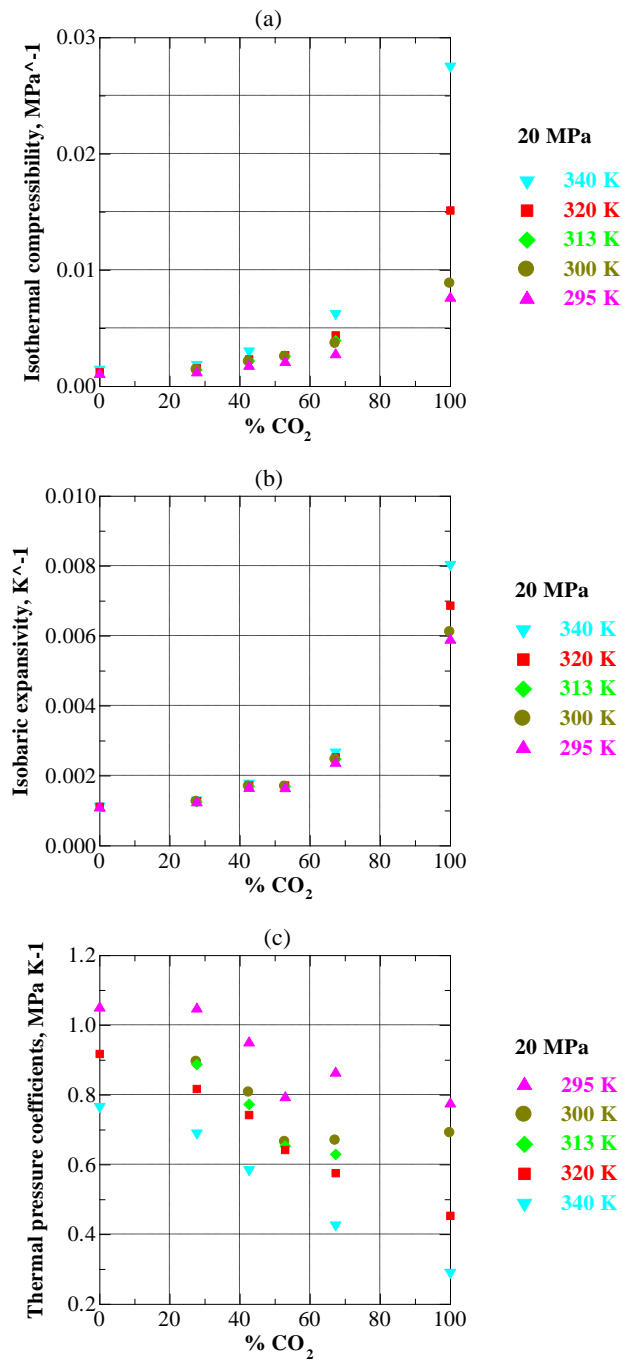
Figure V.35(a-c) *Compositional dependence of the (a) isothermal compressibility, (b) isobaric expansivity and (c) thermal pressure coefficient of pure CO_2, pure ethyl acetate and $EA+CO_2$ mixtures containing 27.7, 42.6, 52.9, 67.3 wt % CO_2 at selected temperatures.*

V.1.6 Excess volume

The excess volumes for the mixtures were determined from the experimental density values using the following relationship in which the densities are on mass basis, whereas excess volume is on molar basis:

$$V^E = \frac{1}{\rho_m} \sum_{i=1}^{2} x_i M_i - \sum_{1=1}^{2} \frac{x_i M_i}{\rho_i}$$

(V.5)

Here ρ_m is the density of the mixture, and x_i, M_i, and ρ_i are the mole fraction, the molar mass and the density of the component *i*, respectively. In these evaluations, density values were calculated from the correlation equations obtained in the present study for a given temperature and pressure.

In Figures V.36-38 excess volumes are shown respectively at 295, 320 and 340 K for different pressures as a function of carbon dioxide mole fraction. As shown, the excess volumes are negative and become more negative with decreasing pressure and increasing temperature. The excess volume goes through its highest negative value for the mixture containing 52.9 wt % (69.2 mole %) CO_2. This composition appears to represent the mixture composition with the highest degree of packing. This is further reflected in the higher densities that are displayed with this mixture, which can be observed from comparisons of Figures V.16-19. The negative values of excess volume in mixtures is indicative of better packing, often arising in asymmetric systems that involve molecules of different sizes displaying differences in free volumes (Pensado et al., 2008). Negative excess volumes are common in mixtures of carbon dioxide with organic solvents and have been reported for mixtures of CO_2 with pentaerythritol tetra-2-ethylhexanoate (Pensado et al., 2008), toluene (Pöhler and Kiran, 1996) ethanol (Pöhler and Kiran, 1997a) and acetone (Pöhler and Kiran, 1997b). As would be anticipated, when pressure is increased, the magnitude of the negative excess volume should be reduced. This is clearly observed in Figures V.39-41, which show the excess volumes at 16, 20 and 28 MPa at the respective temperatures.
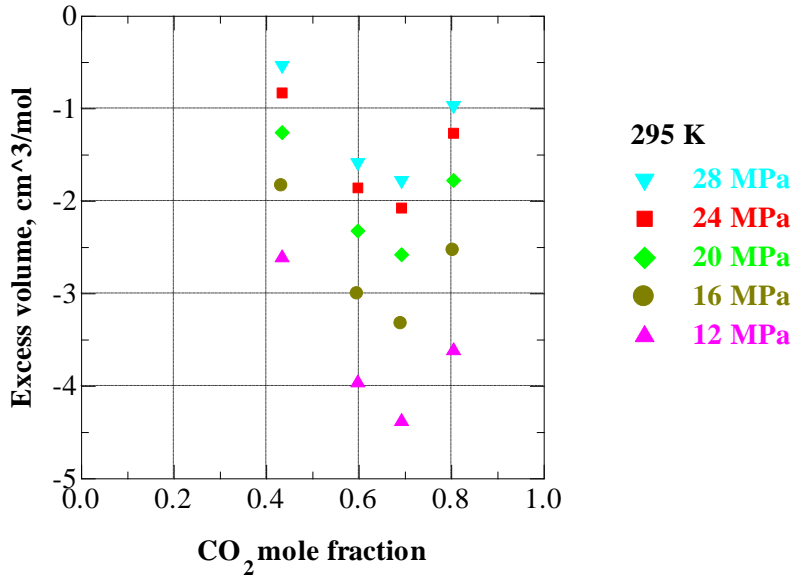
Figure V.36 *Excess volume in EA+CO₂ mixtures at 295 K.*
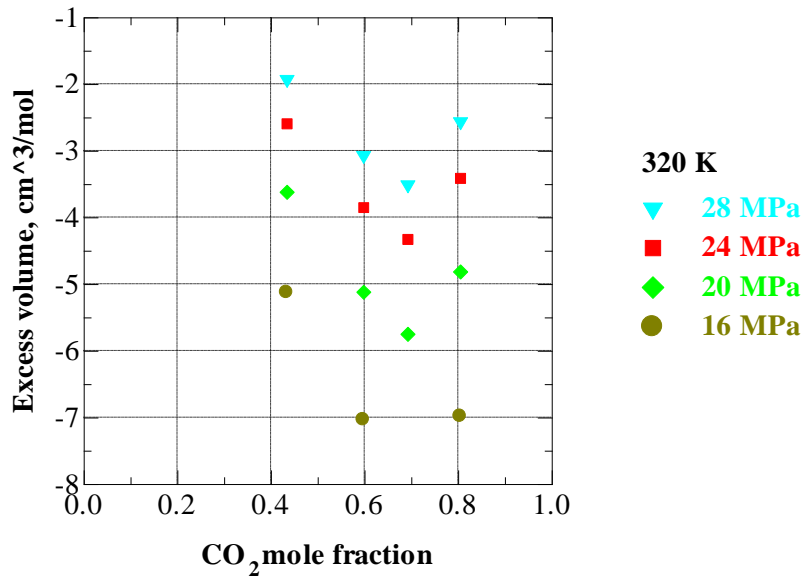
Figure V.37 *Excess volume in EA+CO₂ mixtures at 320 K.*
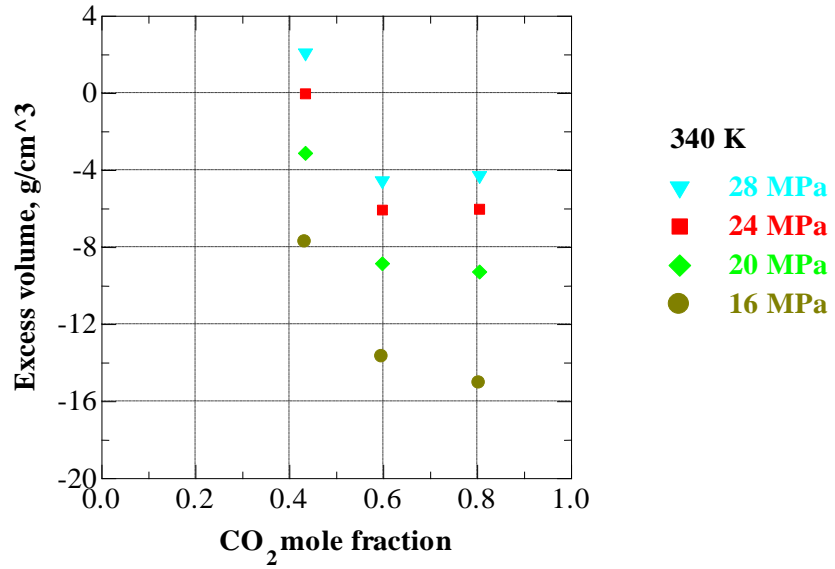
Figure V.38 *Excess volume in EA+CO₂ mixtures at 340 K.*
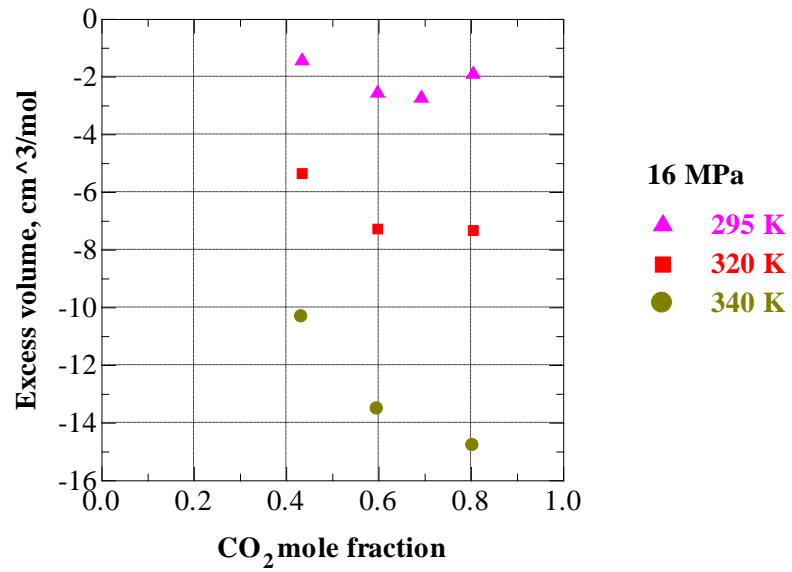
Figure V.39 *Excess volume in EA+CO₂ mixtures at 16 MPa.*
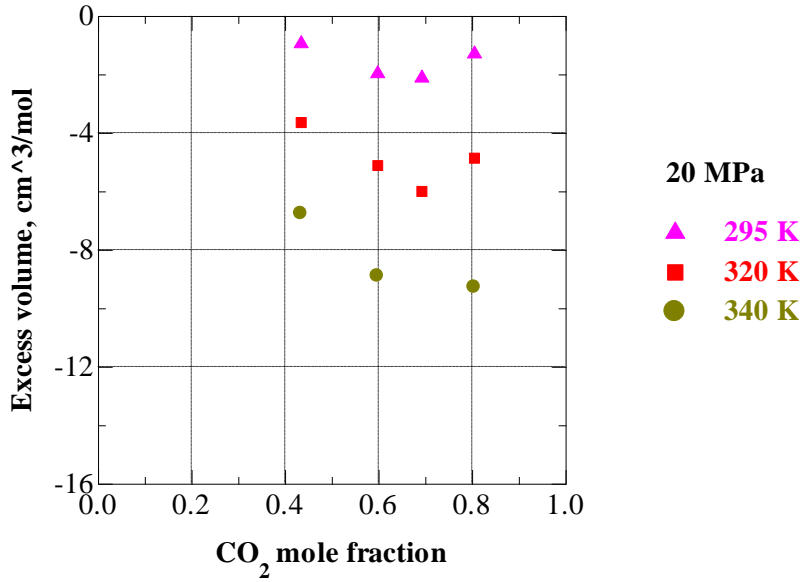
Figure V.40 *Excess volume in EA+CO₂ mixtures at 20 MPa.*
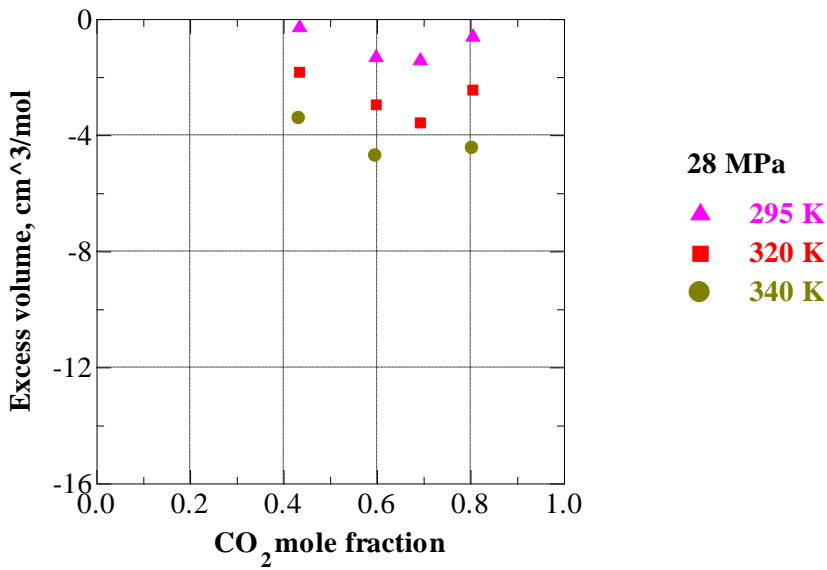
Figure V.41 *Excess volume in EA+CO₂ mixtures at 28 MPa.*

V.2 SEE-C operating parameters

Operating pressure and temperature conditions were selected to enhance the extraction of the oily dispersed phase of the emulsion. Extraction pressure and temperature conditions of 80 bar and 38°C, respectively, were selected for processing emulsions, according to the following considerations:

✓ T = 38°C is compatible with several drugs or peptides to be encapsulated and lower than the PLGA glass transition that occurs at about 40°C (De and Robinson, 2004);

✓ solubility of EA in CO_2: these process conditions assure the complete miscibility of EA in SC-CO_2 (Smith et al., 1998);

✓ solubility of H_2O in CO_2: at these operating conditions the solubility of the continuous phase of the emulsion in CO_2 is very small, so it is very small and can be neglected (Sabirzyanov et al., 2002; King et al., 1992; Wiebe and Gaddy, 1940);

✓ the difference in density between the emulsion and SC-CO_2 is very large (~1 g/cm^3 for the liquid phase against 0.310 g/cm^3 for CO_2). Since the countercurrent operation in the packed column is favoured by large density differences between the two phases involved in the process, for a fixed temperature the lower is the pressure the larger is the density difference, therefore, pressures higher than 100 bar were not considered.

V.3 Flooding calculations

In a countercurrent packed column, efficient mass transfer conditions are reached when the liquid flowing down over the packing begins to be held in the void spaces between the packing; this is called *loading condition* and the pressure drop in the column begins to increase. Further increases in gas or liquid velocity will produce further increases of the pressure drop until the liquid completely fills the void spaces in the packing, no more liquid can flow down through the column and it is forced to flow up, together with the gas stream. This condition is referred as *flooding* and the column is no more operative. Given a packed column, for a fixed gas rate, there is a definite liquid rate above which the column will flood; similarly, at any given liquid rate there is a definite gas rate above which the column gives flooding. The *flooding point* represents the upper limiting condition of pressure drop and liquid and/or gas flow rates for practical tower operation, therefore, it must be avoided. A typical operating range for the gas velocity through the columns is 50 to 75% of the flooding velocity. It is assumed that, by operating in this range, the gas velocity will also be below the loading point. The flooding condition depends on density difference between the two

phases involved, the characteristics of the packing material and the liquid and gas rates.

Experiments on flooding conditions at different CO_2 densities were performed on SEE-C apparatus, using water as the liquid phase and supercritical carbon dioxide as the dense gas phase. For each experiment, gas flow rate and CO_2 density (i.e. pressure and temperature conditions) were fixed; whereas, the liquid velocity was increased by small increments to measure the increase of the pressure drop, until the flooding point was reached. Firstly, the limit in density difference between the liquid and gas phase that allows countercurrent operation was measured; the results are reported in Figure V.42 at fixed L/G ratios. For CO_2 densities below ~0.6 g/cm^3 (below the dashed line), the gas to liquid (water) density difference allows the proper interaction of the two phases; for CO_2 densities above ~0.6 g/cm^3 (above the dashed line), entrainment of the liquid phase increases rapidly until flooding occurs; small changes in the flow rates near the limit conditions lead to an unstable process. A similar value of the density difference was also found by Brunner and co-workers that, operating a continuous supercritical fractionation process of fish oil ethyl esters, found that the operating point at 0.603 g/cm^3 was close to the flooding point (Riha and Brunner, 2000). Flooding velocities (G_f) as a function of the liquid/gas ratio for different densities are also illustrated in Figure V.43: at constant L/G ratio, the flooding velocity decreases with the increase of CO_2 density.
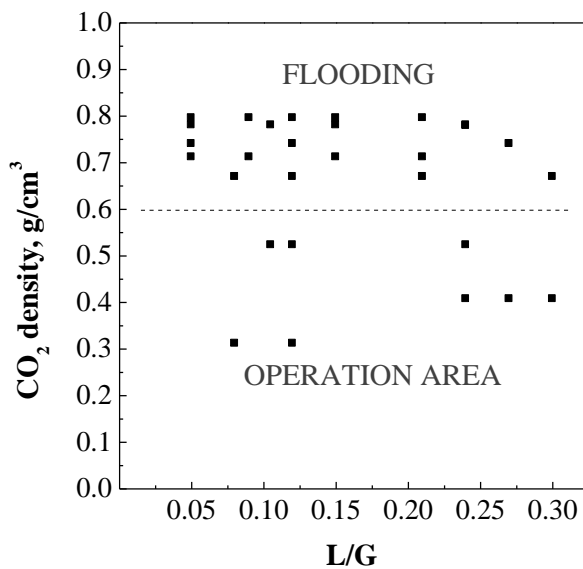
Figure V.42 *Effect of the gas density upon flooding for different L/G ratios (dashed line: boundary line between proper process conditions and flooding).*
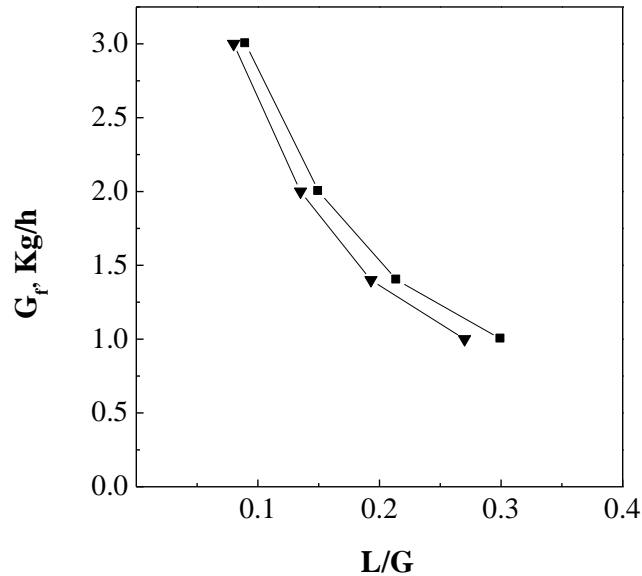
Figure V.43 *Flooding velocities (G_f) as a function of the liquid/gas ratio (L/G) for different CO_2 densities: (■) P = 100 bar, T = 57°C, ρ = 0.31 g/cm^3 and (▼) P = 100 bar, T = 44°C, ρ = 0.52 g/cm^3.*

Flooding points can also be calculated using standard procedures based on the use of graphs of experimental data reported in the literature.

- *"Generalized Pressure Drop Correlation" (GPDC)*

A common and relatively simple procedure for estimating flooding velocity is to use a generalized flooding and pressure drop correlation. One version of this relationship for a packed tower is in the Sherwood correlation, shown in Figure V.44 (Richardson et al., 2002). The "*Generalized Pressure Drop Correlation*" (GPDC) describes the balance between the up-flowing gas momentum force and the gravitational forces acting on the liquid droplets. It is a function of the physical properties of the gas and of the liquid stream; therefore, mass flow rates, gas and liquid densities, viscosity of the liquid, as well as a packing factor must be known. All the versions of the GPDC are based on random packing only.
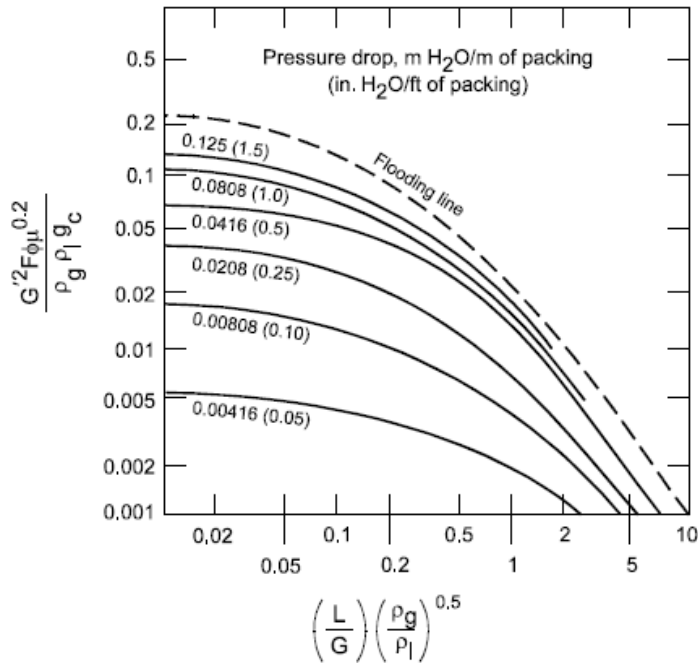
Figure V.44 "*Generalized Pressure Drop Correlation" (GDPC) (L = liquid mass flow rate, Kg/s; G = gas mass flow rate, Kg/s; ρ_l = density of the absorbing liquid (Kg/m^3); ρ_g = density of the gas stream (Kg/m^3); G' = mass flow rate of gas per unit cross sectional area of column, Kg/m$^2\cdot$s; g_c = gravitational constant, m/s^2; F = packing factor, m^{-1}; ϕ = ratio of specific gravity of the scrubbing liquid to that of water; μ_l = viscosity the of liquid, N$\cdot$s/m^2).*

- *"Brunner correlation"*, that is the GPDC correlation modified by Brunner for towers operating with supercritical CO_2.

The correlation proposed by *Brunner* (Brunner, 2009) allows to calculate flooding points for packed columns with structured packings (Figure V.45). Particularly, the gas capacity factor on the ordinate is a measure for the gas velocity necessary to suspend a liquid droplet, and the flow parameter on the abscissa rates the kinetic energy of the liquid phase to the kinetic energy of the gas phase. The *"Brunner correlation"* differs only marginally (i.e., only for the term used for the ordinate) from the correlation originally suggested by Sherwood et al. (1938).
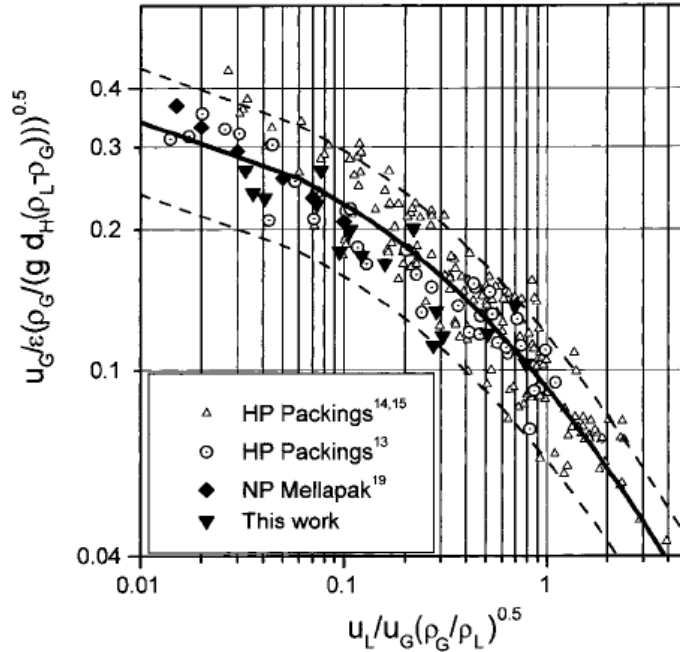
Figure V.45 *"Brunner correlation" (u_G = superficial velocity of gas phase, m/s; u_L = superficial velocity of liquid phase, m/s; ρ_G = density of the supercritical phase, Kg/m^3; ρ_L = density of the liquid phase, Kg/m^3; ε = fractional void volume of the packing; g = gravitational acceleration, m/s^2; d_H = hydraulic diameter, m).*

- *"Random packing correlation"(RPC)*

The *"Random packing correlation"* (Peters and Timmerhaus, 1968) depends on liquid and gas flow rates, surface area of packing per unit lower volume, fractional void volume of dry packing, liquid viscosity, local acceleration due to gravity, liquid and gas densities (Figure V.46). This correlation is based on the method proposed by Sherwood et al. in 1938, with the modification of experimental determination of appropriate packing factor (a_P/ε^3) values as given by Lobo et al. (1945). The correlation shows three separate curves: the intermediate curve can be used for random packings, the upper curve is used for stacked packings and the lower curve is useful for indicating an approximate lower limit when random packings are loaded. The flooding line for random packings is based on experimental data obtained with 15 different liquids, 3 gases and various random packings such as rashig rings, berl, saddles and helices.

The y-axis is labeled $\dfrac{G^2 (a_p/\varepsilon^3)(\mu_L')^{0.2}}{g\,\rho_G\,\rho_L}$ and the x-axis is labeled $\dfrac{L}{G}\sqrt{\dfrac{\rho_G}{\rho_L}}$.

Curve labels: "Flooding with stacked packing", "Flooding with random packing", "Lower limit for loading with random packing". Legend: a_p/ε^3 = packing factor; μ_L' = liquid viscosity, cp.
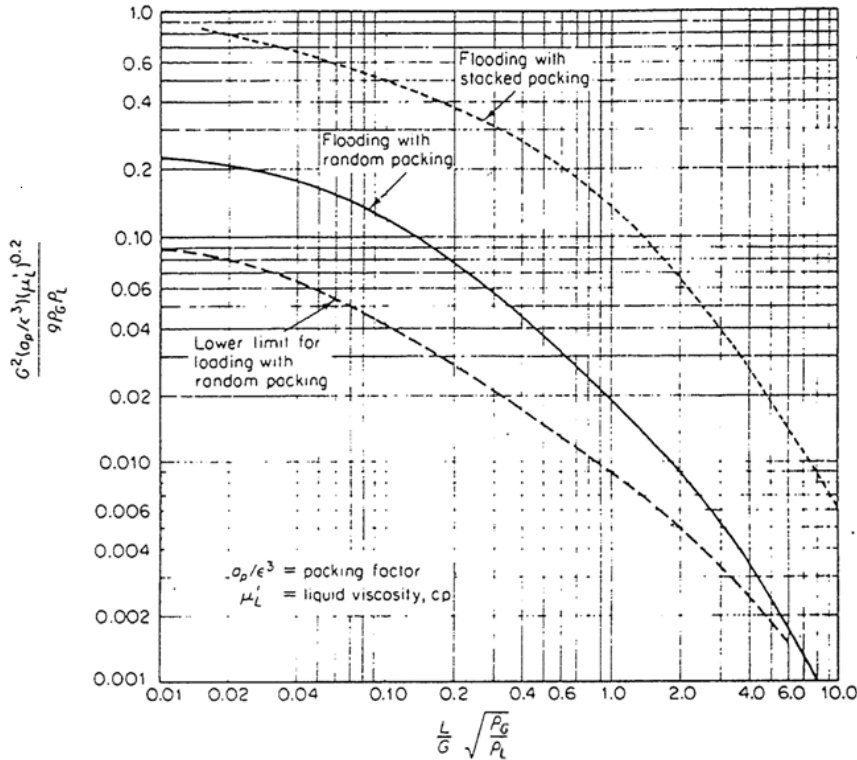
Figure V.46 "*Random packing correlation*" *(RPC) (L = liquid flow rates, lb/h·ft²; G = gas flow rate, lb/h·ft²; a_P/ε = packing factor ft⁻¹, μ_L = liquid viscosity, c_P; ρ_G = density of the supercritical phase, lb/ft³; ρ_L = density of the liquid phase, lb/ft³; g = gravitational acceleration, ft/h²).*

CO₂ flow rates at flooding conditions, calculated using the various correlations discussed above, are reported in Table V.7 and Table V.8 at different L/G ratios and at different densities, respectively. In the same tables, flooding values experimentally measured are also reported. Looking at the results reported in Table V.7, SC-CO₂ flooding flow rate (Gf) decreases with the increase of L/G for all literature correlations and the same trend has been found for the experimental values produced in this work. But, the Gf values calculated from the literature are from about 2.5 to 4 times larger than experimental data; moreover, their variation with L/G is also less pronounced. Possible explanations for these differences are that literature correlations have been produced for processes using gases at ordinary pressure conditions, i.e. near the atmospheric pressure, where gas densities are very small compared to those of supercritical CO₂. The only exception is the Brunner correlation, that has been developed for SC-CO₂; however, in that case, structured packings have been used, that allow a larger void section through the column to which correspond larger possibilities for gas

to flow up with reduced interactions with the liquid. Very small random packings have been used, instead, in the SEE-C tower. Table V.8 shows also that looking at the literature correlations and at our experimental data, for CO_2 densities largely smaller than 0.6 g/cm^3 there is no influence of the gas density on flooding conditions. An exception is given by RPC correlation that indicates a larger G_f at larger pressures, that is the contrary of what one can expect for a dense gas.

Using the results discussed until now, efficient separations in the column used, can be obtained with a flow rate of 1.4 kg/h of CO_2 that corresponds to the 50% of the flooding experimental value, when operating at 80 bar, 38°C with an L/G ratio of 0.1. When, L/G is varied between 0.1 and 0.4, the corresponding limits for liquid flow are indicated in Table V.9.

Table V.7 *Evaluation of the G_f conditions varying the L/G ratio between 0.1 and 0.4 at fixed T = 38°C and P = 80 bar (ρ = 0.31 g/cm^3) using the correlations previously discussed.*

L/G	G_f (Kg/h)			
	GPDC	*Brunner*	*RPC*	*This work*
0.1	10.25	11.26	7.50	3.0
0.2	8.68	9.38	6.64	1.4
0.4	7.09	7.51	5.21	1.0

Table V.8 *Evaluation of the flooding conditions varying the density at fixed L/G = 0.1, using the correlations previously discussed.*

ρ (g/cm³)	G_f (Kg/h)			
	GPDC	*Brunner*	*RPC*	*This work*
0.31	10.25	11.26	7.50	3.0
0.52	10.24	11.23	9.26	3.0

Table V.9 *Liquid and SC-CO$_2$ flow rates used at different values of L/G.*

L/G	SC-CO$_2$ flow rate (Kg/h)	liquid flow rate (Kg/h)
0.1	1.4	0.14
0.2	1.4	0.28
0.4	1.4	0.56

Chapter VI
PLGA microparticles production by SEE-C technology

PLGA microparticles can be administered by *in-situ* injection, achieving a precise and localized drug delivery which is more effective in many cases, such as for chemioterapy, hormone therapy, DNA/protein or vaccine delivery (Verrijk et al., 1992; Meinel et al. 2001; Walter et al., 2001; Luten et al., 2008). Moreover, PLGA microparticles with a specific size and distribution have also been proposed for the use in tissue engineering as building blocks of implantable 3D scaffolds because can offer several benefits, like the control over morphology and physicochemical characteristics (Mercier et al., 2005; Singh et al., 2010) and the versatility of the release kinetics of encapsulated specific growth factors for cellular function orienting and directing (Jaklenec et al., 2008). PLGA microparticles have also been suggested as biodegradable carrier for cell culture and/or cell administration in the so-called "*injectable scaffolds*" which may affect stem cells lineage restriction and, after polymer degradation, allow a complete integration of the grafted cells in the host tissue (Declercq et al., 2005; Kang et al., 2005; Hong et al., 2005).

Starting from the optimized operating conditions, the SEE-C process has been applied to the production of PLGA microparticles with an engineered size and distribution, from single and double emulsions. Polymer microparticles have been characterized by scanning electron microscopy, size distribution, differential scanning calorimetry and X-Ray diffractometry. A study of the PLGA microdevices degradation has also been performed to monitor morphological differences in time of the devices produced.

VI.1 Droplets and microparticles size and morphology

The size of the particles is mainly related to the emulsion droplet size and, therefore, depends on the emulsion formulation. Particularly, the increase of the oily solution viscosity, due to a higher polymer concentration

in the solvent, can produce larger droplets when using the same dispersion shear force and surfactant concentration (Li et al., 2008). As a consequence, SEE-C experiments (at steady state conditions) have been performed by processing 100 g of single (*o-w*, 20:80 w/w) and/or double (*w-o-w*, 1:19:80 w/w/w) emulsions in each run, varying the PLGA content in the oily phase from 5 to 10% w/w to obtain PLGA microparticles of increased mean size (MS). All the distribution data of the droplets and of the microparticles produced are summarized in Table VI.1 (Della Porta et al., 2011).

Table VI.1 *Laser scattering size distribution data of droplets (DSD) and of microparticles (PSD) produced at different PLGA concentrations in the oily phase using SEE-C of single (o-w) and double (w-o-w) emulsions. Legend: MS = mean size; SD = standard deviation; CV = coefficient of variation; SF = shrinking factor.*

	Droplet Size Distributions (DSDs)				**Particles Size Distributions (PSDs)**			
	o-w			*w-o-w*	*o-w*			*w-o-w*
PLGA (% w/w)	**5**	**7.5**	**10**	**10**	**5**	**7.5**	**10**	**10**
MS (µm)	2.4	2.6	4.1	4.1	1.0	1.8	3.3	3.5
SD (µm)	1.0	1.2	2.1	2.1	0.4	0.8	1.6	1.8
$CV_{(SD/MS)}$ (%)	42	46	51	51	40	44	48	51
$SF(MS_S/MS_E)$	--	--	--	--	0.42	0.69	0.80	0.85
D_{10} (µm)	1.1	1.1	1.5	1.5	0.4	0.7	1.1	1.2
D_{50} (µm)	1.8	1.8	3.0	3.1	0.7	1.3	2.3	2.6
D_{90} (µm)	2.8	2.7	4.9	5.1	1.2	2.1	3.8	4.6

Optical microscope images of two different emulsions (single *o-w* emulsion produced at PLGA concentration of 5% w/w and double *w-o-w* emulsion with a PLGA concentration of 10% w/w in the oily phase) are reported in Figure VI.1(a-b). From the images it is clear that the emulsions were stable with non-coalescing droplets.

(a) **Single** **PLGA 5% w/w**	*Mean Size 2.4 μm (SD 1.0 μm)*
(b) **Double** **PLGA 10% w/w**	*Mean Size 4.1 μm (SD 1.8 μm)*
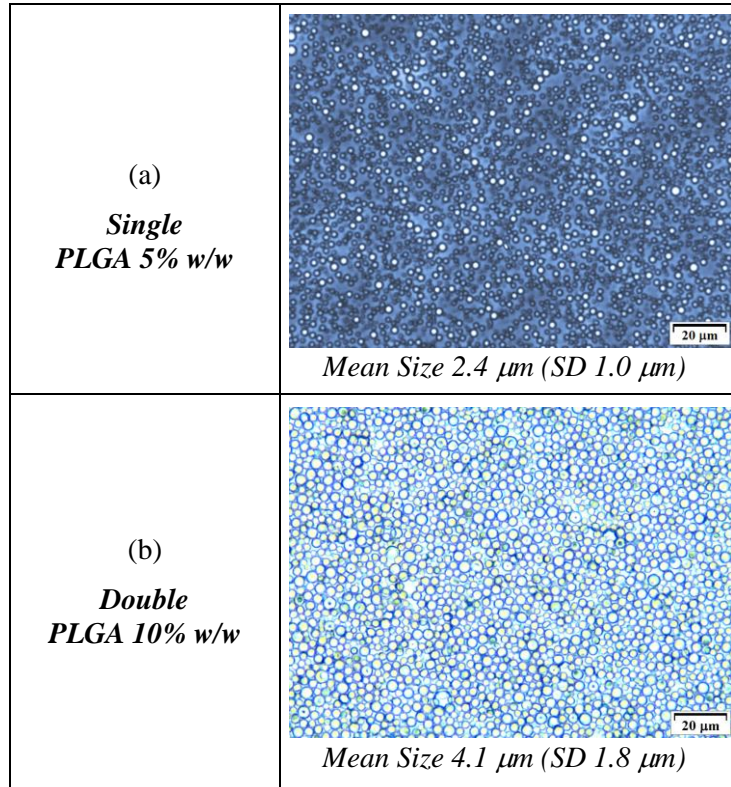
Figure VI.1(a-b) *Optical microscope images of two different emulsions: (a) single o-w and (b) double w-o-w emulsions.*

The produced PLGA microparticles were spherical and non coalescing, as illustrated in the FE-SEM images reported in Figure VI.2(a-c). These images are related to particles obtained from single emulsions prepared with PLGA concentrations in the oily phase of 5% w/w, 7.5% w/w and 10% w/w, respectively. It is clear the increase of the mean particle size from about 1 to 3 μm when PLGA concentration in the oily phase was increased from 5 to 10% w/w.
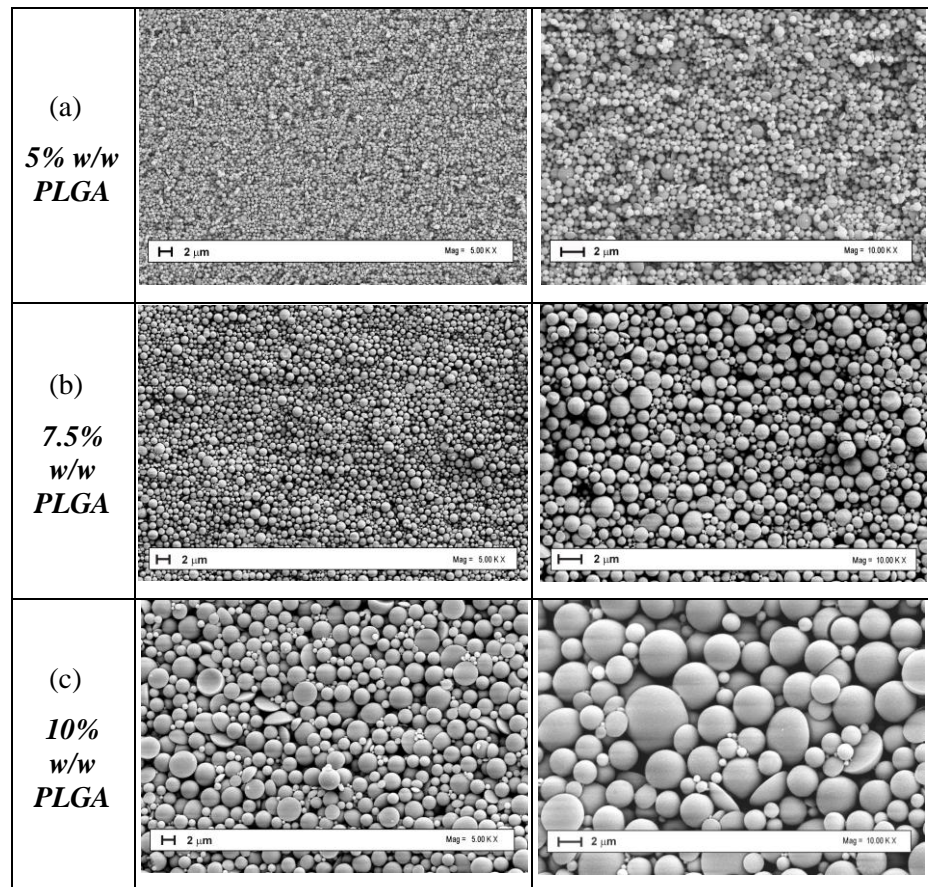
Figure VI.2(a-c) *FE-SEM images of PLGA microparticles obtained using SEE-C by processing single emulsions containing PLGA in concentrations of (a) 5% w/w, (b) 7.5% w/w and (c) 10% w/w. Operating conditions: 80 bar and 38°C, L/G ratio 0.1.*

Looking at the distribution data reported in Table VI.1, it is evident that the mean size of the microspheres is always smaller and the distributions narrower than the droplet mean sizes from which they were generated (the gap between PSD and DSD at D_{50} values is 1.1 μm, 0.5 μm and 0.7 μm for the PLGA concentration of 5%, 7.5% and 10% w/w in the oily phase of single emulsions, respectively).

The PSD of the particles obtained from single emulsions containing 5% and 7.5% w/w of PLGA in the oily phase are also reported in a cumulative representation in Figure VI.3. The DSDs of the two emulsions processed by SEE-C are reported in the same figure, for comparison purposes. DSDs of the two emulsions practically overlap, showing that the variation of PLGA concentration from 5 to 7.5% w/w in the oily phase produced very similar

droplet sizes. Mean droplet sizes of 2.4 μm (SD 1.0) and 2.6 μm (SD 1.2) were obtained with PLGA amounts of 5% and 7.5% w/w, respectively. However, the PSD of the microparticles originated from the droplets containing 5% w/w of PLGA is sharper than the PSD of the microparticles from droplets containing 7.5% w/w of PLGA. This fact is due to the droplet shrinking factor (defined as the ratio between the particles and droplets mean sizes, $SF = MS_S/MS_E$) that also plays a relevant role in determining the final size of the microparticles. The droplets containing a higher percentage of polymer have a lower possibility to shrink when the solvent is eliminated; therefore larger particles are produced (Rosca et al., 2004). The shrinking factor (SF) has been measured for all the different PLGA concentrations explored in the oily phase and the obtained values are reported in Table VI.1. Particularly, the produced particles are about 60% and 33% smaller, respectively, than the original droplets (Della Porta et al., 2011).
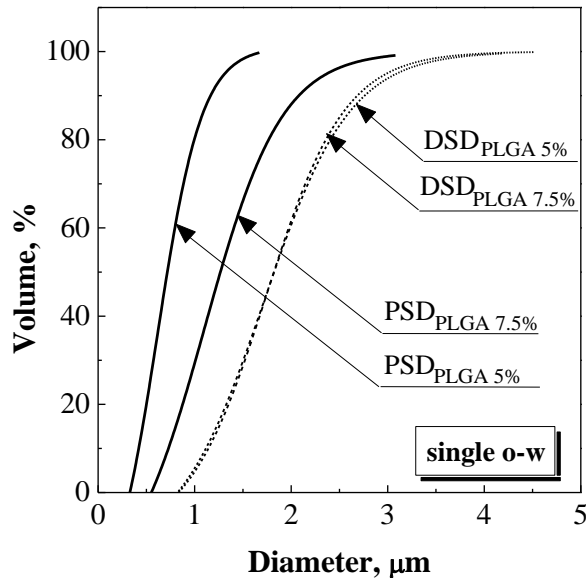
Figure VI.3 *PSDs of PLGA particles produced from single (o-w) emulsions containing 5% and 7.5% w/w of PLGA in the oily phase. The DSDs of the two emulsions processed by SEE-C are also reported (dashed curves), for comparison.*

DSDs of the emulsion containing 10% w/w of PLGA in the oily phase and PSDs of the related microparticles have also been studied using single (*o-w*) and double (*w-o-w*) emulsions and the related size distribution curves are reported in Figure VI.4. PLGA concentration of 10% w/w in the oily phase produced droplets with almost the same distribution in the case of single and double emulsions. The PSD cumulative curve of the

microparticles generated from single emulsion showed a larger shift from the DSD related curve, indicating a larger droplet shrinking (the gap between PSD and DSD at D_{50} values is 0.74 µm); whereas, when a double emulsion was processed, the size distribution curve of the generated particles showed a smaller shift (gap between PSD and DSD at D_{50} values is 0.49 µm) (Della Porta et al., 2011).
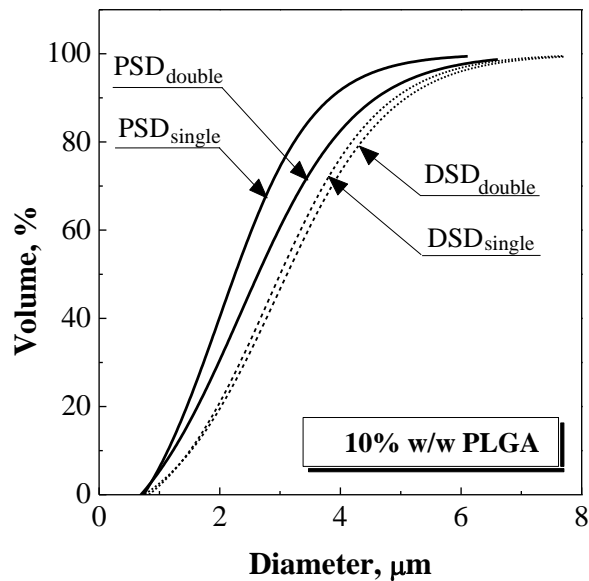
Figure VI.4 *PSDs of PLGA particles produced from single and double emulsions containing 10% w/w of PLGA in the oily phase. The DSDs of the two emulsions processed by SEE-C are also reported (dashed curves), for comparison.*

The coefficient of variation (CV), defined as the ratio between the standard deviation (SD) and the mean size (MS) of the same distribution, has been evaluated for both droplet and particle distributions and its values are reported in Table VI.1. It gives an indication of the sharpness of the distribution, since put the variability in relation to the magnitude of the measured diameters. The CV of the particle size distributions obtained by SEE-C are in the range of 40-50 and always lower or, at least, the same of the ones of the original emulsions, confirming the fine reproduction of the size distribution from droplets to particles of the supercritical continuous process. Increasing the PLGA concentration, CV values increase; therefore the polydispersity of the particles tends to increase with the particle mean size, as expected. The increase of the CV value is mainly related to the type of the emulsion produced. Obviously, if emulsion with monodispersed droplets are produced, monodispersed microspheres can be obtained.

A single *o-w* emulsion using a PLGA concentration of 20% w/w has also been prepared to obtain particles with larger size. In this case, the produced PLGA microparticles covered approximately a range between 1.4 and 88.2 μm. As illustrated in the FE-SEM image reported in Figure VI.5, broken particles were obtained when their size was larger than about 50 μm. This fact demonstrates that particles larger than 50 μm probably cannot be processed by continuous operating mode in the packed tower, due to the droplets/particles interaction by contact with the packing elements.
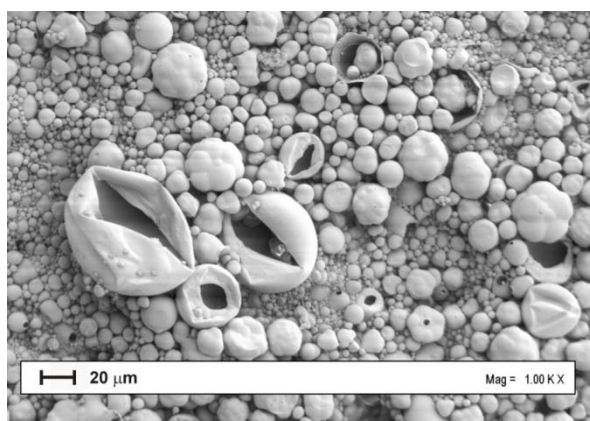
Figure VI.5 *FE-SEM image of PLGA broken microparticles obtained processing an o-w emulsion (20:80) containing PLGA in concentration of 20% w/w in the oily phase. Operating conditions: 80 bar and 38°C, L/G ratio 0.1.*

VI.2 Comparison between SEE-C and solvent evaporation (SE)

Double emulsions are more difficult to be processed by conventional solvent evaporation, since the emulsion is less stable and the produced microspheres are expected to be porous due to the entrapped internal water phase. Coalescence phenomena are frequent, as well as, the formation of concave particles due to the loss of the water internal phase and the formation of collapsed empty particles (Rosca et al., 2004).

A systematic comparison between the characteristics of the microspheres obtained by SEE-C process and by conventional solvent evaporation technique (SE) has been performed, starting from the same *w-o-w emulsion* (ratio 1:19:80) containing 10% w/w of PLGA in the oily phase and processed using the two different technologies/process layouts. The corresponding PSDs of the microspheres obtained by SEE-C and SE are reported in Figure VI.6. The DSD of the emulsions processed is also reported in the same figure, for comparison purposes. The experimental evidence is that microspheres obtained by SEE-C process showed a PSD

narrower than the one obtained by the conventional process and than the DSD of the starting emulsion.
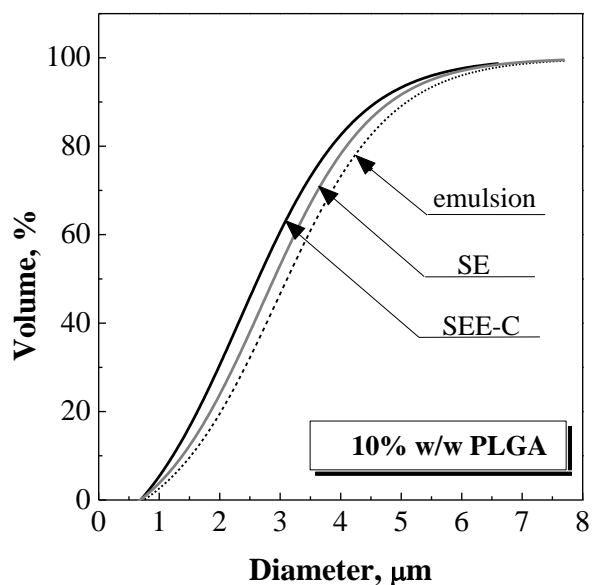
Figure VI.6 *Particle Size Distributions (PSDs) of microspheres produced by SEE-C and SE processes using a w-o-w emulsion containing a PLGA content in the oily phase of 10 % w/w. The Droplets Size Distribution (DSD) of the emulsion processed by the two technologies is also reported, for comparison.*

The observed behavior can be confirmed evaluating the shrinking factor (SF) between the droplets and the related microspheres. The SF values are reported in Table VI.2. In the case of the microspheres produced by SEE-C process it is interesting to observe that the SF value is 0.86, indicating that the particles are about 10% smaller than the original droplets; whereas, in the case of the SE process, the microsphere mean size is equal to the original mean droplet size and the SF value is 1.00.

Mean sizes and distributions of the microspheres obtained by SEE-C and by conventional SE are also reported in Table VI.2, together with the DSD data of the treated emulsion.

Table VI.2 *Laser scattering size distribution data of droplets (DSD) and of microspheres (PSD) produced using SEE-C and SE processes from a w-o-w emulsion containing 10% w/w of PLGA. Legend: MS = mean size; SD = standard deviation; CV = coefficient of variation; SF = shrinking factor.*

	Droplets µm	Microspheres µm	
		SEE-C	**SE**
PLGA (% w/w)		**10**	
MS (µm)	4.1	3.5	4.1
SD (µm)	2.1	1.8	2.1
$CV_{(SD/MS)}$ (%)	51	51	51
SF (MS_S/MS_E)	---	0.86	1.00
D_{10} (µm)	1.5	1.2	1.4
D_{50} (µm)	3.1	2.6	2.9
D_{90} (µm)	5.1	4.6	4.8

Both technologies produced spherical particles; however, concave particles were also produced by SE. An example of the different results obtained is illustrated in the FE-SEM images reported in Figure VI.7(a) and Figure VI.7(b), respectively for SEE-C and SE microparticles:

| (a) **SEE-C microspheres from *w-o-w emulsion* with 10% w/w PLGA** | (b) **SE microspheres from *w-o-w emulsion* with 10% w/w PLGA** |
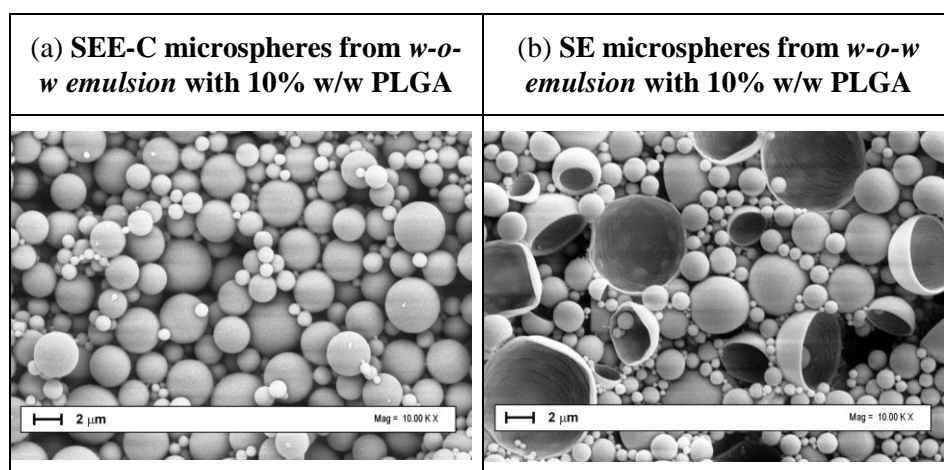
Figure VI.7(a-b) *FE-SEM images of PLGA microspheres produced by SEE-C (left side) and by SE (right side) from a double emulsion containing a PLGA amount of 10% w/w. Operating conditions: 80 bar and 38°C, L/G ratio 0.1.*

Ethyl acetate residues measured in the microspheres after the continuous process ranged between 100 and 300 ppm, that are values considerably lower than the ones measured during the SE operation. Indeed, particles produced by SE showed a mean solvent residue of 500 ppm. This result confirms that the continuous process produces a better contact between the two phases (emulsion/SC-CO_2), enhancing mass transfer. The higher solvent residue obtained in the case of SE can be explained considering the mechanism of solvent elimination of the two processes. In the case of the evaporation technology, EA evaporates from the continuous (aqueous) phase of the emulsion, according to the vapor-liquid equilibrium conditions for the system EA-water at the selected operating pressure and temperature (Reichl et al., 1998). EA content in the aqueous system tends to reduce by evaporation and this reduction induces the diffusion of EA from the liquid droplets of the dispersed phase that balances this reduction, until the droplets are completely dried. Only at this point of the process, the content of EA in the continuous phase starts to reduce until it reaches the lower boundary of the liquid equilibrium curve. When this condition has been reached, no more vapor-liquid fractionation of the EA-water mixture is possible. Therefore, a lower solvent residue is very difficult to be obtained by this technology. On the contrary, in the case of SC-CO_2 processing, due to the complete miscibility of EA in CO_2 at the process conditions and the very small solubility of water in CO_2, EA is almost completely extracted from water during the extraction process without any equilibrium limitation.
The reduced solvent residue is another important advantage of supercritical emulsion processing with respect to conventional SE.

The reasons of the success of the continuous process are in the very short processing time of the emulsion treated by SEE-C. Indeed, considering as a reference time, the residence time of the liquid phase that crosses the packed column, the continuous processing requires a residence time of the emulsion/suspension in the column of about 5 minutes; whereas, 4-6 hours are necessary to perform the conventional SE (often also at higher temperatures). The enhanced mass transfer characteristic of SC-CO_2 generates a faster extraction avoiding coalescence or aggregation phenomena typically occurring during the solvent evaporation process.

VI.3 Microparticles solid state analyses

Thermal analysis (DSC) has been performed on microparticles obtained by SEE-C and on raw PLGA, for comparison purpose. The obtained thermograms are reported in Figure VI.8. PLGA shows a glass transition between 39 and 45°C (onset 39.98°C; endset 45.32°C) and the decomposition that occurs at above 300°C. The produced microparticles show the same glass transition and degradation event of the unprocessed polymer (Della Porta et al., 2011).
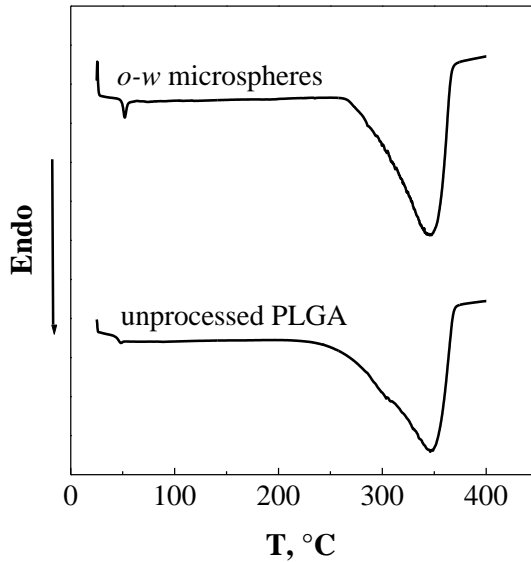
Figure VI.8 *DSC traces of unprocessed and PLGA microparticles produced by SEE-C.*

X-ray analysis has also been performed on the untreated polymer and on PLGA microparticles, to have information about the solid state of the produced materials. The X-ray patterns are reported in Figure VI.9; they indicate that both unprocessed polymer and microparticles are amorphous, confirming the fast polymer precipitation inside the droplets during the microparticle formation by SEE-C.
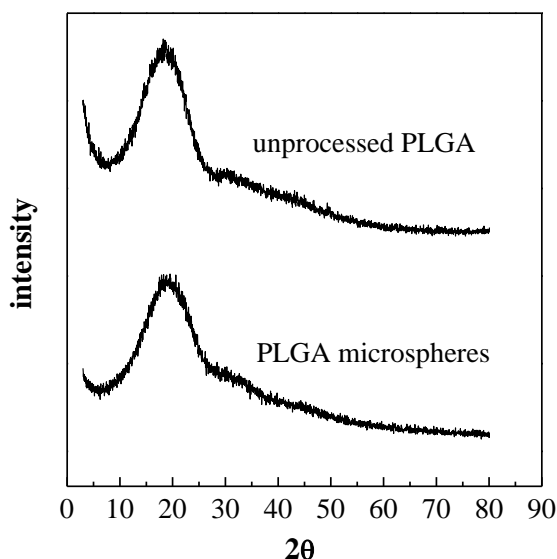
Figure VI.9 *X-ray profiles of unprocessed and PLGA microparticles produced by SEE-C.*

VI.4 PLGA microparticles degradation: morphological study

PLGA is well known for its bulk erosion properties (Von Burkersroda et al., 2002). In order to study the degradation of the microparticles produced by the supercritical process, two different batches of particles produced using single and double emulsions containing 10% w/w PLGA (with a fixed MS of 3 μm; SD 1.5 μm) have been suspended in distilled water at 37°C with an agitation of 50 rpm. The PLGA particles degradation started in the first 48 h, as indicated by the pH lowering of the suspension that decreased from 6.8 to 4.5. From each suspension, 10 μl were sampled every 7 days, dried and prepared for the morphological analysis by FE-SEM. The microparticles surface modification after 14, 28 and 35 days are reported in Figure VI.10(a-c, left side). A smooth surface is still present on the particles sampled after 14 days of degradation (Figure VI.10(a, left side)). The progressive erosion starts to be evident after 35 days, when the microdevices became nanoporous (Figure VI.10(c, left side)). The microparticles produced by double emulsion showed a complete erosion in 60 days. Their surface morphologies after 14, 28 and 35 days are also reported in Figure VI.10(a-c, right side). A smooth surface can be still observed after 14 days of residence in distilled water (Figure VI.10(a, right side)); whereas, the circular structures observed on the microparticles surface should due to the polymer precipitation on the internal water phase of the double emulsion. Nanoporous and near-collapsed particles were observed after 35 days, indicating the polymer bulk depolimerization (Figure VI.10(c, right side)). The overall

period between 50-60 days required for PLGA microparticles complete degradation in water, coupled with a maximum pH lowering of the suspension to a value of 4.5, is in agreement with the literature data (Okada and Toguchi, 1995), which suggest a degradation time of 60 days for similar PLGA particles obtained by conventional solvent evaporation.

Days	PLGA microparticles evolution in water from single *o-w emulsion*	PLGA microparticles evolution in water from double *w-o-w emulsion*
(a) **14**		
(b) **28**		
(c) **35**		
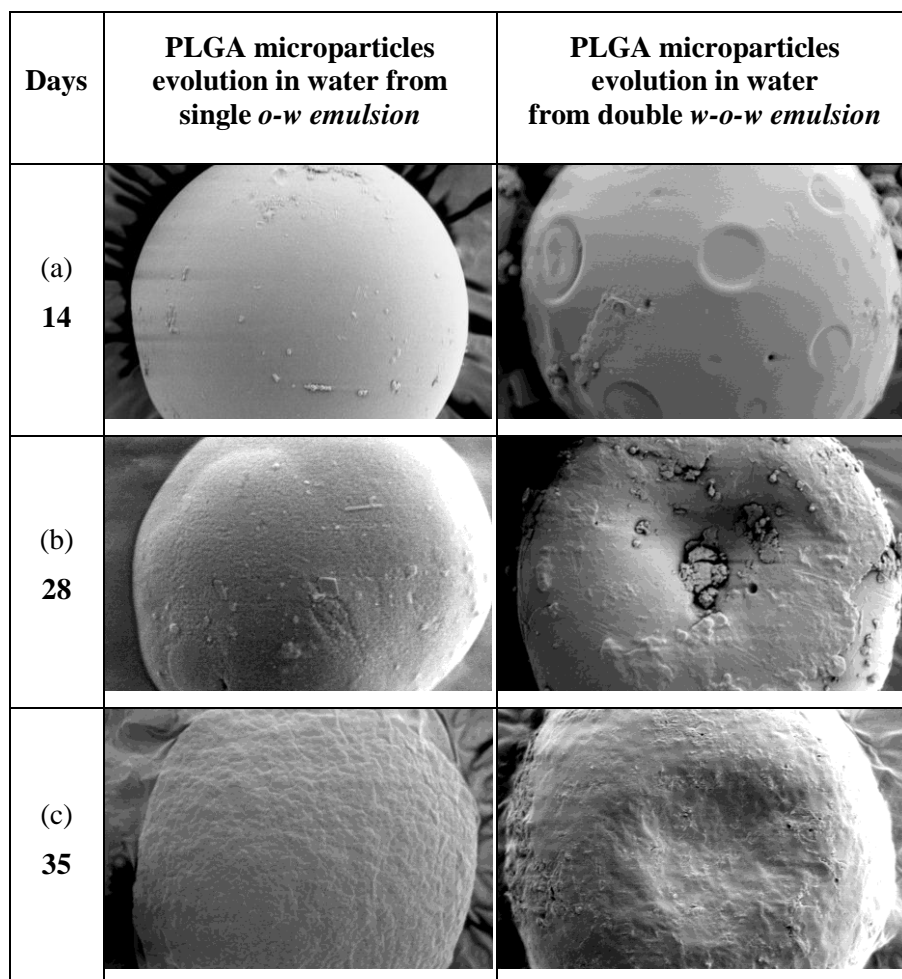
Figure VI.10(a-c) *FE-SEM images (Mag = 50.00 KX) related to a morphological study of PLGA microparticles degradation in water after (a) 14, (b) 28 and (c) 35 days, respectively. The particles have a diameter of almost 3 µm and were produced by SEE-C using a single (left side) and double w-o-w emulsions (right side).*

Chapter VII
NSAID/PLGA injectable microspheres: continuous *versus* batch operation layouts

Nonsteroidal anti-inflammatory drugs (NSAIDs) are the most commonly prescribed medications in the world. Due to their short half-lives and a strong relationship between concentration and response, it is necessary to dose them at regular, frequent time intervals to maintain the drug concentration within the therapeutic range. However, almost all NSAIDs available in the market show severe side effects such as gastrointestinal (GI) mucose damage, irritation, and bleeding. High doses at frequent time intervals may also generate toxicity. As a consequence, a trend in NSAIDs formulation is the development of controlled release dosage form.

In this chapter, the production of NSAID/PLGA microspheres with high drug encapsulation efficiency by using less toxic solvents, such as EA, and by applying SEE-C process is proposed. Among the non-steroidal anti-inflammatory drugs (NSAIDs), Piroxicam (PX) and Diclophenac Sodium (DS) have been chosen as model compounds to be entrapped within microspheres, to obtain extended release devices. The microdevices produced by SEE-C have also been compared with the ones obtainable by SEE and conventional SE. A detailed characterization of the produced microspheres has been performed comparing morphologies, size distributions and physico-chemical properties of the different products obtained using the three different technologies/process layouts. Drug release profiles of microspheres have also been monitored to check the structure of the microspheres produced by SEE-C technology.

VII.1 Microspheres produced by SEE-C: particle size control

To obtain injectable PLGA microspheres charged with PX of DS, single and double emulsions were prepared, respectively, using EA as oily phase. A

single *o-w emulsion* (20:80 w/w) was used to encapsulate PX in PLGA, due to the good solubility of both PX and PLGA in EA. A double *w-o-w emulsion* (2:18:80 w/w/w) was used to encapsulate DS in PLGA, due to the good solubility of DS in water and its insolubility in EA. This type of emulsion decreases contact between the organic phase and the active substance and improves the encapsulation efficiency of water-soluble drugs. To produce particles with different mean sizes, the PLGA amount in the oily phase of the emulsions has been varied. Particularly, single emulsions with o-w ratio of 20:80 w/w have been formulated fixing the PX loading in EA at 10% w/w and varying the PLGA concentration from 5% to 7.5% w/w; whereas, double emulsions with w-o-w ratio of 2:18:80 w/w/w have been prepared maintaining the DS concentration fixed at 10% w/w and varying the PLGA amount from 2.5% to 5% w/w.

The DSDs obtained are shown in a cumulative representation in Figure VII.1(a) for the single emulsions and in Figure VII.1(c) for the double emulsions. As already reported, an increase of PLGA concentration induces an enlargement of the droplets and the formation of wider DSDs (Della Porta e al., 2010). Particularly, mean droplet sizes of 2.1 μm (SD 0.9) and 3.5 μm (SD 1.8) were obtained in the case of *o-w emulsions* with PLGA amounts of 5% and 7.5% w/w, respectively. Mean droplet sizes of 1.1 μm (SD 0.5) and 2.4 μm (SD 1.0) were obtained in the case of *w-o-w emulsions* for PLGA concentrations of 2.5% and 5% w/w, respectively.

The corresponding PSDs are reported in Figure VII.1(b) for microspheres produced from the single emulsions, and in Figure VII.1(d), for microspheres obtained from the double emulsions. The increase of the emulsion droplets size with the PLGA concentration produces a significant increase in PSDs of the obtained microspheres. In the case of microspheres produced from single emulsions, the mean size varied from 1.4 μm (SD 0.6) to 3.1 μm (SD 1.6) when the PLGA concentration was varied from 5% to 7.5% w/w, respectively; in the case of microspheres produced from double emulsions, the mean size varied from 1.0 μm (SD 0.5) to 1.9 μm (SD 0.8) when the PLGA concentration was varied from 2.5%, to 5% w/w, respectively.

Comparing the DSDs with the related PSDs, it is evident that the relative position of the two PSDs has been maintained: i.e., there is approximately the same gap between the two distribution curves; but, the PSDs are always narrower than the corresponding DSDs. As example, cumulative size distributions of the droplets and of the related microspheres obtained with a PLGA concentration of 5% w/w are plotted together in Figure VII.2(a-b) for a single and a double emulsion, respectively.
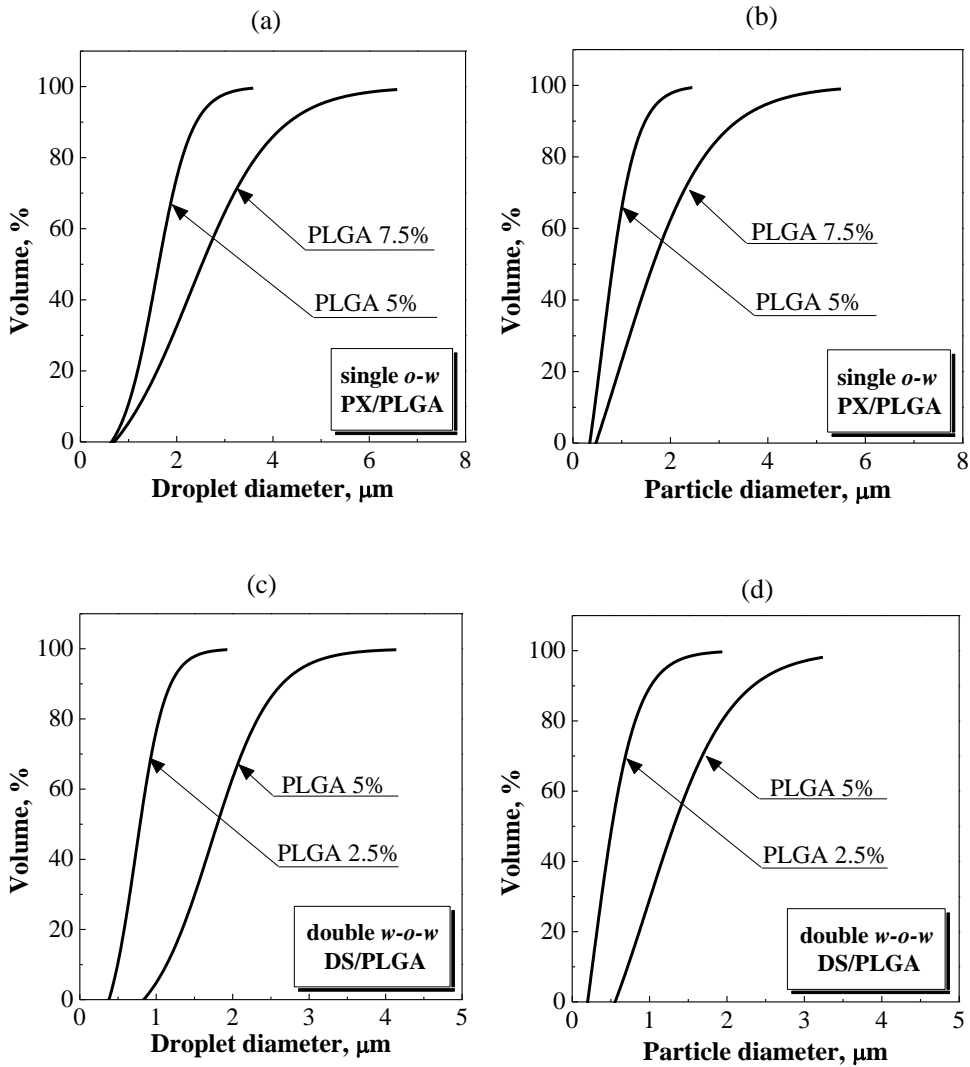
Figure VII.1(a-d) *Cumulative size distribution curves describing the droplets in (a) single and (b) double emulsions obtained varying the PLGA concentration in the oily phase, and the related microspheres produced by SEE-C from (c) single and (d) double emulsions.*
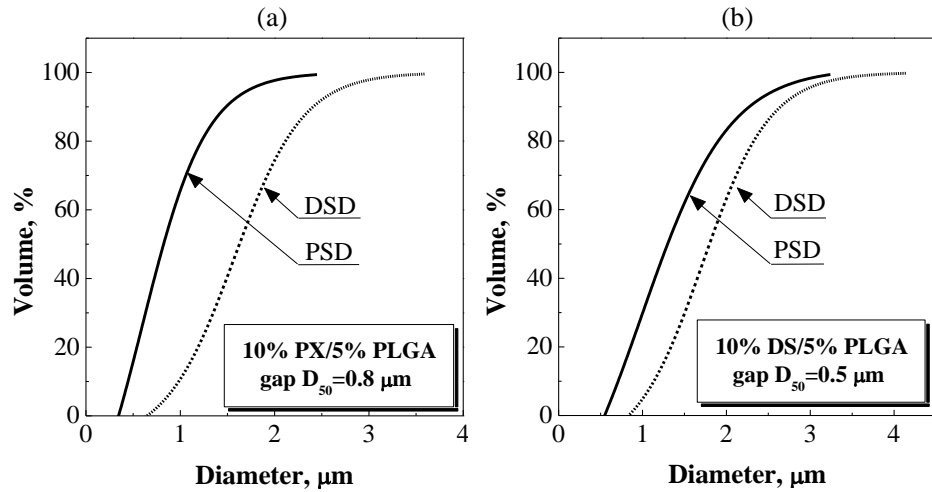
Figure VII.2(a-b) *Cumulative size distributions of the droplets and of the relative microspheres obtained from (a) single (o-w) emulsion containing 5% w/w of PLGA and 10% w/w of PX, and (b) double (w-o-w) emulsion containing 5% w/w of PLGA and 10% w/w of DS.*

All the microspheres produced were spherical and not agglomerated. Examples of microspheres are shown in the FE-SEM images reported in Figure VII.3(a-b) and related to particles obtained from single and double emulsions prepared with a PLGA amount of 5% w/w in the oily phase.

(a) **SEE-C microspheres from *o-w* emulsion with 5% w/w PLGA and 10% w/w PX**	(b) **SEE-C microspheres from *w-o-w emulsion* with 5% w/w PLGA and 10% w/w DS**
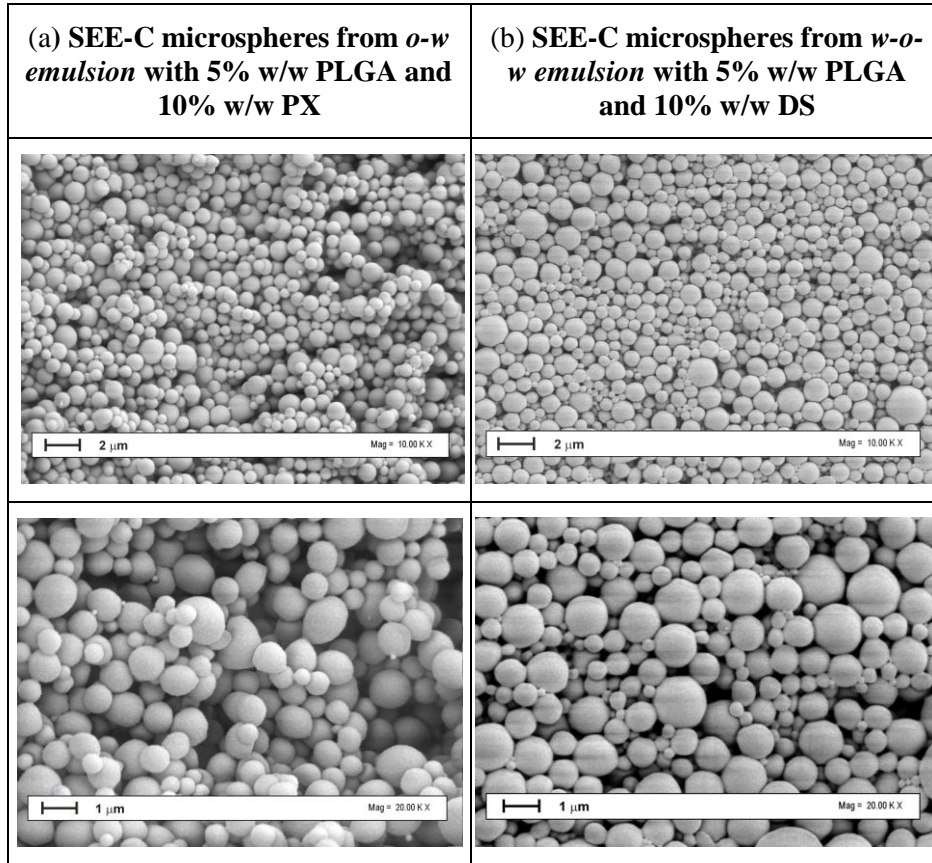
Figure VII.3(a-b) *FE-SEM images of (a) PX/PLGA microspheres obtained by SEE-C from a single (o-w) emulsion and (b) DS/PLGA microspheres obtained from a double (w-o-w) emulsion, both containing PLGA in concentration of 5% w/w. Operating conditions: 80 bar and 38°C, L/G ratio 0.1.*

VII.2 Comparison between SEE, SEE-C and SE

VII.2.1 PSD and morphology

A comparison between the products obtained by SEE, SEE-C and conventional solvent evaporation technique (SE) has been performed from single (*o-w*) and double (*w-o-w*) emulsions that were processed using the three different technologies/process layouts. Microspheres size and distribution are the first parameters considered for the comparison of the results obtained by SEE, SEE-C and SE. These parameters were measured by dynamic laser scattering. All the PSDs data of the PX/PLGA and

DS/PLGA microspheres recovered using the three process layouts are reported in Table VII.1 and Table VII.2, respectively. In the same tables, the DSDs of the treated emulsions are also reported, for comparison purposes.

Table VII.1 *o-w emulsion:* *laser scattering size distribution data of droplets (DSD) and of microspheres (PSD) containing different PLGA concentrations in the oily phase and produced using standard SEE layout, SEE-C, and SE process. Legend: MS = mean size; SD = standard deviation; CV = coefficient of variation.*

| | Droplets μm | | Microspheres μm | | | | | |
| | | | SEE | | SEE-C | | SE | |
PLGA (% w/w)	5	7.5	5	7.5	5	7.5	5	7.5
MS (μm)	2.1	3.5	1.9	3.1	1.4	3.1	2.8	4.0
SD (μm)	0.9	1.8	0.8	1.5	0.6	1.6	1.3	1.9
CV $_{(SD/MS)}$ (%)	43	51	42	48	43	52	46	48
SF (MS$_S$/MS$_E$)	---	---	0.90	0.89	0.67	1.00	1.33	1.14
D$_{10}$ (μm)	1.0	1.2	0.9	1.3	0.4	0.7	0.9	1.3
D$_{50}$ (μm)	1.6	2.5	1.5	2.4	0.8	1.7	1.6	2.4
D$_{90}$ (μm)	2.4	4.3	2.3	4.0	1.5	3.4	2.4	4.1

Table VII.2 *w-o-w emulsion*: *laser scattering size distribution data of droplets (DSD) and of microspheres (PSD) containing different PLGA concentrations in the oily phase and produced using standard SEE layout, SEE-C, and SE process. Legend: MS = mean size; SD = standard deviation; CV = coefficient of variation.*

| | Droplets μm | | Microspheres μm | | | | | |
| | | | SEE | | SEE-C | | SE | |
PLGA (% w/w)	2.5	5	2.5	5	2.5	5	2.5	5
MS (μm)	1.1	2.4	1.0	2.3	1.0	1.9	1.5	2.6
SD (μm)	0.5	1.0	0.4	1.0	0.5	0.8	0.7	1.2
CV$_{(SD/MS)}$ (%)	45	42	40	43	50	42	47	46
SF (MS$_S$/MS$_E$)	---	---	0.91	0.96	0.91	0.79	1.36	1.08
D$_{10}$ (μm)	0.5	1.1	0.5	1.1	0.3	0.7	0.5	1.0
D$_{50}$ (μm)	0.8	1.8	0.8	1.7	0.5	1.3	0.7	1.7
D$_{90}$ (μm)	1.2	2.7	1.2	2.5	1.1	2.3	1.3	2.7

SEE-C allows the recovery of microspheres with MSs and SDs identical or slightly smaller than the ones produced by SEE and smaller than the ones produced by SE. Indeed, for example, starting from an *o-w emulsion* (containing 5% w/w PLGA) with a droplet mean size of 2.1 μm (SD 0.9), microspheres with mean sizes of 1.4 μm (SD 0.6), 1.9 μm (SD 0.8) and 2.8 μm (SD 1.3) were obtained by SEE-C, SEE and SE, respectively; whereas, starting from a *w-o-w emulsion* (containing 5% w/w PLGA) with a droplet mean size of 2.4 μm (SD 1.0), microspheres with mean sizes of 2.3 μm (SD 1.0), 1.9 μm (SD 0.8) and 2.6 μm (SD 1.2) were obtained by SEE-C, SEE and SE, respectively. As a consequence, the PDSs of microspheres produced by SEE-C are narrower than the ones produced by SEE and SE; the PSDs of microspheres produced by SEE and SE have, instead, practically the same D_{50} and similar D_{90}, but SE produces a fraction of microspheres that is not present in the sample produced by SEE and, of course, in the original emulsion droplets. This behavior is better evidenced in Figure VII.4(a-b), where two examples of cumulative size distributions of microspheres obtained by SEE-C, SEE and SE from single and double emulsions containing 5% w/w of PLGA are reported, respectively.
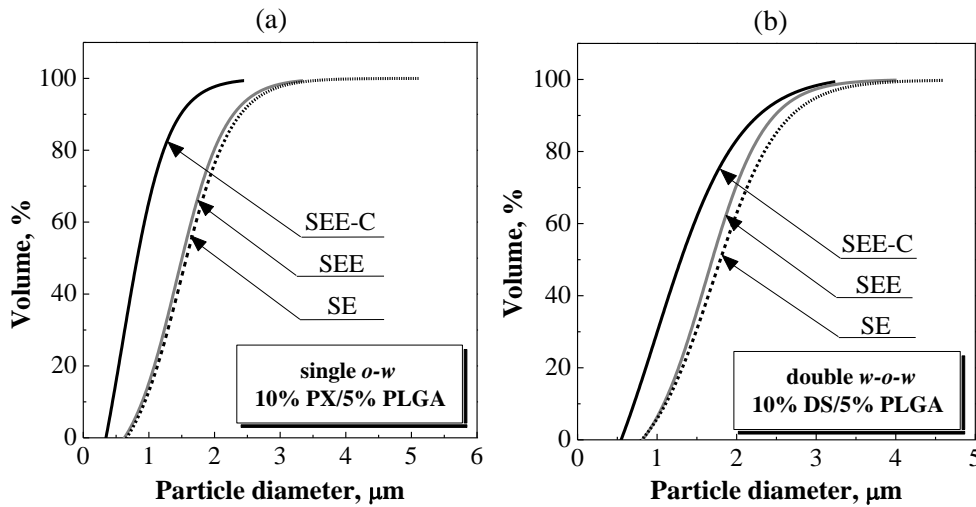
Figure VII.4(a-b) *Comparison between PDSs of (a) PX/PLGA and (b) DS/PLGA microspheres obtained by SEE-C, SEE and SE processes starting from the same single or double emulsion with a PLGA content in the oily phase of 5 % w/w.*

These results confirm that the PSD of the produced particles is mainly related to the emulsion droplet size; but, the solvent elimination process also plays a relevant role in determining the final size of the produced microspheres. Indeed, the faster precipitation route obtained in SEE-C

processing (only 5 min necessary to perform the SEE-C against 30 min for SEE and 4-6 h for the conventional SE) prevents droplets coalescence or aggregation phenomena occurring during SE. With respect to the SEE standard layout, the SEE-C offers other advantages such as, complete absence of aggregated particles that may occur during the depressurization step when impacting against to the wall of the reactor, and minimized lost of particles in the CO_2 gas stream released during the final depressurization step. Indeed, SEE usually showed a recovery percentage (defined as: *PLGA charged in emulsion/PLGA recovered after the processing x 100*) variable from 40 to 60% and SE allowed the recovery of maximum 50% of the charged material; whereas, a recovering percentage of about 90% was measured in SEE-C.

A systematic comparison between microspheres morphology obtained using SEE-C and SE processes has also been performed. Examples of the obtained results are reported in Figure VII.5(a-b), where FE-SEM images of DS/PLGA microspheres produced by SEE-C and SE from a double emulsion containing 2.5% w/w of PLGA and 10% w/w of DS are showed, respectively. The two technologies produced well-defined spherical particles; however, the FE-SEM images show that SE also produced large DS crystals, suggesting that part of the drug went out from the emulsion droplets during the SE. This would result in poor drug loading and initial rapid release of the drug (burst effect) (O'Donnell and McGinity, 1997; Ghaderi et al., 2000; Della Porta et al., 2010).

(a) **SEE-C microspheres from *w-o-w emulsion* with 2.5% w/w PLGA and 10% w/w DS**	(b) **SE microspheres from *w-o-w emulsion* with 2.5% w/w PLGA and 10% w/w DS**
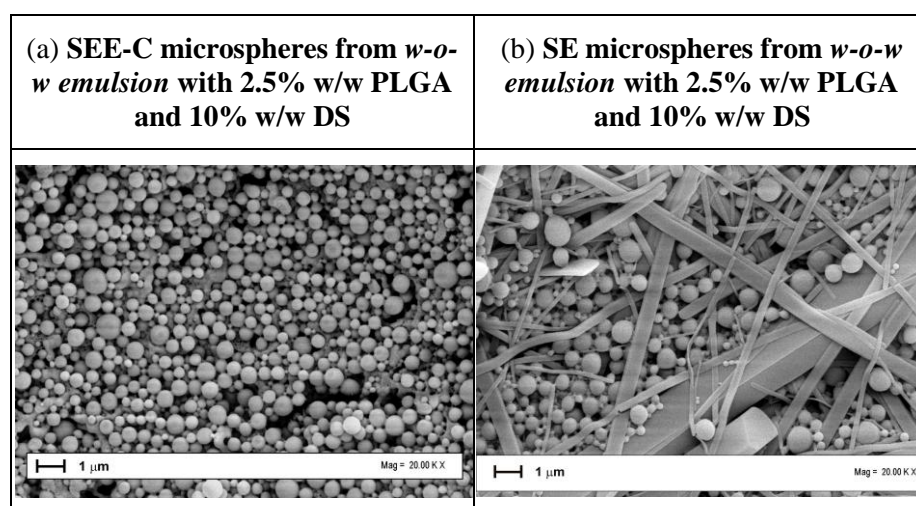
Figure VII.5(a-b) *FE-SEM images of DS/PLGA microspheres produced by SEE-C (left side) and by SE (right side) from a double emulsion containing a PLGA amount of 2.5% w/w (DS is 10% w/w of PLGA). Operating conditions: 80 bar and 38°C, L/G ratio 0.1.*

VII.2.2 Drug loading

The theoretical and experimental drug loading, and the encapsulation efficiency of all discussed microspheres are summarized in Table VII.3. From the data reported, the encapsulation efficiency into PLGA microspheres produced by SEE-C and SEE technologies is higher than 95% in the case of PX and maximum 90% in the case of DS; whereas, microspheres produced by SE show lower encapsulation efficiencies of about 70% in the case of PX and only 30% in the case of DS (Della Porta et al., 2010). These measured values are in agreement with the results reported in literature in the case of SE; indeed, a mean of 60% of the drug can be conventionally encapsulated in microspheres produced starting from a single o-w emulsion; whereas, only about the 30% of the drug is charged in the microspheres in the case of a double w-o-w emulsion (Rosca et al., 2004; Herrmann and Bodmeier, 1998; Li et al., 2008). Indeed, according to Rosca et al. (2004), especially when a double emulsion is used, during the solvent elimination and the consequent droplet shrinkage, the polymer walls around the inner microdroplets may break forming holes inside and on the microsphere surface, through which the inner aqueous phase is partly expelled, affecting the loading efficiency. The above mechanism description also justifies the formation of porous microspheres, when a double emulsion is evaporated. During the supercritical extraction of emulsions, on the contrary, an excellent drug loading is observed, even in the case of double emulsions, due to the very fast solvent elimination and polymer precipitation; that is, microsphere wall breakage is reduced and the water soluble drug has a reduced time to migrate to the external continuous phase. Moreover, according to Herrmann and Bodmeier (1998), the drug encapsulation efficiency is strongly reduced in the SE methods especially when EA is used, as the dispersed phase, due to the higher solubility of ethyl acetate in water compared to that one of methylene chloride. Therefore, methylene chloride is still the most favorable solvent (even if more toxic than EA) when the SE technology is used. The SC-CO$_2$ emulsion extraction can give, instead, more process alternatives since a high encapsulation efficiency is obtained even if EA is used as solvent of the dispersed phase.

Table VII.3 *Theoretical and measured drug loading in the microspheres recovered using SEE-C, SEE and SE processes.*

	PX/PLGA			DS/PLGA		
	SEE-C	SEE	SE	SEE-C	SEE	SE
Theoretical drug loading (% w/w)	10					
Experimental drug loading (% w/w)	9.7 (±0.08)	9.6 (±0.09)	7.3 (±0.09)	9.0 (±0.11)	8.8 (±0.12)	3.3 (±0.42)
Encapsulation efficiency (% w/w)	97.0 (±0.8)	95.8 (±0.9)	72.6 (±0.9)	90.0 (±1.1)	87.8 (±1.2)	32.8 (±4.2)

VII.2.3 Solid state characterization

The particles solid state has been studied comparing the X-ray patterns of the untreated materials with those of the produced microspheres. The X-ray profiles of untreated PX and PLGA and of the microspheres produced by supercritical emulsion extraction (SEE or SEE-C) and by SE are reported in Figure VII.6. In the case of DS/PLGA microspheres, the X-ray patterns of the untreated materials and of the produced microspheres are reported in Figure VII.7. Untreated drugs (PX and DS) show a crystalline structure, whereas PLGA is substantially amorphous. PX/PLGA and DS/PLGA microspheres produced by SC-CO_2 technology show an amorphous pattern, suggesting the formation of a polymer/drug solid solution; whereas, the microspheres produced by SE show a pattern with some small peaks due to the presence of drug crystals not encapsulated in the polymer microspheres. This result indicates that microspheres with a more accurate polymer/drug solid solution can be obtained by SC-CO_2 processing.
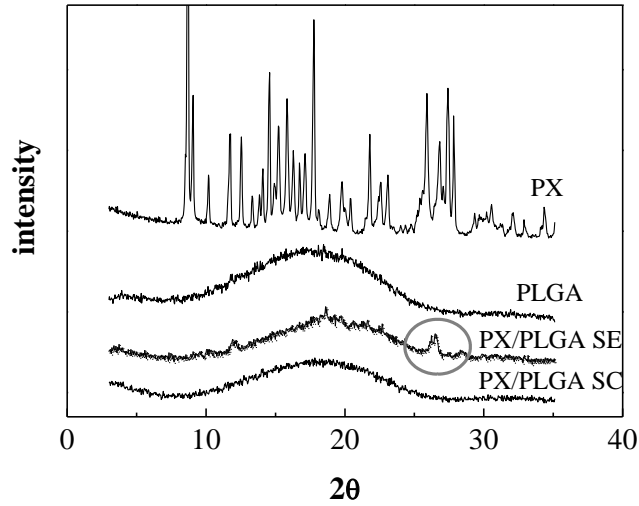
Figure VII.6 *Comparison of X-ray patterns of untreated PX and PLGA compared with PX/PLGA microspheres obtained by supercritical emulsion extraction (SEE or SEE-C) and SE technology.*
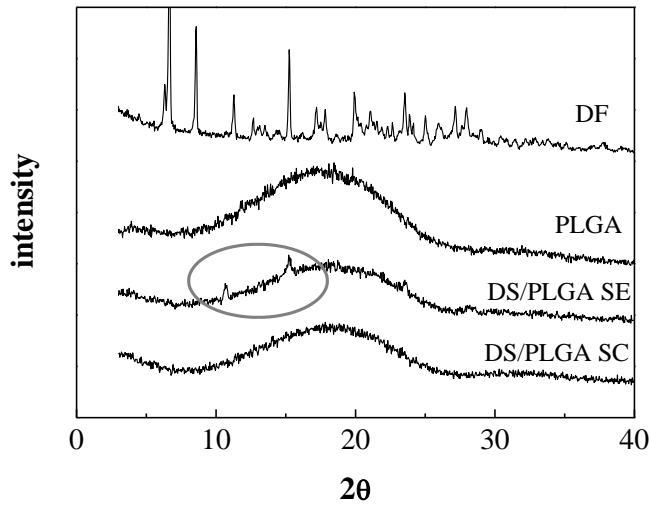
Figure VII.7 *Comparison of X-ray patterns of untreated DS and PLGA compared with DS/PLGA microspheres obtained by supercritical emulsion extraction (SEE or SEE-C) and SE technology.*

VII.3 Microspheres produced by SEE-C: release study

Drug release mechanisms from PLGA can be described in two steps: diffusion through the polymer and liberation from the matrix via bulk

erosion (Siepmann et al., 2001). In the recent literature, several studies have been focused on the interpretation of the predominant release mechanism related to the selected PLA/PGA copolymer ratio (Faisant et al., 2006; Klose et al., 2006). These two mechanisms can overlap or operate in sequence, depending on the polymer molecular weight and mainly on the polymer composition (PLA/PGA). According to Siepmann et al. (2001), drug release from PLGA can be initially diffusion-controlled and, after a certain period of time, overcompensated by the polymer bulk erosion. The length of the diffusion step is also influenced by the content of poly-lactic acid that will erode more slowly that the poly-glycolic acid.

PLGA microspheres produced by SEE-C with a mean size of 3.1 μm (SD 1.6) and with PX theoretical loading of 10% w/w have been tested for drug release studies in a release medium of phosphate buffered solution (PBS 0.2 M, pH 7.4) with 0.5% Tween-80 at 37°C. The release profile data are reported in Figure VII.8(a), where it is evident that the diffusion-controlled drug release prevails in the first days, followed by a fast bulk erosion which characterizes the second part of the drug release. About the 50% of the drug seems available for diffusion; whereas, the remaining part seems to be blocked inside the polymer and cannot be reached by diffusion alone. A complete drug release was obtained in about 8 days.

The release profile from PLGA microspheres produced by SEE-C with a mean size of 1.0 μm (SD 0.5) and with DS theoretical loading of 10% w/w is reported in Figure VII.8(b). In this case, a complete drug release is obtained in about 2 days and a moderate ''burst effect'' can be observed (30% of the charged drug). The release curve show again the presence of two distinct zones: the first, in which diffusion is the controlled mechanism; the second, in which the DS release is related to the bulk erosion. The overall drug release times measured for DS are one fourth of those measured for PX. This behavior may be due to the fact that probably DS is not blocked into the polymer forming the microspheres, since the microspheres resulting from double emulsion have a completely different internal and surface structure with respect to those coming from single emulsion. Indeed, it is well know that microspheres produced starting from double emulsions can be porous due to the presence, during their formation, of a water internal phase that will induce the formation of partially empty structures with micropores distributed inside the microsphere (Li et al., 2008). In such porous PLGA structures, the diffusion of water from the external medium is expected to be facilitated and, consequently, the resulted diffusion times are shorter (Della Porta et al., 2010).

(a)

(b)
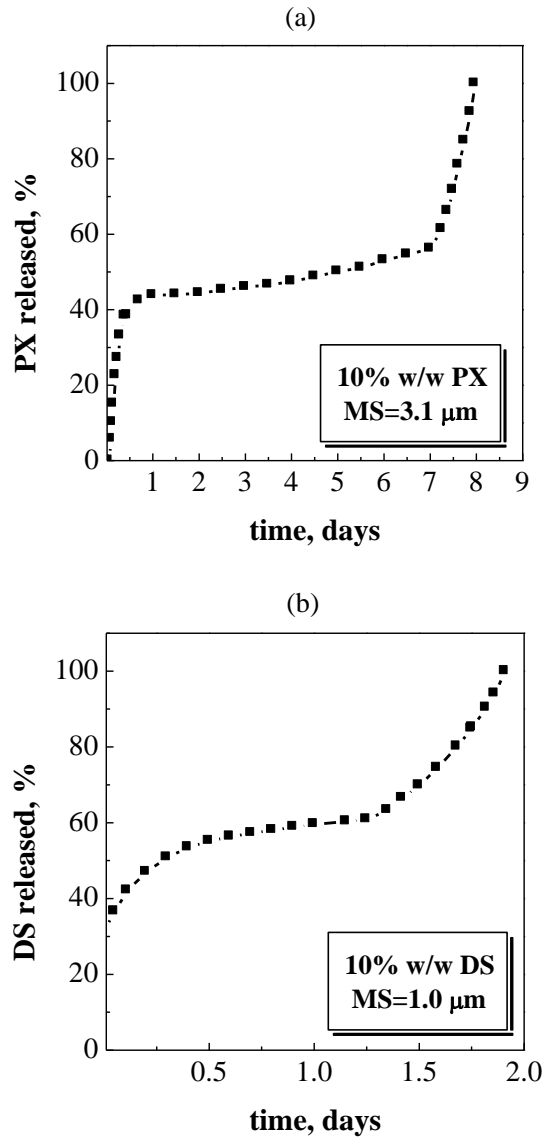
Figure VII.8(a-b) *In vitro release profiles of (a) PX from PLGA microspheres with a mean diameter of 3.1 μm and PX theoretical loading of 10% w/w, and of (b) DS from PLGA microspheres with a mean diameter of 1.0 μm and DS theoretical loading of 10% w/w.*

CHAPTER VIII
Hydrocortisone/PLGA microspheres production and drug release study

A critical problem for implantable devices used for monitoring and treatment of patients is the inflammatory response of the body caused by the tissue injury, that results from implantation of the devices as well as their presence in the body (Onuki et al., 2008). The inflammatory response consists of several phases: acute inflammation, chronic inflammation and fibrotic encapsulation (Ratner and Bryant, 2004). The acute inflammatory response is of relatively short duration (24-48 h) and is mostly responsible for matrix formation and cleaning of the wound site (Anderson, 2001). Persistent inflammatory stimuli lead to a chronic inflammatory reaction (Johnston, 1988), that usually continues for 1-2 weeks, after that a fibrotic tissue is formed or normal tissue re-growth occurs. These tissue reactions affect the normal function of numerous implantable devices; therefore, to increase their longevity and functionality, inflammatory reactions have to be prevented or suppressed.

It has been suggested (Hickey et al., 2002a, 2002b) that, to control inflammatory reactions produced by implanted devices, it should be possible to load these structures with glucocorticoid/polymer microspheres, engineered to release the anti-inflammatory principle during the first weeks after implantation. Glucocorticoids are usually used to prevent or suppress inflammation because they can inhibit the production of factors that are critical in generating the inflammatory response (Hardman et al., 1996); among these, Hydrocortisone Acetate (HA) is one of the most broadly used. However, HA can have serious systemic side effects; therefore, its controlled local release at the specific implantation site via microsphere-based formulations can be significant to avoid the adverse effects and suppress local inflammatory reactions. Moreover, this drug is poorly soluble and

unstable in aqueous media, and both solubility and stability of HA can be improved by forming drug/polymer microspheres.

In this work, the applicability of the SEE-C process has been explored for the production of PLGA microspheres loaded with HA and for controlling their characteristics. The influence of kind and formulation of emulsion on the produced microspheres has been investigated in terms of morphology, particle size distribution, solid state properties and encapsulation efficiency. The produced microspheres have been also studied for in vitro HA release, to obtain further information about the particles structure and to verify their applicability to continuous localized delivery of HA at a specific implant site, to suppress the inflammatory response.

VIII.1 Particle size and morphology

VIII.1.1 HA/PLGA microspheres from w_1-o-w_2 emulsion (w_1: EtOH)

Different w_1-o-w_2 emulsions (1:19:80 w/w/w), with ethanol as solvent in the internal water phase, have been prepared varying the PLGA percentage from 5% to 10% w/w (at fixed drug concentration) or the HA percentage from 2.3% to 4.1% w/w (at fixed PLGA content). PSDs data of the microspheres recovered using the SEE-C process are reported in Table VIII.1; DSDs data of the emulsions treated are also reported in the same table.

Table VIII.1 *Laser scattering size distribution data of droplets (DSD) and of microspheres (PSD) produced from w_1-o-w_2 emulsions (1:19:80 w/w/w, w_1: EtOH) at different HA contents or PLGA concentrations, using SEE-C process. Legend: MS = mean size; SD = standard deviation; CV = coefficient of variation.*

Emulsion kind	w_1-o-w_2 emulsion (w_1: EtOH)					
HA (% w/w)	2.3		4.1		4.1	
PLGA (% w/w)	5		5		10	
Distribution data	DSD	PSD	DSD	PSD	DSD	PSD
MS (µm)	1.8	0.8	1.2	1.0	3.2	2.3
SD (µm)	0.8	0.4	0.5	0.4	1.5	1.1
CV (%)	44	50	42	40	47	48
D_{10} (µm)	0.9	0.4	0.5	0.4	1.5	0.9
D_{50} (µm)	1.4	0.6	0.9	0.7	2.7	1.7
D_{90} (µm)	2.0	1.0	1.3	1.1	4.2	2.8

An optical microscope image of the droplets and a FE-SEM image of the related particles containing 2.3% w/w of HA and 5% w/w of PLGA are reported in Figure VIII.1, showing the formation of very uniform droplets and particles. This result is confirmed by CV values reported in Table VIII.1, ranging between 40 and 50 for DSDs and PSDs; i.e., sharp particle size distributions have been obtained.
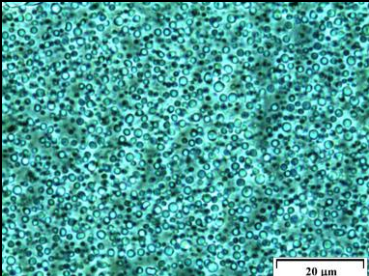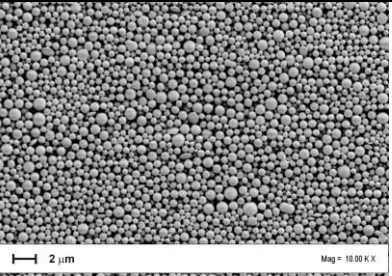
Emulsion composition	Optical microscope image	FE-SEM image
5% w/w PLGA/ 2.3% w/w HA		

Figure VIII.1 *Optical microscope image of the droplets and FE-SEM image of the microspheres produced by SEE-C process from a w_1-o-w_2 emulsion (w_1: EtOH) containing 2.3% w/w of HA and 5% w/w of PLGA.*

The effect of the variation of the PLGA concentration in the oily phase from 5% to 10% w/w has been studied with respect to the microspheres size distribution, at fixed HA concentration. DSDs and PSDs obtained by laser scattering analysis are reported in a cumulative representation in Figure VIII.2. As expected, the increase in the oily phase viscosity produced a significant increase in the PSDs of the corresponding microspheres; the mean particles size varied from 1.0 μm (SD 0.4) to 2.3 μm (SD 1.1) when the PLGA concentration was varied from 5% to 10% w/w, respectively.
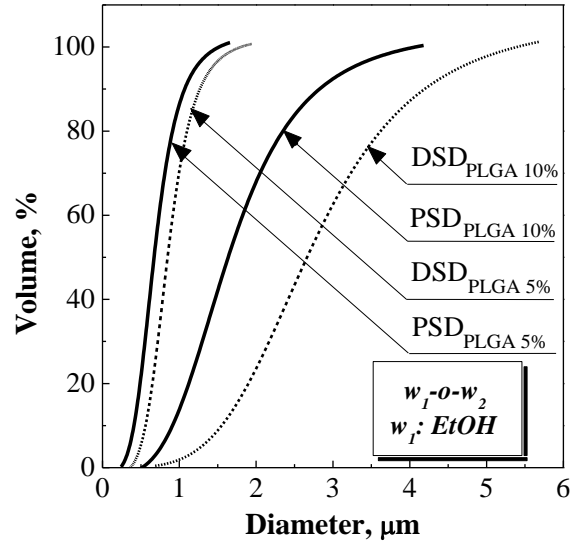
Figure VIII.2 *Cumulative size distributions of the droplets and of the corresponding microspheres obtained by SEE-C process from w_1-o-w_2 emulsions prepared using EtOH as solvent in the internal water phase and varying the PLGA content in the oily phase from 5% to 10% w/w. The drug loading was fixed at 4.1% w/w.*

VIII.1.2 HA/PLGA microspheres from w_1-o-w_2 emulsion (w_1: DMSO)

w_1-o-w_2 *emulsions* (1:19:80 w/w/w) have also been prepared dissolving HA in dimethyl sulfoxide, at different drug loadings of 4.5% and 9% w/w; whereas, the PLGA concentration was set at 10% w/w. Distribution data of the droplets and of the microspheres produced are reported in Table VIII.2:

Table VIII.2 *Laser scattering size distribution data of droplets (DSD) and of particles (PSD) produced from w_1-o-w_2 emulsions (1:19:80 w/w/w, w_1: DMSO) at different HA concentrations of 4.5% and 9% w/w, using SEE-C process; PLGA concentration was fixed at 10% w/w. Legend: MS = mean size; SD = standard deviation; CV = coefficient of variation.*

Emulsion kind	w_1-o-w_2 emulsion (w_1: DMSO)			
PLGA (% w/w)	10			
HA (% w/w)	4.5		9	
Distribution data	DSD	PSD	DSD	PSD
MS (μm)	3.4	2.7	3.4	3.1
SD (μm)	1.5	1.3	1.7	1.5
CV (%)	44	48	50	48
D_{10} (μm)	1.6	0.8	1.5	1.2
D_{50} (μm)	2.9	1.7	2.8	2.3
D_{90} (μm)	4.3	3.2	4.4	4.0

An optical microscope image of the droplets and a FE-SEM image of the corresponding particles containing 10% w/w of PLGA and 9% w/w of HA are reported in Figure VIII.3: the droplets and the microspheres produced were very uniform in size and non-coalescing. This result is confirmed by CV values reported in Table VIII.2, that range between 44 and 50 for DSDs and PSDs.

Emulsion composition	Optical microscope image	FE-SEM image
10% w/w PLGA/ 9% w/w HA		
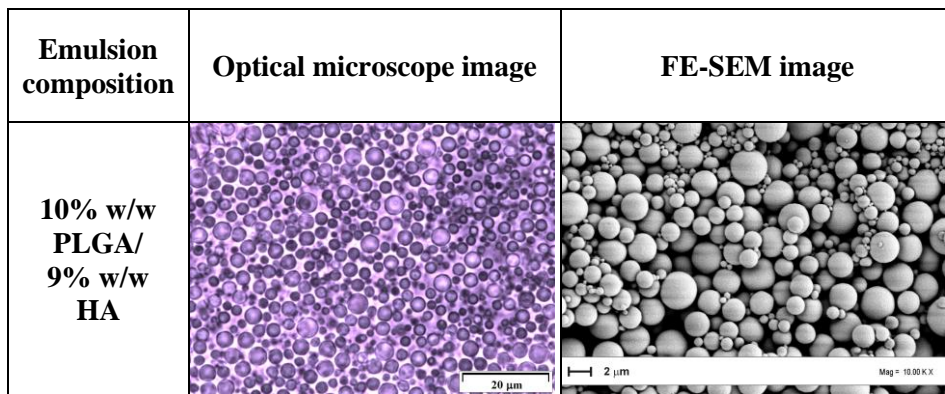
Figure VIII.3 *Optical microscope image of the droplets and FE-SEM image of the microspheres produced by SEE-C process from a w_1-o-w_2 emulsion (w_1: DMSO) prepared with 9% w/w of HA and 10% w/w of PLGA.*

VIII.1.3 HA/PLGA microspheres from s-o-w suspension emulsion

s-o-w suspension emulsions have been prepared with different HA contents of 4.5% and 9% w/w, at a fixed PLGA concentration of 10% w/w. FE-SEM images of the microspheres obtained in this case showed the presence of large HA crystals, identified via shape. An example of the microspheres obtained is reported in Figure VIII.4 and is related to particles charged with 4.5% w/w of HA; HA isolate crystals are clearly identifiable. This result indicates that part of the drug was lost from the droplets during the emulsion formation.
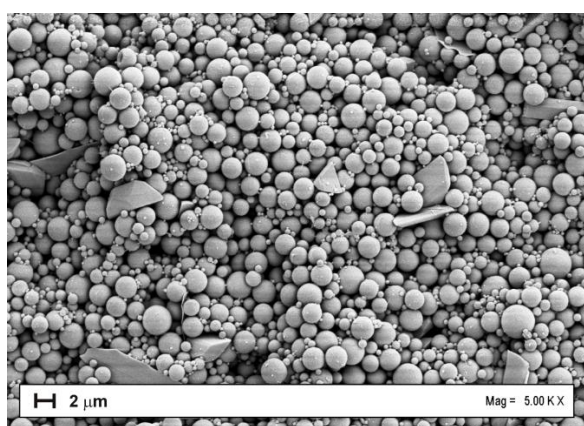
Figure VIII.4 *FE-SEM image of HA/PLGA microspheres prepared by SEE-C from a s-o-w suspension emulsion containing 4.5% w/w of HA and 10% w/w of PLGA.*

For this reason, the preparation of *s-o-w suspension emulsions* was modified; to obtain a better drug encapsulation, HA was micronized using SAA processing (Supercritical Assisted Atomization). SAA is a micronization process based on the solubilization of controlled quantities of SC-CO_2 in a liquid solution (in which was previously dissolved the solute to be micronized), using a saturator that contains high surface packings and ensures long residence times. Therefore, a near-equilibrium solution is formed, that is subsequently atomized through a nozzle and microparticles are obtained after droplet evaporation with warm nitrogen. In this case, SC-CO_2 acts both as a *co-solute* being partially miscible with the solution to be treated, as well as a pneumatic agent to atomize the solution in fine droplets. The liquid solvent, meanwhile, acts as a carrier for the product to be treated (Della Porta et al., 2006). In the specific case, ethanol was tested as liquid solvent and the best results in terms of precipitated HA particles morphology and size were observed operating in the saturator at 90 bar and 80°C, in the

precipitator at 0.7 bar and 35°C, and with a G/L ratio of 1.8 and a nitrogen flow rate of 1000 nL/h. HA particles in the micrometric range (mean size of 0.95 μm (SD 0.11)) were obtained using this process and were used as the solid phase in the experiments on *s-o-w emulsions*.

Distribution data of the droplets and of the related microspheres produced using micronized and not-micronized HA are summarized in Table VIII.3:

Table VIII.3 *Laser scattering size distribution data of droplets (DSD) and of microspheres (PSD) produced from s-o-w suspension emulsions (20:80 w/w) at different HA concentrations of 4.5% and 9% w/w; PLGA concentration was fixed at 10% w/w. Legend: MS = mean size; SD = standard deviation; CV = coefficient of variation.*

Emulsion kind	s-o-w suspension emulsion with not μ-ized HA				s-o-w suspension emulsion with μ-ized HA			
PLGA (% w/w)	10				10			
HA (% w/w)	4.5		9		4.5		9	
Distribution data	DSD	PSD	DSD	PSD	DSD	PSD	DSD	PSD
MS (μm)	3.5	3.0	3.2	5.4	3.2	2.5	3.9	3.0
SD (μm)	1.6	1.5	1.5	2.9	1.4	1.1	1.9	1.6
CV (%)	46	50	47	54	44	44	49	53
D_{10} (μm)	1.6	0.7	1.4	0.7	1.5	1.3	1.3	0.9
D_{50} (μm)	2.9	1.5	2.5	1.5	2.5	2.2	2.6	2.1
D_{90} (μm)	4.4	2.9	3.9	3.2	3.8	3.3	4.2	3.8

Examples of the results obtained are reported in Figure VIII.5, where an optical microscope image of the droplets and a FE-SEM image of the related microspheres containing 4.5% w/w of SAA-micronized HA and 10% w/w of PLGA are shown. The produced droplets and microparticles were very uniform and not aggregated. Indeed, CV values reported in Table VIII.3 for both droplet and particle distributions range between 44 and 54, confirming the uniformity of the products obtained.
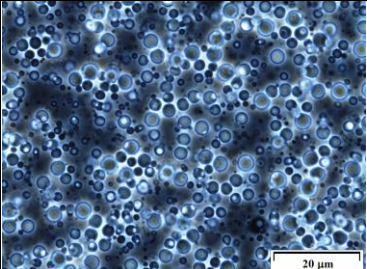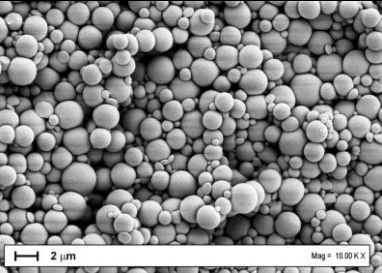
| Emulsion composition	Optical microscope image	FE-SEM image
10% w/w PLGA/ 4.5% w/w HA		

Figure VIII.5 *Optical microscope image of the droplets and FE-SEM image of the microspheres produced by SEE-C process from a s-o-w suspension emulsion loaded with 4.5% w/w of micronized HA and 10% w/w of PLGA.*

VIII.2 Solid state characterization

Thermal analysis (DSC) has been systematically performed on the produced microspheres and on raw PLGA and HA, for comparison. An example of the corresponding thermograms is reported in Figure VIII.6. PLGA (50:50) shows a glass transition that remains relatively constant (onset 39.98°C; endset 45.32°C) in the observed samples and a polymer decomposition that occurs above 300°C; raw HA shows an endothermic peak at about 220°C, due to its melting point. The HA/PLGA microspheres exhibit only the PLGA degradation event, confirming that the supercritical process does not modify the polymer structure; whereas, the characteristic peak of HA is no more visible in the produced microspheres. This fact suggests the formation of an amorphous HA intimate dispersion inside the polymer microspheres.
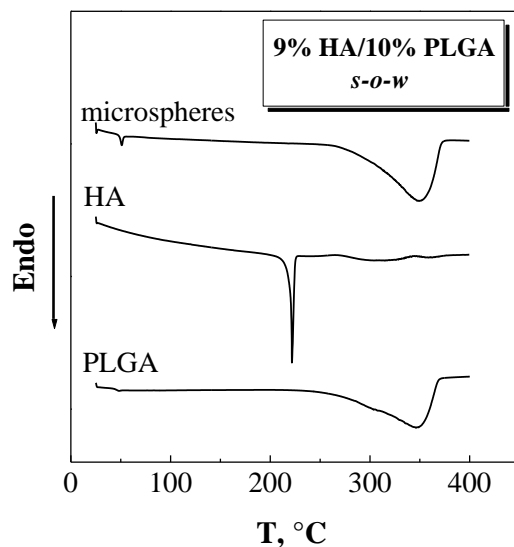
Figure VIII.6 *Example of DSC traces of untreated PLGA, HA and SEE-C microspheres prepared from a s-o-w suspension emulsion containing HA loading of 9% w/w and PLGA content of 10 % w/w.*

VIII.3 Hydrocortisone Acetate encapsulation efficiency

Systematic analysis has been performed on the produced microspheres to measure the effective HA encapsulation, related to the quantity of HA initially loaded, the kind of emulsion used and the mean size of the microspheres. HA content (effective and theoretical) and encapsulation efficiency details for the different emulsion kinds and formulations are summarized in Table VIII.4.

Table VIII.4 *Theoretical and experimental HA loading in the microspheres recovered using SEE-C technology.*

	Microsphere mean size, μm	Theoretical HA loading, % w/w	Effective HA loading, % w/w	Encapsulation efficiency, %
w_1-o-w_2 (w_1: EtOH)	1	2.3	1.8	80
	1	4.1	2.3	55
	2	4.1	2.1	51
w_1-o-w_2 (w_1: DMSO)	3	4.5	1.4	32
	3	9.0	3.3	37
s-o-w (not μ-ized HA)	3	4.5	1.4	30
	5	9.0	5.5	50
s-o-w (μ-ized HA)	3	4.5	2.2	48
	3	9.0	6.8	76

Data reported in Table VIII.4 show a wide variation of the encapsulation efficiency of HA into PLGA microspheres, ranging between 30 and 80%. Particularly, in the case of microspheres produced from w_1-o-w_2 *emulsions* with EtOH as solvent in the w_1 phase, increasing the theoretical HA loading from 2.3 to 4.1% w/w (at fixed microspheres size) the encapsulation efficiency decreases from 80% to 55%. Increasing the size of the microspheres from 1 to 2 μm (at fixed drug loading), the encapsulation efficiency is almost the same.

For microspheres produced from w_1-o-w_2 *emulsions* with DMSO as solvent in the w_1 phase, encapsulation efficiency is poor and the increase of the theoretical HA loading from 4.5 to 9% w/w does not produce appreciable variations.

In the case of microspheres produced from *s-o-w suspension emulsions*, an increase of the theoretical HA content from 4.5 to 9% w/w (at fixed drug loading) improves the encapsulation efficiency. It is evident that a *s-o-w suspension emulsion* using micronized HA allows better encapsulation

performances than a *s-o-w suspension emulsion* using not-micronized HA. The optimized *s-o-w suspension emulsion* can be also favorable to be used when compared with the w_1-*o*-w_2 *emulsion* because only the solvent of the oily phase is used, due to the absence of an internal water phase.

Comparing the encapsulation efficiency values shown in Table VIII.4 with those reported in literature for the entrapment of Hydrocortisone, the success of SEE-C processing is immediately evident; indeed, encapsulation efficiencies of maximum 22% were obtained entrapping Hydrocortisone in PLGA microspheres (with mean size of 3, 13 and 39 μm) produced using a modified SEDS process (Ghaderi et al., 2000). Gelatin nanoparticles encapsulating Hydrocortisone were also produced using a desolvation method. In this case, drug encapsulation efficiencies varying from 35 to 45% were observed (Vandervoort and Ludwig, 2004). Very low encapsulation efficiencies were also obtained encapsulating other glucocorticoids; i.e., PLGA microspheres loaded with Dexamethasone (with mean size of 11 μm) were prepared by o-w emulsion-solvent evaporation method using a mixture of dichlorometane and methanol in the oily phase, and the encapsulation percentage was ∼ 4% (Hickey et al., 2002a).

VIII.4 *In vitro* Hydrocortisone Acetate release

Drug release studies have been performed on the produced microspheres to try to evidence the influence of particle sizes, drug loadings and structural differences between microspheres on the controlled release of HA.

First, PLGA microspheres (produced from w_1-*o*-w_2 *emulsions*, w_1: DMSO) with a mean size of 3 μm and charged with different effective HA loadings of 1.4% and 3.3% w/w have been studied. The release profiles obtained are reported in Figure VIII.7 and show that, when the HA content in the matrix is increased, a slower drug release is initially obtained. A complete drug release was obtained in almost 11 days for both charges. This behavior can seem surprising and is particularly relevant in the first part of the drug release curve, where the diffusion is the prevalent release mechanism. Indeed, one expects that a higher loading will correspond to a faster drug release, since the diffusion rate is ordinarily controlled by the difference of concentration between the inside of the polymer microspheres and the external medium. However, the release behavior at different drug loadings observed in this study can be explained considering the low solubility of HA in the release medium (water). Indeed, as suggested by Lee (1980), two moving fronts can be established in PLGA particles (diffusion followed by bulk erosion) and they are synchronized (the second motion of the front is influenced by the first one). When the concentration of the drug in the polymer is much higher than its solubility in water, the diffusion front is slow and can move towards the internal of the particles only when the concentration in the solid phase decreases to values lower than the

equilibrium value; as a consequence, the higher is the drug concentration in the polymer, the slower is the movement of the diffusion front (Chakraborty et al., 2009).
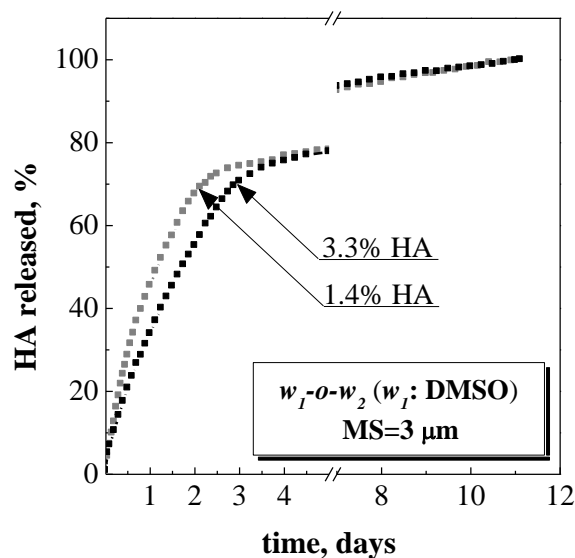
Figure VIII.7 *Comparison between the release profiles of HA from PLGA microspheres (produced from w_1-o-w_2 emulsions, w_1: DMSO) with the same mean diameter (3 μm) and charged with different effective HA loadings of 1.4% and 3.3% w/w.*

HA release profiles from PLGA microspheres (produced from w_1-o-w_2 *emulsions*, w_1: EtOH) with different mean sizes of 1 μm and 2 μm but containing the same effective HA loading of 2.1% w/w are reported in Figure VIII.8. As expected, the drug release curves show a dependence of the release profiles on the mean particle diameter: the smaller is the mean size the faster is the drug release, since the diffusion path is shorter. The total drug release from the microspheres was obtained in about 6 days. However, the complete release is not sensibly dependent on the particle diameter and the overall duration of the release kinetics is relatively similar.
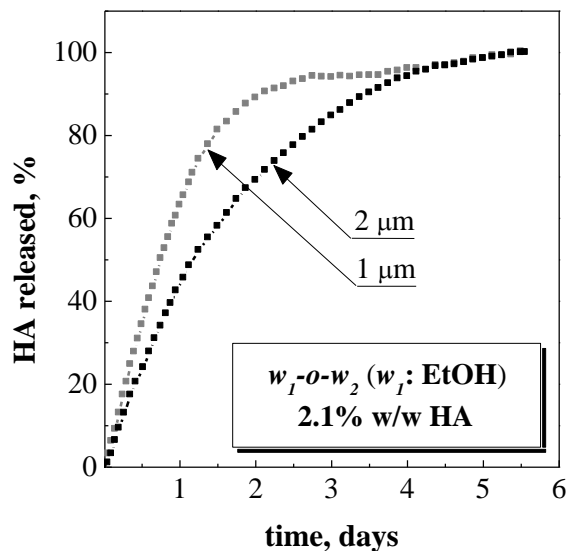
Figure VIII.8 *Comparison between the release profiles of HA from PLGA microspheres (produced from w_1-o-w_2 emulsion with w_1: EtOH) with different mean sizes of 1 μm and 2 μm and charged with the same effective HA loading of 2.1% w/w.*

A comparison between HA release profiles from PLGA microspheres with the same mean size of 3 μm but produced from *s-o-w suspension emulsions* using micronized and not-micronized HA has also been performed. As illustrated in Table VIII.4, at fixed microspheres size, a *s-o-w suspension emulsion* prepared with micronized HA allows a higher drug loading than that prepared using not-micronized HA. Particularly, the percentage of HA encapsulated was 1.4% w/w when using a *s-o-w suspension emulsion* with not-micronized HA and 2.2% w/w when using a *s-o-w suspension emulsion* with micronized HA. As a consequence, increasing the HA loading the HA release rate of microspheres decreases, as illustrated in Figure VIII.9:
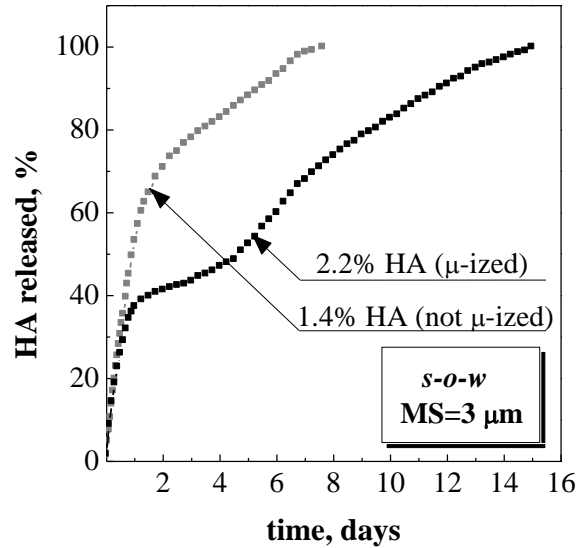
Figure VIII.9 *Comparison between the release profiles of HA from PLGA microspheres with the same mean sizes of 3 μm and produced from s-o-w suspension emulsions using micronized and not micronized HA.*

The overall drug release times measured for microspheres produced from w_1-o-w_2 *emulsions* are smaller than those measured for microspheres produced from *s-o-w suspension emulsions* using micronized HA. This behavior may be due to the fact that in the case of w_1-o-w_2 *emulsion* the resulting microspheres have a different internal structure.

Therefore, *s-o-w suspension emulsions* give better encapsulation efficiencies (see Table VIII.4) and also longer HA release times (around two weeks) in comparison with the other kinds of emulsion tested, covering the time required to control chronic inflammation step after devices implantation.

CHAPTER IX
Preparation and characterization of Insulin-loaded PLGA microdevices

Efficient delivery of peptides or proteins to target cells or organs has received considerable attention in medicine. In the last years, biodegradable microspheres have been extensively investigated as controlled release dosage forms for proteins and peptides to prolong their therapeutic effect. Most traditional devices are realized suspending the bioactive agents in a polymeric monolith and surgically implanting them into the body or encapsulating the bioactive agents in polymeric microspheres and injecting them subcutaneously (Gombotz and Pettit, 1995). The intrinsic physico-chemical properties of proteins severely obstacle the development of new protein-based therapeutics (Talmadse et al., 1993). One major reason is the inherent instability of proteins when they are exposed to the conditions normally encountered during microparticle fabrication using conventional emulsion/solvent removal techniques. Indeed, the three dimensional structure of proteins, which is crucial for biological activity, can be damaged by heat and mechanical stresses, determining aggregation and formation of insoluble precipitates (Oliva et al., 1996; Shnek et al., 1998).

To overcome the solvent evaporation limitations, the SEE-C technology has been applied to the production of controlled-size protein-loaded biopolymer microspheres to be used for locally injectable sustained release formulations, starting from a double emulsion system. Insulin has been chosen as model protein to be encapsulated within PLGA microspheres, for its wide use in the treatment of diabetes mellitus (Kang and Singh, 2005; Yeh et al., 2004; Bao et al., 2006). A detailed characterization of the produced microspheres in terms of morphology, size distribution, encapsulation efficiency and release profile is proposed.

IX.1 Size tailoring and morphology

The decrease of the stirring rate or the increase of the polymer concentration in the oily phase during the emulsion preparation can produce larger droplets (Kluge et al., 2009a; Della Porta et al., 2010). The influence of the emulsion stirring rate has been measured on droplets/microspheres size and size distribution decreasing the stirring rate from 2800 to 1000 rpm during the formation of the secondary emulsion, to explore the possibility of microspheres size tailoring. A constant PLGA concentration of 10% w/w in the organic phase was used for all these experiments.

Examples of the w_1-o-w_2 *emulsions* (1:19:80 w/w/w) produced at different stirring rates are shown in the optical microscope images reported in Figure IX.1(a-c, left side). All the emulsions were formed by stable, non-coalescing droplets. After SC-CO$_2$ solvent extraction in the continuous tower, microspheres were produced that maintained the spherical shape of the starting emulsion and formed no aggregates, as shown in the corresponding FE-SEM images reported in Figure IX.1(a-c, right side).

DSDs of the emulsions and PSDs of the related microspheres, obtained by laser scattering analysis, are reported in Figure IX.2(a-c). The experimental evidence is that the microspheres are smaller and the distributions are narrower than the droplet mean sizes and distributions from which they were generated, due to shrinkage of the droplets during solvent elimination.

Emulsion stirring rate	Optical microscope images	FE-SEM images
(a) 2800 rpm		
(b) 1400 rpm		
(c) 1000 rpm		
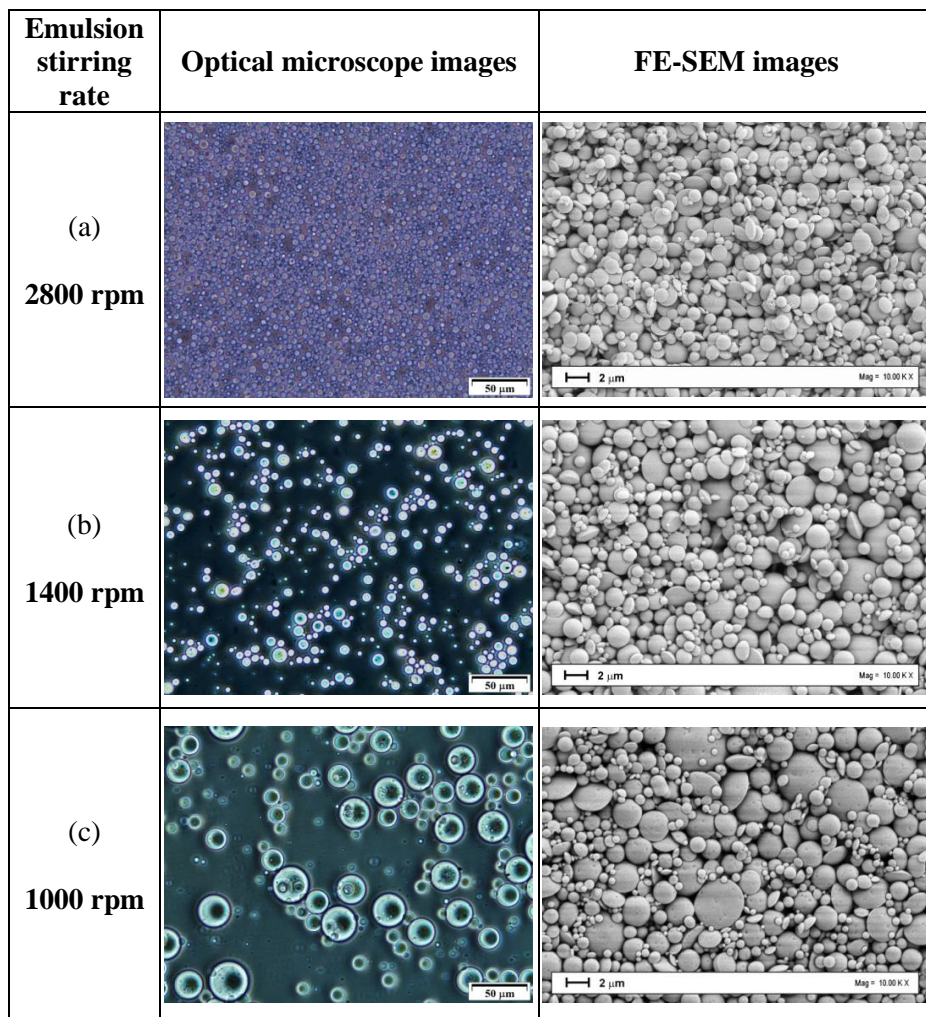
Figure IX.1(a-c) *Optical microscope images of the droplets and FE-SEM images of the microspheres produced from w_1-o-w_2 emulsions prepared at different stirring rates and treated by SEE-C.*
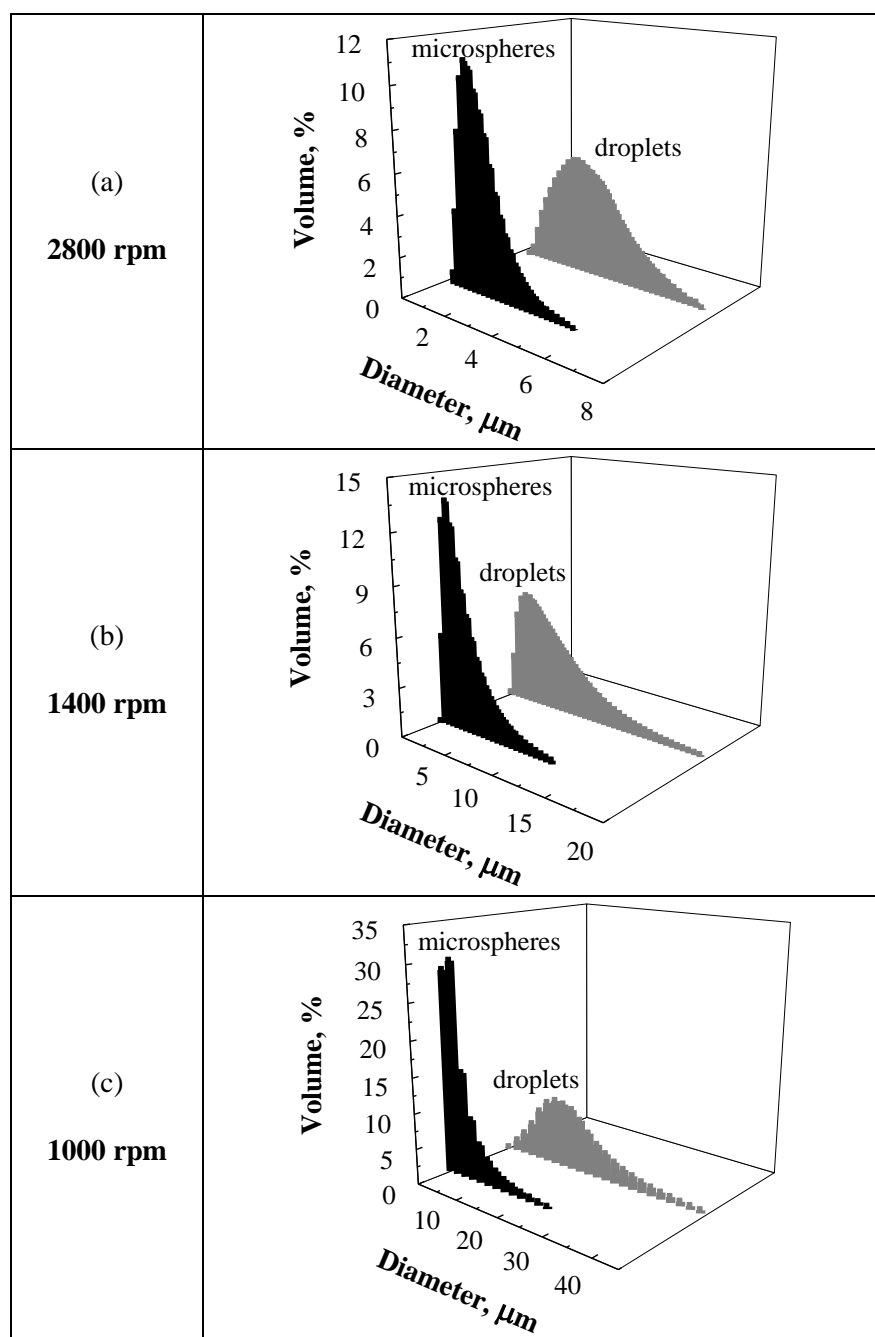
Figure IX.2(a-c). *Size distribution curves of the droplets and of the relative microspheres obtained from w_1-o-w_2 emulsions prepared at different stirring rates and treated by SEE-C.*

The PSDs curves are comparatively reported in Figure IX.3 and confirm the general evidences obtained in Figure IX.1(a-c) and Figure IX.2(a-c). However, a further information can be qualitatively deduced from this figure and quantitatively measured by the data summarized in Table IX.1: the mode of the three distributions are very similar; whereas, the PSD strongly enlarges when the emulsion stirring rate is reduced. Mean droplet sizes from 3.2 μm (SD ±1.2) to 16.9 μm (SD ±7.7) were obtained for emulsion stirring rates of 2800 and 1000 rpm, respectively. Correspondingly, microspheres with mean diameters varying from 1.8 μm (SD ±0.9) to 4.8 μm (SD ±2.8) were obtained. This result is in good agreement with those observed by other authors (Kluge et al., 2009a) and may be explained as follows: there is a minimum droplet size distribution that can be stabilized by the surfactant molecules and it is reasonable that at higher energy inputs, this lower bound is gradually approached.
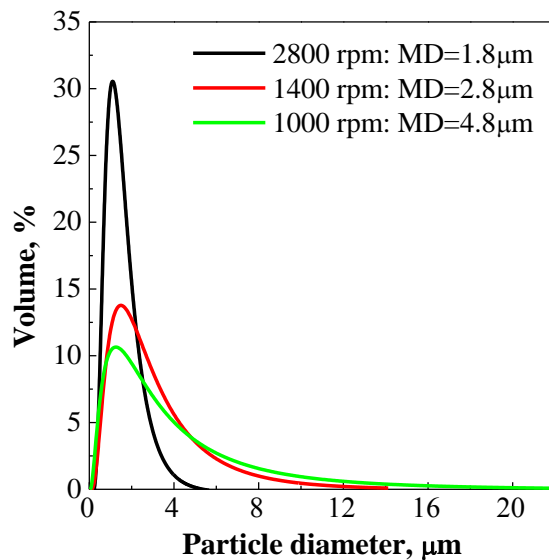
Figure IX.3 *PSDs of Insulin-loaded PLGA microspheres produced from SC-CO$_2$ extraction of w_1-o-w_2 emulsions, decreasing the stirring rate from 2800 to 1000 rpm.*

Table IX.1 *Laser scattering size distribution data of droplets (DSD) and of microspheres (PSD) produced using SEE-C from w_1-o-w_2 emulsions prepared at different stirring rates. Legend: MS = mean size; SD = standard deviation; SF = shrinking factor.*

PLGA (% w/w)		10				
INS (% w/w)	0.5		0.5		0.5	
Emulsion stirring rate (rpm)	2800		1400		1000	
Distribution data	*DSD*	*PSD*	*DSD*	*PSD*	*DSD*	*PSD*
MS (µm)	3.2	1.8	5.6	3.2	16.9	4.8
SD (µm)	±1.2	±0.9	±2.3	±2.2	±7.7	±2.8
D_{10} (µm)	1.6	0.9	1.5	1.1	4.4	0.9
D_{50} (µm)	3.2	1.8	4.8	2.9	15.7	3.4
D_{90} (µm)	5.4	3.1	11.1	6.5	29.7	9.9

IX.2 Insulin encapsulation efficiency

Encapsulation efficiency of proteins within polymeric microspheres is a complex phenomenon controlled by several factors. There are usually three main factors which are considered to affect the drug encapsulation efficiency during emulsification and solidification of double emulsions:

- (1) coalescence between inner water phase and outer water phase, leading to the leakage of the drug into the outer water phase. Therefore, the more is stable the inner water phase, the higher is drug encapsulation efficiency. For example, Insulin molecules are highly loaded in PLGA microspheres when a hydrophilic component is added to the primary solution. In the specific emulsions prepared, glycerol has been added to the inner water phase to increase the inner phase viscosity and reduce the Insulin diffusion to the outer water phase, as suggested by some authors (Yamaguchi et al., 2002).

- (2) coalescence and break-up of double emulsions, also leading to the leakage of drug;

- (3) diffusion of drug from inner to outer water phase through oil phase, during the processes of droplets formation and solvent removal (Liu et al., 2006; Bittner et al., 1998).

The influence of the microsphere size on the encapsulation efficiency has been investigated: when Insulin was entrapped in larger microspheres, higher encapsulation efficiencies were obtained (Table IX.2). This result is

also confirmed by traditional process literature data, where it is reported that when Insulin was entrapped in large microparticles, larger entrapment efficiencies were obtained (Uchida et al., 1997b; Shao and Bailey, 2000). However, SEE-C is more efficient than solvent evaporation, since the encapsulation efficiencies obtained (up to about 70%, see Table IX.2) are higher than those observed in previous traditional studies, mainly obtained from emulsions formulated using dichloromethane as the oily phase solvent, more toxic than ethyl acetate (Kawashima et al., 1999; De Rosa et al., 2000).

The effect of the protein loading on the encapsulation efficiency was also investigated and reported in Table IX.2: at a fixed particle mean size of 3 μm, increasing the Insulin loading from 0.5% to 1% w/w there is no effect on the encapsulation efficiency that is similar (~60%), as illustrated.

Table IX.2 *Theoretical and measured Insulin loading in the microspheres recovered using SEE-C technology.*

Microspheres mean size, μm	Theoretical Insulin loading, % w/w	Effective Insulin loading, % w/w	Encapsulation efficiency, %
2	0.5	0.35	63 (±2.9)
3	0.5	0.30	60 (±1.5)
3	1.0	0.58	58 (±3.4)
5	0.5	0.36	71 (±2.5)

IX.3 *In vitro* Insulin release study

Insulin-loaded microspheres with different sizes (2 and 3 μm) and protein loadings (0.3 and 0.6% w/w) have been tested to monitor the Insulin release profiles at 37°C, in two different release mediums: PBS and DMEM. The effect of different microsphere sizes (at fixed Insulin loading of 0.3% w/w) on the release profiles is shown in Figure IX.4(a) for microsphere suspended in PBS medium, and in Figure IX.4(b) for microspheres suspended in DMEM medium. The experimental data showed that the smaller is the microspheres size, the faster is the Insulin release from the microspheres. All the microspheres showed a fast release of a fixed amount of the charged Insulin in the first 2 hours. Indeed, both microdevices of 2 and 3 μm in size, when suspended in PBS, released about 55% of the encapsulated Insulin in the first 2 hours; whereas, the same microdevices suspended in DMEM showed a release of Insulin ranging between 10 and 40% in the first 2 hours. Microspheres with a mean size of 2 μm showed always a release of a higher

Insulin amount in the first 2 hours with respect to the ones with a mean size of 3 μm, in the two tested media. A possible explanation is that microspheres smaller in size have larger surface area and exhibit increased buffer penetration and a higher initial protein release. High initial release typically seen for proteins in PLGA microspheres is often ascribed to the rapid diffusion of protein molecules located at or close to the surface of the microsphere matrices (Zolnik et al., 2006). Furthermore, since Insulin is a small protein, molecules can diffuse fast as soon as the pores are formed due to water penetration after incubation (Yamaguchi et al., 2002).

The complete Insulin release was obtained after about 30 days in PBS and in 21 days in DMEM. When the DMEM medium was used, a more adequate profile in terms of sustained release was observed. The shape of the two Insulin release profiles obtained from microspheres of 2 and 3 μm also suggests the predominance of diffusion-controlled mechanism in the first part of the drug release curve, followed by a polymer bulk erosion mechanism when the two release curves of microspheres with different size start to overlap.

The effect of different Insulin loadings of 0.3 and 0.6% w/w has also been monitored on release profiles of microspheres with the same mean size (3 μm); the results obtained are shown in Figure IX.5(a) and in Figure IX.5(b) for microspheres suspended in PBS and DMEM, respectively. The higher Insulin loading of 0.6% w/w generated a faster release from microspheres and a higher amount of Insulin was released in the first 2 hours in both media. The difference in release rate is due to the fact that at higher Insulin loading there is a larger Insulin concentration gradient between the inside of the polymer microspheres and the external medium. Since the gradient is the driving force for Insulin diffusion, 0.6% w/w loading leads to a higher initial Insulin released and a more rapid release rate. Moreover, at a higher loading, there is more Insulin distributed near the surface area of microspheres. This also leads to a greater initial release. As Insulin is released, it leaves more pores and interconnecting channels for the release of the remaining protein. However, Insulin has to travel a longer path under a lower concentration gradient. Therefore, the release rate of Insulin from the microspheres decreases at the later stage, as shown in Figure IX.5(a) and in Figure IX.5(b) (Liu et al., 2006). From the comparison of the curves obtained in the two different release media, release profiles in DMEM show again reduced amounts of Insulin released in the first 2 hours and more adequate profiles in terms of sustained release than those in PBS.
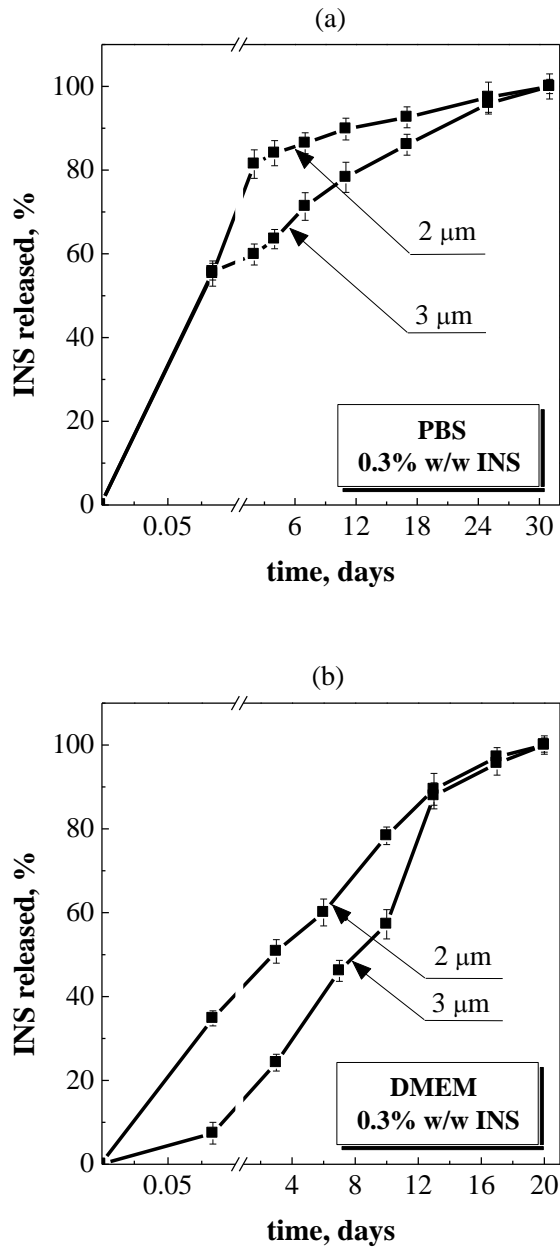
Figure IX.4(a-b) *Comparison between the release profiles of Insulin from microspheres suspended in (a) PBS and (b) DMEM, with different mean diameters (MD) and charged with the same loading of 0.3% w/w.*
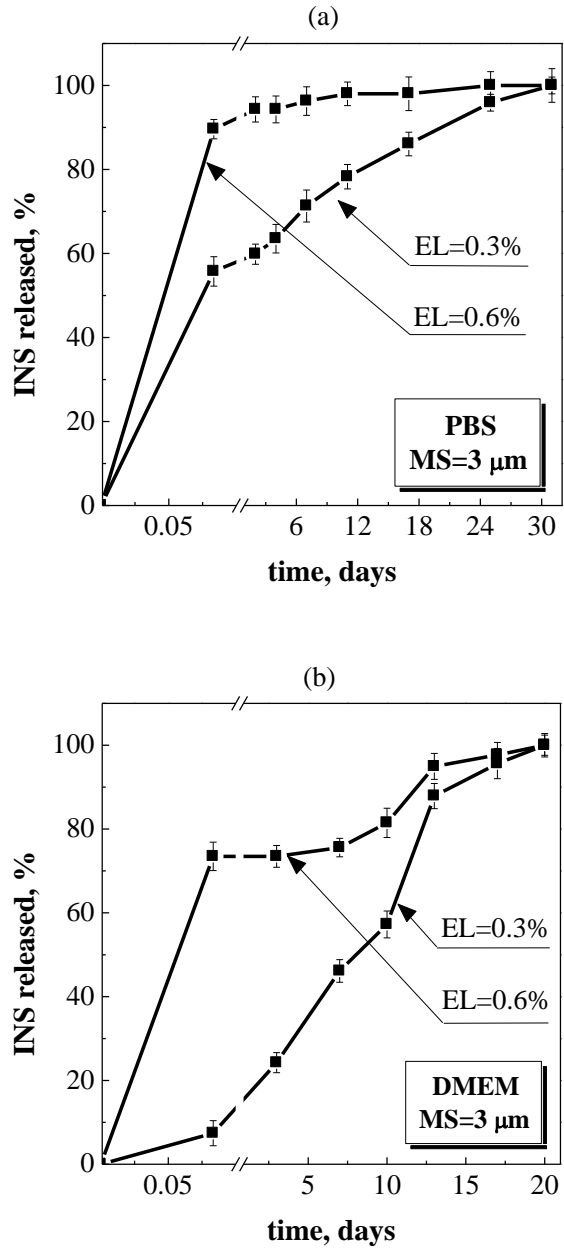
Figure IX.5(a-b) *Comparison between the release profiles of Insulin from microspheres suspended in (a) PBS and (b) DMEM, with different loadings and the same mean size of 3 µm.*

CHAPTER X
CONCLUSIONS AND FUTURE
DEVELOPMENTS

The aim of this thesis was the optimization and characterization of the SEE-C process to investigate its capabilities and performances in the production of microparticles with engineered size and distribution. The innovative process arrangement is obtained by using a high pressure packed column operating in countercurrent, in which mass transfer between the liquid and the gaseous phase is improved by the internal packing elements.

This work was developed in two main parts: a process optimization followed by the production of different AP/PLGA systems for controlled drug delivery. The process optimization included a fluidodynamic study of the packed tower, together with the analysis of the process operating parameters. Moreover, a thermodynamic study of the selected system (ethyl acetate+CO_2) was carried out. In the second part of the work, firstly drug-free PLGA microparticles were successfully produced by SEE-C process. Then, different active principles were tested for their encapsulation within PLGA microspheres: anti-inflammatory drugs (such as Piroxicam and Diclofenac Sodium), corticosteroids (such as Hydrocortisone acetate) and proteins (such as Insulin) were chosen as model compounds. Due to the very high solubility of the organic solvents commonly adopted in the formation of emulsions, the SEE-C technology can be readily extended to the preparation of microspheres from many emulsions.

The results obtained in this thesis confirm that the SEE-C technology offers a new strategy to produce tailored composite microspheres for controlled drug delivery formulations. Taking the advantage of the large contact area between SC-CO_2 and emulsion in the packed tower, SEE-C allows the production of PLGA microspheres with different size in a robust and reproducible mode in only few minutes. Well shaped and not collapsed spherical microspheres were obtained. The faster solvent extraction rate did not influence the particles morphological structure but had a significant effect on the size distribution of the precipitated particles, which were

always smaller (or at least reproduce exactly) than the size of the original droplets, avoiding the aggregation phenomena that occur during conventional processes.

Narrow particle size distributions resulted, showing a dependence on emulsion formulation parameters such as the polymer concentration and the stirring rate: increasing the polymer concentration or decreasing the emulsion stirring rate, larger particles can be obtained. Furthermore, systematic analyses confirmed that the active principles were entrapped and homogeneously dispersed, in an amorphous solid state, into the PLGA matrix.

In vitro drug release analyses showed a controlled release of the active principle from microspheres produced by SEE-C process. A characteristic drug release profile of controlled release formulations was observed, in which both diffusion and degradation mechanisms have a significant contribution. In addition, emulsion kind, microspheres size and drug concentration were clearly controlling parameters for drug release.

A comparison between the characteristics of the microspheres obtained by SEE-C and those produced by SEE and conventional SE was also proposed starting from several fixed emulsions. It was evident that SEE-C extraction is a faster process that allows a better control of the PSDs for all the systems studied.

Greater product uniformity, higher throughput with small plant volumes and elimination of the batch-to-batch repeatability problems are important advantages of the SEE-C technology respect to the batches processes. Improved recovery efficiencies, shorter processing times, less residual solvents and good drug encapsulations are other advantages of the SEE-C operation.

Future developments of these studies lie in the production of Pharmacologically Active Microcarriers (PAMs) that can be used in the regenerative medicine field to overcome problems of cell survival, lack of cell differentiation and integration in the host tissue. PAMs are biocompatible and biodegradable microparticles coated with adhesion molecules, that may serve as a support for cell culture and may be used as cell carriers presenting a controlled delivery of target growth factor. In this configuration, they can thus support the survival and differentiation of the transported cells as well as their microenvironment.

REFERENCES

Aida, T., Aizawa, T., Kanakubo, M., Nanjo, H. (2010). Analysis of volume expansion mechanism of CO_2-acetate systems at 40°C. *J. Supercrit. Fluids*, **55(1)**, 56-61.

Amass, W., Amass, A., Tighe, B. (1998) A review of biodegradable polymers: Uses, correct development in the synthesis and characterization of biodegradable polyesters, blends of polymers and recent advances in biodegradation studies. *Polym. Int.*, **47(2)**, 89-144.

Anderson, J.M., Shive, M.S. (1997) Biodegradation and biocompatibility of PLA and PLGA microspheres. *Adv. Drug Deliv. Rev*., **28(1)**, 5-24.

Anderson, J.M. (2001) Biological responses to materials. *Annu. Rev. Mater. Res*., **31**, 81-110.

André-Abrant, A., Taverdet, J.-L., Jay, J. (2001) Microencapsulation par évaporation de solvant. *Eur. Polym. J.*, **37(5)**, 955-967.

Arshady, R. (1991) Preparation of biodegradable microspheres and microcapsules: 2. Polylactides and related polyesters. *J. Contr. Rel*., **17(1)**, 1-22.

Bahl, Y., Sah, H. (2000) Dynamic changes in size distribution of emulsion droplets during ethyl acetate-based microencapsulation process. *AAPS Pharm. Sci. Technol.*, **1(1)**, 41-49.

Bancroft, W.D. (1913) Theory of emulsification. *J. Phys. Chem.*, **17**, 501-519.

Bandi, N., Roberts, C.B., Gupta, R.B., Kompella, U.B. (2004) Formulation of controlled-release drug delivery systems. In *Drugs and the pharmaceutical sciences* (P. York, U.B. Kompella, B.Y. Shekunov Eds), Marcel Dekker, New York.

Bao, W., Zhou, J., Luo, J., Wu, D. (2006) PLGA microspheres with high drug loading and high encapsulation efficiency prepared by a novel solvent evaporation technique. *J. Microencapsul.*, **23(5)**, 471-479.

References

Berchane, N.S., Jebrail, F.F., Carson, K.H., Rice-Ficht, A.C., Andrews, M.J. (2006) About mean diameter and size distributions of poly(lactide-co-glycolide) (PLG) microspheres. *J. Microencapsul.*, **23(5)**, 539-552.

Berkland, C., King, M., Cox, A., Kim, K.K., Pack, D.W. (2002) Precise control of PLG microsphere size provides enhanced control of drug release rate. *J. Contr. Rel.*, **82(1)**, 137-147.

Berkland, C., Kim, K., Pack, D. (2003) PLG microsphere size controls drug release rate through several competing factors. *Pharm. Res.*, **20(7)**, 1055-1062.

Bilati, U., Allémann, E., Doelker, E. (2005) Nanoprecipitation versus emulsion-based techniques for the encapsulation of proteins into biodegradable nanoparticles and process-related stability issues. *AAPS Pharm. Sci. Tech.*, **6(4)**, E594-604.

Bittner, B., Morlock, M., Koll, H., Winter, G., Kissel, T. (1998) Recombinant human erythropoietin (rhEPO) loaded poly(lactide-co-glycolide) microspheres: Influence of the encapsulation technique and polymer purity on microsphere characteristics. *Eur. J. Pharm. Biopharm.*, **45(3)**, 295-305.

Bitz, C., Doelker, E. (1996) Influence of the preparation method on residual solvents in biodegradable microspheres. *Int. J. Pharm.*, **131(2)**, 171-181.

Boisdron-Celle, M., Menei, P., Benoit, J.P. (1995) Preparation and characterization of 5-fluorouracil-loaded microparticles as a biodegradable anticancer drug carrier. *J. Pharm. Pharmacol.*, **47(2)**, 108-114.

Brunner, G. (2009) Counter-current separations. *J. Supercrit. Fluids*, **47(3)**, 574-582.

Burgess, D.J., Hickey, A.J. (1994) Microsphere technology and applications. In *Encyclopedia of pharmaceutical technology* (J. Swarbrick, J.C. Boylon Eds), Marcel Dekker, New York and Basel, p. 1-29.

Byun, H.S., Choi, M.Y., Lim, J.S. (2006) High-pressure phase behavior and modeling of binary mixtures for alkyl acetate in supercritical carbon dioxide. *J. Supercrit. Fluids*, **37(3)**, 323-332.

Cao, X., Schoichet, M.S. (1999) Delivering neuroactive molecules from biodegradable microspheres for application in central nervous system disorders. *Biomaterials*, **20(4)**, 329-339.

Carrio, A., Schwach, G., Coudane, J., Vert, M. (1995) Preparation and degradation of surfactant-free PLAGA microspheres. *J. Contr. Rel.*, **37(1-2)**, 113-121.

Chacón, M., Berges, L., Molpeceres, J., Aberturas, M.R., Guzman M. (1996) Optimized preparation of poly D,L (lactic-glycolic) microspheres and nanoparticles for oral administration. *Int. J. Pharm.*, **141(1-2)**, 81-91.

Chakraborty, S., Khanday, M., Patra, C.N., Patro,V.J., Sen, K.K. (2009) Effects of drug solubility on the release kinetics of water soluble and insoluble drugs from HPMC based matrix formulations. *Acta Pharm.*, **59(3)**, 313-323.

Chattopadhyay, P., Gupta, R.B. (2003) Supercritical CO_2 based formation of silica nanoparticles using water-in-oil microemulsions. *Ind. Eng. Chem. Res.*, **42(3)**, 465-472.

Chattopadhyay, P., Shekunov, B.Y., Seitzinger, J., Huff, R. (2004) Particles from supercritical fluid extraction of emulsion. *US Patent* no. US2004/0026319 A1.

Chattopadhyay, P., Huff, R., Shekunov, B.Y. (2006) Drug encapsulation using supercritical fluid extraction of emulsions. *J Pharm. Sci.*, **95(3)**, 667-679.

Chattopadhyay, P., Shekunov, B.Y., Yim, D., Cipolla, D., Boyd, B., Farr, S. (2007) Production of solid lipid nanoparticle suspensions using supercritical fluid extraction of emulsions (SFEE) for pulmonary delivery using the AERx system. *Adv. Drug Del. Rev.*, **59(6)**, 444-453.

Chester, T.L., Haynes, B.S. (1997) Estimation of pressure-temperature critical loci of CO_2 binary mixtures with methyl-*tert*-butyl ether, ethyl acetate, methyl-ethyl ketone, dioxane and decane. *J. Supercrit. Fluids*, **11(1-2)**, 15-20.

Chulia, D., Deleuil, M., Pourcelot, Y. (1994) *Powder Technology and Pharmaceutical Processes*, Elsevier Science Publishing Company, New York.

Chung, T.-W., Huang, Y.-Y., Liu, Y.-Z. (2001) Effects of the rate of solvent evaporation on the characteristics of drug loaded PLLA and PDLLA microspheres. *Int. J. Pharm.*, **212**, 161-169.

Cohen, S., Yoshioka, T., Lucarelli, M., Hwang, L.H., Langer, R. (1991) Controlled delivery systems for proteins based on poly(lactic/glycolic acid) microspheres. *Pharm. Res.*, **8(6)**, 713-720.

Costa, H.F., Gardas, R.L., Johnson, I., Fonseca, I.M.A., Ferreira, A.G.M. (2009) PVT property measurements for ethyl propionate, ethyl butyrate, and ethyl pentanoate esters from (298 to 393) K and up to 35 MPa. *J. Chem. Eng. Data*, **54(2)**, 256-262.

References

Cowsar, D.R., Tice, T.R., Gilley, R.M., English, J.P. (1985) Poly(lactide-co-glycolide) microspheres for controlled release of steroids. *Methods Enzymol.*, **112**, 101-116.

da Silva, M.V., Barbosa, D., Ferreira, P.O., Mendonça, J. (2000) High pressure phase equilibrium data for the systems carbon dioxide/ethyl acetate and carbon dioxide/isoamyl acetate at 295.2, 303.2, and 313.2 K. *Fluid Phase Equil.*, **175(1-2)**, 19-23.

Dass, C.R., Burton, M.A. (1999) Microsphere-mediated targeted gene therapy of solid tumors. *Drug Deliv.*, **6(4)**, 243-252.

De, S., Robinson, D.H. (2004). Particle size and temperature effect on the physical stability of PLGA nano-spheres and micro-spheres containing Bodipy. *AAPS Pharm. Sci. Tech.*, **5(4)**, 18-24.

De Rosa, G., Iommelli, R., La Rotonda, M.I., Miro, A., Quaglia, F. (2000) Influence of the co-encapsulation of different non-ionic surfactants on the properties of PLGA insulin-loaded microspheres. *J Contr. Rel.*, **69(2)**, 283-295.

Debenedetti, P.G., Tom J.W., Yeo S.D., Lim G.B. (1993) Application of supercritical fluids for the production of sustained delivery devices. *J. Contr. Rel.*, **24(1-3)**, 27-44.

Declercq, H.A., Gorski, T.L., Tielens, S.P., Schacht, E.H., Cornelissen, M.J. (2005) Encapsulation of osteoblast seeded microcarriers into injectable, photopolymerizable three-dimensional scaffolds based on d,l-lactide and ε-caprolactone. *Biomacromol.*, **6(3)**, 1608-1614.

Della Porta, G., De Vittori, C., Reverchon, E. (2005) Supercritical assisted atomization: A novel technology for micro-particles preparation of an asthma-controlling drug. *AAPS Pharm. Sci. Tech.*, **6(3)**, E421-428.

Della Porta, G., Ercolino, S.F., Parente, L., Reverchon, E. (2006) Corticosteroids micro-particles produced by supercritical assisted atomization: Process optimization, product characterization and ''in vitro'' performance. *J. Pharm. Sci.*, **95(9)**, 2062-2076.

Della Porta, G., Reverchon E. (2008a). Supercritical fluid-based technologies for particulate drug delivery. In *Handbook of particulate drug delivery* (M.N.V. Ravi Kumar Ed), American Scientific Publishers, New York, p.35-59.

Della Porta, G., Reverchon, E. (2008b) Nanostructured microspheres produced by supercritical fluid extraction of emulsion. *Biotech. Bioeng.*, **100(5)**, 1020-1033.

156

Della Porta, G., Falco, N., Reverchon, E. (2010) NSAID drugs release from injectable microspheres produced by supercritical fluid emulsion extraction. *J Pharm. Sci.*, **99(3)**, 1484-1499.

Della Porta, G., Falco, N., Reverchon, E. (2011) Continuous Supercritical Emulsions Extraction: A new technology for biopolymer microparticles production. *Biotech. Bioeng.*, **108(3)**, 676-677.

Dillow, A.K., Dehghani, F., Hrkach, J.S., Foster, N.R., Langer, R. (1999) Bacterial inactivation by using near- and supercritical carbon dioxide. *Proc. Natl. Acad. Sci. USA*, **96(18)**, 10344-10348.

Emami, J., Hamishehkar, H., Najafabadi, A.R., Gilani, K., Minaiyan, M., Mahdavi, H., Mirzadeh, H., Fakhari, A., Nokhodchi, A. (2009) Particle size design of PLGA microspheres for potential pulmonary drug delivery using response surface methodology. *J. Microencapsul.*, **26(1)**, 1-8.

Evora, C., Soriano, I., Rogers, R.A., Shakesheff, K.M., Hanes, J., Langer, R. (1998) Relating the phagocytosis of microparticles by alveolar macrophages to surface chemistry: The effect of 1,2-dipalmitoylphosphatidylcholine. *J. Contr. Rel.*, **51(2-3)**, 143-152.

Faisant, N., Akiki, J., Siepmann, F., Benoit, J.P., Siepmann, J. (2006) Effects of the type of release medium on drug release from PLGA-based microparticles: Experiment and theory. *Int. J. Pharm.*, **314(2)**, 189-197.

Falco, N., Kiran E. (2012) Volumetric properties of ethyl acetate + carbon dioxide binary fluid mixtures at high pressures, *J. Supercrit. Fluids*, **61**, 9-24.

Federal Register (1997). International Conference on Harmonisation. Guidance on impurities: Residual solvents. *Fed. Regist.*, **62(247)**, 67377-67388.

Freiberg, S., Zhu, X.X. (2004) Polymer microspheres for controlled drug release. *Int. J. Pharm.*, **282(1-2)**, 1-18.

Freitas, S., Merkle, H.P., Gander B. (2005) Microencapsulation by solvent extraction/evaporation: Reviewing the state of the art of microsphere preparation process technology. *J. Contr. Rel.*, **102(2)**, 313-332.

Freytag, T., Dashevsky, A., Tillman, L., Hardee, G.E., Bodmeier, R. (2000) Improvement of the encapsulation efficiency of oligonucleotide-containing biodegradable microspheres. *J. Contr. Rel.*, **69(1)**, 197-207.

Fusaro, F., Mazzotti, M., Muhrer, G. (2004) Gas antisolvent recrystallization of paracetamol from acetone using compressed carbon dioxide as antisolvent. *Cryst. Growth Des.*, **4(5)**, 881-889.

References

Gardas, R.L., Johnson, I., Vaz, D.M.D., Fonseca, I.M.A., Ferreira, A.G.M. (2007) PVT property measurements for some aliphatic esters from (298 to 393) K and up to 35 MPa. *J. Chem. Eng. Data*, **52(3)**, 737-751.

Ghaderi, R., Artursson, P., Carlfors, J. (2000). A new method for preparing biodegradable microparticles and entrapment of hydrocortisone in DL-PLG microparticles using supercritical fluids. *Eur. J. Pharm. Sci.*, **10(1)**, 1-9.

Ginty, P.J., Whitaker, M.J., Shakesheff, K.M., Howdle, S.M. (2005) Drug delivery goes supercritical? *Mater. Today*, **8(8)**, 42-48.

Gombotz, W.R., Pettit, D.K. (1995) Biodegradable polymers for protein and peptide drug delivery. *Bioconjug. Chem.*, **6(4)**, 332-351.

Hardman, J., Limbird, L., Molinoff, P., Ruddon, R., Gilman, A. (1996) *Goodman and Gilman's The pharmacological basis of therapeutics*, 9th ed., McGraw-Hill, New York.

Herrmann, J., Bodmeier, R. (1995) Somatostatin containing biodegradable microspheres prepared by a modified solvent evaporation method based on W/O/W-multiple emulsions. *Int. J. Pharm.*, **126(1-2)**, 129-138.

Hickey, T., Kreutzer, D., Burgess, D.J., Moussy, F. (2002a) Dexamethasone/PLGA microspheres for continuous delivery of an anti-inflammatory drug for implantable medical devices. *Biomaterials*, **23(7)**, 1649-1656.

Hickey, T., Kreutzer, D., Burgess, D.J., Moussy, F. (2002b) *In vivo* evaluation of a Dexamethasone/PLGA microsphere system designed to suppress the inflammatory tissue response to implantable medical devices. *J. Biomed. Mater. Res.*, **61(2)**, 180-187.

Hong, Y., Gao, C.Y., Xie, Y., Gong, Y.H., Shen, J.C. (2005) Collagen-coated polylactide microspheres as chondrocyte microcarriers. *Biomaterials*, **26(32)**, 6305-6313.

Hou, Y., Chen, X., Ren, S., Song, Z., Wu, W. (2010) Phase behavior, densities, and isothermal compressibility of (carbon dioxide + dimethyl carbonate). *J. Chem. Eng. Data*, **55(4)**, 1580-1587.

Hsu, Y.Y, Hao, T., Hedley, M.L. (1999) Comparison of process parameters for microencapsulation of plasmid DNA in poly(D,L-lactic-co-glycolic) acid microspheres. *J. Drug Target.*, **7(4)**, 313-323.

Huang, Y.-Y., Chung, T.-W., Tzeng, T.-W. (1997) Drug release from PLA/PEG microparticulates. *Int. J. Pharm.*, **156(1)**, 9-15.

Jaklenec, A., Wan, E., Murray, M.E., Mathiowitz, E. (2008) Novel scaffolds fabricated from protein-loaded microspheres for tissue engineering. *Biomaterials*, **29(2)**, 185-192.

Jain, R.A. (2000) The manufacturing techniques of various drug loaded biodegradable poly(lactide-co-glycolide) (PLGA) devices, *Biomaterials*, **21(23)**, 2475-2490.

Jeyanthi, R., Mehta, R.C., Thanoo, B.C., Deluca, P.P. (1997) Effect of processing parameters on the properties of peptide-containing PLGA microspheres. *J. Microencapsul.*, **14(2)**, 163-174.

Johnston, R.B., Jr. (1988) Current concepts: immunology. Monocytes and macrophages. *N. Engl. J. Med.*, **318(12)**, 747-752.

Kang, S.W., Jeon, O., Kim, B.S. (2005) Poly(lactic-co-glycolic acid) microspheres as an injectable scaffold for cartilage tissue engineering. *Tissue Eng.*, **11(3-4)**, 438-447.

Kang, F., Singh, J. (2005) Preparation, in vitro release, in vivo absorption and biocompatibility studies of insulin-loaded microspheres in rabbits. *AAPS Pharm. Sci. Tech.*, **6(3)**, E487-494.

Kang, Y.Q., Yin, G.F., Ping, O.Y., Huang, X.B., Yao, Y.D., Liao, X.M., Chen, A.Z., Pu, X.M. (2008) Preparation of PLLA/PLGA microparticles using solution enhanced dispersion by supercritical fluids (SEDS). *J. Coll. Interf. Sci.*, **322(1)**, 87-94.

Kawashima, Y., Yamamoto, H., Takeuchi, H., Fujioka, S., Hino, T. (1999) Pulmonary delivery of insulin with nebulized DL-lactide/glycolide copolymer (PLGA) nanospheres to prolong hypoglycemic effect. *J. Contr. Rel.*, **62(1-2)**, 279-287.

Kim, H., Lee, H., Park, T.G. (2002) Pegylated recombinant human epidermal growth factor for sustained release from biodegradable PLGA microspheres. *Biomaterials*, **23**, 2311-2317.

King, M.B., Mubarak, A., Kim, J.D., Bott, T.R. (1992). The mutual solubilities of water with supercritical and liquid carbon dioxide. *J. Supercrit. Fluids*, **5(4)**, 296-302.

King, T.W., Patrick, C.W. (2000) Development and in vitro characterization of vascular endothelial growth factor (VEGF)-loaded poly(lactic-co-glycolic acid)/poly(ethylene glycol) microspheres using a solid encapsulation/single emulsion/solvent extraction technique. *J. Biomed. Mater. Res.*, **51(3)**, 383-390.

Klose, D., Siepmann, F., Elkharraz, K., Krenzlin, S., Siepmann, J. (2006) How porosity and size affect the drug release mechanisms from PLGA-based microparticles. *Int. J. Pharm.*, **314(2)**, 198-206.

Kluge, J., Fusaro, F., Casas, N., Mazzotti, M., Muhrer, G. (2009a) Production of PLGA micro- and nanocomposites by supercritical fluid

extraction of emulsions: I. Encapsulation of lysozyme. *J. Supercrit. Fluids*, **50(3)**, 327-335.

Kluge, J., Fusaro, F., Mazzotti, M., Muhrer, G. (2009b) Production of PLGA micro- and nanocomposites by supercritical fluid extraction of emulsions: II. Encapsulation of ketoprofen. *J. Supercrit. Fluids*, **50(3)**, 336-343.

Kongsombut, B., Tsutsumi, A., Suankaew, N., Charinpanitkul, T. (2009) Encapsulation of SiO_2 and TiO_2 fine powders with poly-lactic-co-glycolic acid by rapid expansion of supercritical CO_2 incorporated with ethanol cosolvent. *Ind. Eng. Chem. Res.*, **48(24)**, 11230-11235.

Langer, R. (1998) Drug delivery targets. *Nature*, **392**, 5-10.

Langer, R. (2000) Biomaterials in drug delivery and tissue engineering: one laboratory's experience. *Acc. Chem. Res.*, **33(2)**, 94-101.

Lee, P.I. (1980) Diffusional release of a solute from a polymeric matrix-Approximate analytical solution. *J. Membr. Sci.*, **7(3)**, 255-275.

Lewis, D.H. (1990) Controlled release of bioactive agents from lactide/glycolide polymers. In *Biodegradable polymers as drug delivery systems* (M. Chasin and R. Langer Eds), Marcel Dekker, New York, p. 1-41.

Li, W.I., Anderson, K.W., Deluca, P.P. (1995) Kinetic and thermodynamic modelling of the formation of polymeric microspheres using solvent extraction/evaporation method. *J. Contr. Rel.*, **37(3)**, 187-198.

Li, M., Rouand, O., Poncelet, D. (2008) Microencapsulation by solvent evaporation: State of the art for process engineering approaches. *Int. J. Pharm.*, **363(1-2)**, 26-39.

Liu, R., Huang, S.S., Wan, Y.H., Ma, G.H., Su, Z.G. (2006) Preparation of insulin-loaded PLA/PLGA microcapsules by a novel membrane emulsification method and its release in vitro. *Coll. Surf. B: Biointerf.*, **51(1)**, 30-38.

Lobo, W.E., Friend, L., Hashmall, H., Zenz, F.A. (1945) Limiting capacity of dumped tower packings. *Trans. AIChE*, **41**, 693-710.

Luan, X., Skupin, M., Siepmann, J., Bodmeier, R. (2006) Key parameters affecting the initial release (burst) and encapsulation efficiency of peptide containing poly(lactide-co-glycolide) microparticles. *Int. J. Pharm.*, **324(2)**, 168-175.

Luten, J., van Nostrum, C.F., De Smedt, S.C., Hennink, W.E. (2008) Biodegradable polymers as non-viral carriers for plasmid DNA delivery. J. *Contr. Rel.*, **126(2)**, 97-110.

Mason, N., Thies, C., Cicero, T.J. (1976) In vivo and in vitro evaluation of a microencapsulated narcotic antagonists. *J. Pharm. Sci.*, **65(6)**, 847-850.

Matsumoto, A., Kitazawa, T., Murata, J., Horikiri, Y., Yamahara, H. (2008) A novel preparation method for PLGA microspheres using non-halogenated solvents. *J. Contr. Rel.*, **129(3)**, 223-227.

Mattea, F., Martin, A., Schulz, C., Jaeger, P., Eggers, R., Cocero, M.J. (2010) Behavior of an organic solvent drop during the supercritical extraction of emulsions. *AIChE J.*, **56(5)**, 1184-1195.

Meinel, L., Illi, O.E., Zapf, J., Malfanti, M., Merkle, H.P., Gander, B. (2001) Stabilizing insulin-like growth factor-I in poly(lactide-co-glycolide) microspheres. *J. Contr. Rel.*, **70(1-2)**, 193-202.

Meng, F.T., Ma, G.H., Liu, T.D., Qui, W., Su, Z.S. (2004) Microencapsulation of bovine hemoglobin with high bioactivity and high entrapment efficiency using W/O/W double emulsion technique. *Coll. Surf. B: Biointerf.*, **33(3-4)**, 177-183.

Mercier, N.R., Costantino, H.R., Tracy, M.A., Bonassar, L.J. (2005) Poly(lactide-co-glycolide) microspheres as a moldable scaffold for cartilage tissue engineering. *Biomaterials*, **26(14)**, 1945-1952.

Miller, R., Brady, J.M, Cutright, D. (1977) Degradation rates of oral resorbable implants (polylactates and polyglycolates): Rate modification with changes in PLA/PGA copolymer ratios. *J. Biomed. Mater. Res.*, **11(5)**, 711-719.

Muhrer, G. Meier, U., Fusaro, F., Albano, S., Mazzotti, M. (2006) Use of compressed gas precipitation to enhance the dissolution behavior of a poorly water-soluble drug: Generation of drug microparticles and drug-polymer solid dispersions. *Int. J. Pharm.*, **308(1-2)**, 69-83.

Mundargi, R.C., Babu, V.R., Rangaswamy, V., Patel, P., Aminabhavi, T.M. (2008) Nano/micro technologies for delivering macromolecular therapeutics using poly(D,L lactide-co-glycolide) and its derivatives. *J. Contr. Rel.*, **125(3)**,193-209.

National Institute of Standards and Technology (NIST) - http://webbook.nist.gov/chemistry/fluid.

O'Donnell, P.B., McGinity, J.W. (1997) Preparation of microspheres by solvent evaporation technique. *Adv. Drug Deliv. Rev.*, **28(1)**, 25-42.

Okada, H., Toguchi, H. (1995) Biodegradable microspheres in drug delivery. *Crit. Rev. Ther. Drug Carrier Syst*., **12(1)**, 1-99.

Oliva, A., Fariña, J.B, Labrés, M. (1996) Influence of temperature and shaking on stability of insulin preparation: Degradation kinetics. *Int. J. Pharm.*, **143(2)**, 163-170.

References

Onuki, Y., Bhardwaj, U., Papadimitrakopoulos, F., Burgess, D.J. (2008) A review of the biocompatibility of implantable devices: Current challenges to overcome foreign body response. *J. Diabetes Sci. Technol.*, **2(6)**, 1003-1015.

Park, K. (1997) *Controlled drug delivery: Challenges and strategies*, American Chemical Society, Washington, DC.

Pensado, A.S., Pádua, A.A.H., Comuňas, M.J.P., Fernández, J. (2008) High-pressure viscosity and density of carbon dioxide+pentaerythritol ester mixtures: measurements and modeling. *AIChE J.*, **54(6)**, 1625-1636.

Peters, M.S., Timmerhaus, K.D. (1968) *Plant Design and Economics for Chemical Engineers*, 5th ed., McGraw-Hill, New York, p. 698.

Pini, R., Storti, G., Mazzotti, M., Tai, H.Y., Shakesheff, K.M., Howdle, S.M. (2008) Sorption and swelling of poly(D,L-lactic acid) and poly(lactic-co-glycolic acid) in supercritical CO_2: An experimental and modeling study. *J. Polym. Sci. B:Polym. Phys.*, **46(5)**, 483-496.

Pöhler, H., Kiran, E. (1996) Volumetric properties of carbon dioxide+toluene at high pressures. *J. Chem. Eng. Data*, **41(2)**, 482-486.

Pöhler, H., Kiran, E. (1997a) Volumetric properties of carbon dioxide+ethanol at high pressures. *J. Chem. Eng. Data*, **42(2)**, 384-388.

Pöhler, H., Kiran, E. (1997b) Volumetric properties of carbon dioxide+acetone at high pressures. *J. Chem. Eng. Data*, **42(2)**, 379-383.

Ratner, B.D., Bryant, S.J. (2004) Biomaterials: where we have been and where we are going. *Annu. Rev. Biomed. Eng.*, **6**, 41-75.

Reichl, A., Daiminger, U., Schmidt, A., Davies, M., Hoffmann, U., Brinkmeier, C., Reder, C., Marquardt, W. (1998) A non-recycle flow still for the experimental determination of vapor-liquid equilibria in reactive systems. *Fluid Phase Equil.*, **153(1)**, 113-134.

Ren, J.M., Zou, Q.M., Wang, F.K., He, Q.A., Chen, W., Zen, W.K. (2002) PELA microspheres loaded H_pylori lysates and their mucosal immune response. *World J. Gastroenterol.*, **8**, 1098-1102.

Reverchon, E., Adami, R. (2006) Nanomaterials and supercritical fluids. *J. Supercrit. Fluids*, **37(1)**, 1-22.

Reverchon. E., Cardea, S., Schiavo Rappo, E. (2006) Production of loaded PMMA structures using the supercritical CO_2 phase inversion process. *J. Membr. Sci.*, **273(1-2)**, 97-105.

Reverchon, E., De Marco, I. (2006) Supercritical fluid extraction and fractionation of natural matter. *J. Supercrit. Fluids*, **38(2)**,146-166.

Reverchon, E., Antonacci, A. (2007) Drug-polymer microparticles produced by supercritical assisted atomization. *Biotech. Bioeng.,* **97(6)**, 1626-1637.

Reverchon, E., Della Porta, G. (2007) Processo continuo per la produzione di microsfere mediante liquidi espansi. *Italian Patent* no. SA2007A/000024.

Reverchon, E., Della Porta, G., Torino, E. (2010) Production of metal oxide nanoparticles by supercritical emulsion reaction. *J. Supercrit. Fluids*, **53(1-3)**, 95-101.

Richardson, J. F., Harker, J. H., Backhurst, J. R. (2002) Liquid-liquid extraction. In *Coulson & Richardson's Chemical Engineering: Particle Technology and Separation Processes*, 5th ed., Butterworth-Heinemann, Oxford, Tome 2, Chapter 13.

Riha, V., Brunner, G. (2000) Separation of fish oil ethyl esters with supercritical carbon dioxide. *J. Supercrit. Fluids*, **17(1)**, 55-64.

Rolland, A., Wagner, N., Chatelus, A., Shroot, B., Schaefer, H. (1993). Site-specific drug delivery to pilosebaceous structures using polymeric microspheres. *Pharm. Res.*, **10(12)**, 1738-1744.

Rosca, I.D., Watari, F., Uo, M. (2004) Microparticle formation and its mechanism in single and double emulsion solvent evaporation. *J. Contr. Rel.*, **99(2)**, 271-280.

Sabirzyanov, A.N., Il'in, A.P., Akhunov, A.R., Gumerov, F.M. (2002). Solubility of water in supercritical carbon dioxide. *High Temp.*, **40(2)**, 203-206.

Sah, H. (2000) Ethyl formate - alternative dispersed solvent useful in preparing PLGA microspheres. *Int. J. Pharm.*, **195(1-2)**, 103-113.

Shao, P.G., Bailey, L.C. (2000) Porcine insulin biodegradable polyester microspheres: stability and in vitro release characteristics. *Pharm. Dev. Technol.*, **5(1)**, 1-9.

Sherwood, T.K., Shipley, G.H., Holloway, F.A.L. (1938) Flooding velocities in packed columns. *Ind. Eng. Chem.*, **30(7)**, 765-769.

Shnek, D.R., Hostettler, D.L., Bell, M.A., Olinger, J.M., Frank, B.H. (1998) Physical stress testing of insulin suspensions and solutions. *J. Pharm. Sci.*, **87(11)**, 1459-1465.

Siepmann, J., Gopferich, A. (2001) Mathematical modelling of bioerodible, polymeric drug delivery systems. *Adv. Drug Deliv. Rev.*, **48(2-3)**, 229-247.

Singh, M., Sandhu, B., Scurto, A., Berkland, C., Detamore, M.S. (2010) Microspheres-based scaffolds for cartilage tissue engineering: Using subcritical CO_2 as a sintering agent. *Acta Biomater.*, **6(1)**, 137-143.

Smith, R.L., Jr., Yamaguchi, T., Sato, T., Suzuki, H., Arai, K. (1998) Volumetric behavior of ethyl acetate, ethyl octanoate, ethyl laurate, ethyl

linoleate, and fish oil ethyl esters in the presence of supercritical CO_2. *J. Supercrit. Fluids*, **13(1-3)**, 29-36.

Soriano, I., Evora, C., Llabrés, M. (1996). Preparation and evaluation of insulin-loaded poly(DL lactide) microspheres using an experimental design. *Int. J. Pharm.*, **142(2)**, 135-142.

Sturesson, C., Artursson, P., Ghaderi, R., Johansen, K., Mirazimi, A., Uhnoo, I., Svensson, L., Albertsson, A.C., Carlfors, J. (1999) Encapsulation of rotavirus into poly(lactide-co-glycolide) microspheres. *J. Contr. Rel*, **59(3)**, 377-389.

Tadros, T. (2004) Application of rheology for assessment and prediction of the long-term physical stability of emulsions. *Adv. Coll. Interf. Sci.*, **108-109**, 227-258.

Talmadse, J. E. (1993) The pharmaceutics and delivery of therapeutic polypeptides and proteins. *Adv. Drug Del. Rev.*, **10(2-3)**, 247-299.

Tandya, A., Mammucari, R., Dehghani, F., Foster, N.R. (2007) Dense gas processing of polymeric controlled release formulations. *Int. J. Pharm.*, **328(1)**, 1-11.

Ting, S.S.T., Tomasko, D.L., Foster, N.R., Macnaughton, S.J. (1993) Solubility of naproxen in supercritical carbon dioxide with and without cosolvents. *Ind. Eng. Chem. Res.*, **32(7)**, 1471-1481.

Uchida, T., Yoshida, K., Nakada, Y., Nagareya, N., Konoshi, Y., Nakai, A., Nishikata, M., Matsuyama, K. (1997a) Preparation and characterization of polylactic acid microspheres containing water-soluble Anesthetics with small molecular weight. *Chem. Pharm. Bull.*, **45(3)**, 513-517.

Uchida, T., Nagareya, N., Sakakibara, S., Konishi, Y., Nakai, A., Nishikata, M., Matsuyama, K., Yoshida, K. (1997b) Preparation and characterization of polylactic acid microspheres containing bovine insulin by a w/o/w emulsion solvent evaporation method. *Chem. Pharm. Bull. (Tokyo),* **45(9)**, 1539-1543.

Vandervoort, J., Ludwig, A. (2004) Preparation and evaluation of drug-loaded gelatin nanoparticles for topical ophthalmic use. *Eur. J. Pharm. Biopharm.*, **57(2)**, 251-261.

Vargaftik, N.B. (1975) *Tables on the thermophysical properties of liquids and gases*, John Wiley and Sons, New York.

Verrijk, R., Smolde, I.J., Bosnie, N., Begg, A.C. (1992) Reduction of systemic exposure and toxicity of cisplatin by encapsulation in poly(lactide-co-glycolide). *Cancer Res.*, **52(23)**, 6653-6656.

Vert, M., Li, S.M., Spenlehauer, G., Guerin, P. (1993) Bioresorbability and biocompatibility of aliphatic polyesters. *J. Mater. Sci.: Mater. Med.*, **3(6)**, 432-446.

164

Viswanathan, N.B., Thomas, P.A., Pandit, J.K., Kulkarni, M.G., Mashelkar, R.A. (1999) Preparation of non-porous microspheres with high entrapment efficiency of proteins by a (water-in-oil)-in-oil emulsion technique. *J. Contr. Rel.*, **58(1)**, 9-20.

Von Burkersroda, F., Schedl, L., Göpferich, A. (2002) Why degradable polymers undergo surface erosion or bulk erosion. *Biomaterials*, **23(21)**, 4221-4231.

Wagner, Z., Pavlíček, J. (1994) Vapour-liquid equilibrium in the carbon dioxide-ethyl acetate system at high pressure. *Fluid Phase Equil.,* **97**, 119-126.

Walter, E., Dreher, D., Kok, M., Thiele, L., Kiama, S.G., Gehr, P., Merkle, H.P. (2001) Hydrophylic poly(DL-lactide-co-glycolide) microspheres for the delivery of DNA to human derived macrophages and dentritic cells. *J. Contr. Rel.*, **76(1-2)**, 149-168.

Washington, C. (1996) Drug release from microparticulate system. In *Microencapsulation, methods and industrial application* (S. Benita Ed), Marcel Dekker, New York, p. 155-181.

Watts, P.J., Davies, M.C., Melia, C.D. (1990). Microencapsulation using emulsification/solvent evaporation: An overview of techniques and applications. *Int. J. Pharm.*, **7(3)**, 235-250.

Wiebe, R., Gaddy, V. (1940). The solubility of carbon dioxide in water at various temperatures from 12 to 40°C and at pressures to 500 atmospheres. Critical phenomena. *J. Am. Chem. Soc.*, **62(4)**, 815-817.

Wyczesany, A. (2007) Modeling of simultaneous chemical and phase equilibria in esterification of acetic acid with ethanol in high-pressure carbon dioxide. *Ind. Eng. Chem. Res.*, **46(16)**, 5437-5445.

Yamaguchi, Y., Takenaga, M., Kitagawa, A., Ogawa, Y., Mizushima, Y., Igarashi, R. (2002) Insulin-loaded biodegradable PLGA microcapsules: Initial burst release controlled by hydrophilic additives. *J. Contr. Rel.,* **81(3)**, 235-249.

Yang, Y.Y., Chia, H.H., Chung, T.S. (2000) Effect of preparation temperature on the characteristics and release profiles of PLGA microspheres containing protein fabricated by double-emulsion solvent extraction/evaporation method. *J. Contr. Rel.*, **69(1)**, 81-96.

Yang, Y.Y., Chung, T.S., Ng, N.P. (2001) Morphology, drug distribution, and in vitro release profiles of biodegradable polymeric microspheres containing protein fabricated by double emulsion solvent extraction/evaporation method. *Biomaterials*, **22(3)**, 231-241.

References

Yeh, M.K., Chen, J.L., Chiang, C.H. (2004) In vivo and in vitro characteristics for insulin-loaded PLA microparticles prepared by w/o/w solvent evaporation method with electrolytes in the continuous phase. *J. Microencapsul.*, **21(7)**, 719-728.

Yeo, S.D., Kiran, E. (2005) Formation of polymer particles with supercritical fluids: A review. *J. Supercrit. Fluids*, **34(3)**, 287-308.

York, P. (1999). Strategies for particle design using supercritical fluid technologies. *Pharm. Sci. Technol. Today*, **2(11)**, 430-440.

Young, T.J., Johnston, K.P. (1999) Encapsulation of lysozyme by precipitation with a vapor-over-liquid antisolvent. *J. Pharm. Sci.*, **88(6)**, 640-650.

Zhu, K.J., Lin, X., Yang, S. (1990) Preparation,characterization, and properties of polylactide (PLA)-poly(ethylene glycol) (PEG) copolymers: A potential drug carrier. *J. Appl. Polym. Sci.*, **39(1)**, 1-9.

Zhuang, W., Kiran, E. (1996) An automated high pressure PVT apparatus for continuous recording of density and isothermal compressibility of fluids. *Rev. Sci. Instrum.*, **67(1)**, 244-250.

Zolnik, B.S., Leary, P.E., Burgess, D.J. (2006) Elevated temperature accelerated release testing of PLGA microspheres. *J. Contr. Rel.*, **112(3)**, 293-300.

zur Mühlen, A., Schwarz, C., Mehnert, W. (1998) Solid lipid nanoparticles (SLN) for controlled drug delivery - Drug release and release mechanism. *Eur. J. Pharm. Biopharm.*, **45(2)**, 149-155.